Tumor Suppressor p53 in Cerebellar Development, Medulloblastoma Initiation, and Treatment Resistance

by

Daniel M. Treisman

A dissertation submitted in partial fulfillment
of the requirements for the degree of
Doctor of Philosophy
(Cellular and Molecular Biology)
in the University of Michigan
2016

Doctoral Committee:

Professor Andrzej A. Dlugosz, Co-Chair
Adjunct Associate Professor Yuan Zhu, Co-Chair
Assistant Professor Benjamin Allen
Professor Gary D. Hammer
Professor Yi Sun

Dedication

This thesis is dedicated to my loving and supportive wife, Katherine Marshall, my parents, Jonathan and Ruth Treisman, my sisters, Pamela and Rebecca, and the rest of my family.

Acknowledgements

I would like to thank my academic advisor, Professor Yuan Zhu, who has been personally involved with my growth as a scientist since I entered the program. He has provided guidance and support throughout my training, and his mentorship has demonstrated a scientific approach that I will take with me throughout my career.

I would like to acknowledge my thesis committee members, Yi Sun, Ben Allen, Gary Hammer, and Andrzej Dlugosz, who were able to contribute time, thought and effort into helping me to better my study. They provided constructive feedback to improve the project direction during meetings as well as insight into my personal career development. I would especially like to thank Dr. Andrzej Dlugosz for agreeing to serve as my co-chair during my time in Washington.

I would like to thank my program for assisting with oversight during my stay both in Ann Arbor and Washington. Thanks go to Cathy Mitchell, Margarita Bekiares, Director Jessica Schwartz and Director Robert Fuller, for maintaining a professional environment and a positive social atmosphere in Ann Arbor, and for keeping my best interests in the fore while I was in Washington.

I am deeply thankful for my current and former lab members, especially former graduate students Lou Chang, Yuan Wang and Seckin Akgul, as well as current student Emma Jecrois, for their friendship, insight and contributions to my project.

Finally, I would like to thank my family for providing support and encouragement throughout my time in the program. My parents Ruth and Jonathan and sisters Pamela and Rebecca and wife Katherine have been positive and loving during my time in the lab.

Table of Contents

List of Figures

Abstract:

p53 in Cerebellar Development, Medulloblastoma Initiation, and Treatment Resistance

by Daniel Treisman

TP53 is a crucial tumor suppressor inactivated in the majority of human cancers. Medulloblastoma (MB), the most common malignant pediatric brain tumor, is an exception, rarely mutating *TP53*. Within the Sonic Hedgehog (SHH) MB subtype, *TP53* mutation is a prognostic factor, and mutant *TP53* SHH-MBs have the worst prognosis of all subtypes. How most SHH-MBs can form without mutating *TP53* remains unclear. Almost all SHH-MBs with *TP53* mutation arise during childhood, indicating that mutation to TP53 must occur during a limited developmental window. Early postnatal (postnatal day 0.5) granule cell precursors (GCPs) are p53-activation resistant following genotoxic stress, whereas late postnatal (postnatal day 10) GCPs are p53-activation sensitive. I hypothesize that a p53-activation resistant GCP population gives rise to p53 wild type SHH-MBs and that p53-activation sensitive GCPs are eliminated during postnatal development unless they harbor mutant *p53*.

Using two mutant *p53* alleles, a conditional knockout, $p53^{\Delta E5\text{-}6}$, and a hypomorph, $p53^{R172P}$, I demonstrated that p53 activation occurs during cerebellar development, and is activated in the earliest detectable lesions driven by *Ptch1* loss. Consistently, p53-dependent apoptosis plays a major role in both the initiation and progression of SHH-MBs, while p53-dependent cell cycle arrest only delays SHH-MB progression. Surprisingly, a subset of *Ptch1*-deficient pre-neoplastic lesions (PNLs) showed no

evidence of p53 activation, regardless of *p53* mutation, providing a mechanistic basis for the formation of *p53* wild type (WT) SHH-MBs. To test whether these PNL represented a p53-activation resistant population, I designed a clinically relevant treatment scheme to induce genotoxic stress and elicit a heightened p53 response. I found that treatment eliminated all PNL cells and reduced the incidence of SHH-MBs, but only when p53-mediated apoptosis was activated. Activation of p53-mediated cell-cycle arrest alone halted proliferation and induced neuronal differentiation, but failed to eliminate Sox2-positive stem-like cells, which were capable of surviving treatment and generating highly proliferative SHH-MB. Thus, only when p53 activation surpasses a critical threshold will Sox2-positive stem-like cells be eliminated, preventing *p53* recurrence and determining therapeutic outcomes.

Chapter I: Introduction

1.1 A connection between p53 and SHH-medulloblastoma

Tumor suppressor TP53 is one of the most frequently targeted pathways in cancers, with approximately 50% showing alterations to *TP53* (Joerger and Fersht 2016). Curiously, many pediatric brain tumors, including medulloblastoma (MB) and low-grade glioma, the most common malignant and benign pediatric brain tumor types, respectively, rarely harbor mutations to *TP53* (Adesina et. al., 1994). In spite of the scarcity of *TP53* mutation, MB incidence is increased in individuals with Li-Fraumeni, the *TP53*-associated hereditary cancer predisposition syndrome (Northcott et. al., 2012, Kool et. al., 2014). Recent studies have divided MBs into several genetic subtypes, including a subtype linked to the Sonic Hedgehog (SHH) signaling pathway (Thompson et. al., 2006). Li-Fraumeni syndrome is exclusively associated with the SHH-MB subtype, and mutation of *TP53* is one of the chief prognostic indicators, with mutant *TP53* showing a strong correlation with treatment-resistant disease and poor survival (Zhukova et. al., 2013). Mutation of *TP53* is associated with development of aggressive, treatment-resistant MBs in the SHH subgroup (Tabori et. al., 2010, Zhukova et. al., 2013). It remains unclear what role TP53 plays in preventing the initiation of MBs (Gajjar and Robinson 2014). One of the remaining questions in the field is how many SHH-MBs form without requiring *TP53* mutation, and, as a corollary, the role that TP53 plays during MB initiation.

This discrepancy may be explained by differential p53 response in stem and precursor populations found in the developing cerebellum (Pazzaglia et. al., 2006, Yang et. al., 2008). As a pediatric tumor, SHH-MB cell of origin has been identified as belonging to the neuroectodermal lineage, including granule cell precursors (GCPs) of the embryonic and postnatal cerebellum (Marino et. al., 2000, Yang et. al., 2008, Sutter et. al., 2010). Treatment of GCPs with radiation during cerebellar development reveals

differential radiation response from embryonic and early postnatal (postnatal day 0.5) GCPs, which do not activate p53 following irradiation stress, to late postnatal GCPs (postnatal day 10), which respond to radiation stress by inducing p53 activation and apoptosis (Pazzaglia et. al., 2006, Tanori et. al., 2013). One interpretation of this data supports the existence of two types of GCPs, a population resistant to the activation of p53 following stress and a population that is sensitive to stress signals and activates p53 following oncogenic signaling or genotoxic stress. I hypothesize that p53-activation resistant GCPs are capable of giving rise to SHH-MBs retaining a functional p53 pathway, while those GCPs p53-activation sensitive would be eliminated during development unless they had mutated p53, either at the germline or prior to early postnatal development.

To address this hypothesis, I developed a three-tiered approach to assess p53 function, utilizing: 1) a fully functional *p53* allele, 2) a hypomorph allele, $p53^{R172P}$ capable of reduced activation of a subset of effectors, primarily cell cycle arrest associated, and no activation of apoptotic effectors, and 3) a conditionally inactive *p53* allele, $p53^{\Delta E5\text{-}6}$, that can serve as a marker of p53 activation (Liu et. al., 2004, Wang et. al., 2009). Using $p53^{\Delta E5\text{-}6}$ as a marker overcomes several of the constraints preventing investigation of p53 in developmental populations, allowing accumulation of p53 by eliminating the p53-MDM2 negative feedback loop and preventing the removal of cells that would normally be eliminated by p53-mediated apoptosis (Wang et. al., 2009). The $p53^{R172P}$ allele restores partial p53 function, thereby demonstrating the result of functional p53 activity while still preventing the elimination of stressed cells (Liu et. al., 2004). By placing these *p53* mutant alleles into the context of the SHH-MB model subtype the well-characterized $Ptch1^{+/-}$ genetically engineered mouse model (Goodrich et. al., 1997, Wetmore et. al., 2001), and recombining $p53^{\Delta E5\text{-}6}$ in the brain with hGFAP-Cre (Zhuo et. al. 2001), I was able to develop a model capable of testing the activation of p53 activation in cerebellar development and MB initiation.

1.2 MB Epidemiology and Pathology

MB is an aggressive, malignant pediatric tumor arising from the neuroepithelial lineage of the cerebellum (Louis et. al., 2007). MB is primarily a pediatric disease, with 70% of MBs arising in infants and children (Louis et. al., 2007). MBs occur in 0.5 per 100,000 children, and 0.058 per 100,000 in adults (Giordana et. al., 1999, Louis et. al., 2007, Gajjar and Robinson 2014). MBs are typically responsive to combined therapy, which includes surgery, radiation and chemotherapy in individuals older than 3, and chemotherapy and surgery without radiation in infants (Thompson et. al., 1999, Lewandowicz et. al., 2000, Louis et. al., 2007, Crawford et. al., 2007). Based on the quality of surgical resection and the presence of metastatic spread upon initial diagnosis, MBs are divided into average- and high- risk patients. Treatment is effective in 70-80% of average risk MB patients, leading to survival with no recurrent disease (Crawford et. al., 2007). Treatment of MBs in infants is less successful, with average survival of 40%, primarily due to the inability to safely use radiation (Crawford et. al., 2007). Due to the harsh nature of these treatments on developing brain, innovation of therapies capable of targeting the tumor without incurring as great an effect on healthy tissues remains an area of interest in MB research. Pediatric patients treated with a standard radiation dose often suffer a gradual decline in IQ following treatment, with an estimated decline of 20 IQ points in patients younger than 8 years of age (Palmer et. al., 2013, Merchant et. al., 2014, Moxon-Emre et. al., 2014). Thus, translational research for MBs pursue three objectives – predicting which MBs are likely to respond to standard therapy and which are resistant, reducing the side effects associated with modern treatment strategies, and finding a targeted therapy capable of eliminating treatment-resistant MBs.

Several strategies have been developed to diagnose MBs and assess tumor severity. All MBs share some diagnostic characteristics: they are generally comprised of densely packed cells with large nuclei and relatively little cytoplasm, and they typically arise in the cerebellar vermis and fourth ventricle of pediatric patients (Eberhart and Berger 2003, Louis et. al., 2007, Rodriguez et. al., 2007). Immunological markers associated with MBs fall into several categories, including neural markers Synaptophysin, considered the characteristic marker for MB, Neurofilament (NF) and

Paired Box Gene 6 (Pax6); neuroepithelial precursor marker Nestin; glial marker Glial Fibrillary Acidic Protein (GFAP); and Retinal S-antigen, marking retinal features (Schwechheimer et. al., 1987, Louis et. al., 2007). Other characteristic markers detected in MBs include the zinc-finger protein Zic1, a transcription factor associated with granule cell precursors, and neurotrophin receptor TrkC, associated with desmoplastic MBs, with frequent immunostaining in 70% and 40% of MBs, respectively (Segal et. al., 1994, Yokota et. al., 1996, Aruga et. al, 1998, Louis et. al., 2007). MBs are traditionally classified through histopathology, dividing MBs into 5 histological subtypes: classic, desmoplastic, MBEN (medulloblastoma with extensive nodularity and advanced neuronal differentiation), large cell and anaplastic (Louis et. al., 2007). Of these histological groups, MBEN and desmoplastic are often combined into a single group referred to as D/N, and the large cell and anaplastic histology is typically describer as LC/A.

Classical MBs, the most common histological variant, account for 73% of pediatric MBs, and are identified by the presence of rounded cells featuring large, darkly stained nuclei and little cytoplasm, as well as cells arranged into palisades or Homer-Wright rosettes (Louis et. al., 2007, Gajjar and Robinson 2014). Desmoplastic MBs are identified by the pattern of dense, hyper-chromatic cellular regions surrounding eosinophilic nodes, which contain cells at a lower density (Louis et. al., 2007, Gajjar and Robinson 2014). The distinguishing feature of the MBEN subtype is the presence of large, irregular nodes and increased neuronal differentiation of cells within the nodes (Louis et. al., 2007). Staining for a reticulin matrix in the internodular regions is an additional identifier of these subtypes. Additionally, desmoplastic and MBEN subtypes, although only accounting for 10.3% of overall pediatric MBs, occur predominantly within infants, accounting for 57% of infant MBs (Ellison 2010). Anaplastic MBs are characterized by pleomorphic nuclei, frequent nuclear molding and high mitotic frequency (Louis et. al., 2007). Large cell MBs, although often sharing traits with anaplastic MB, are distinguished by the presence of cells with large nuclei, typically 3-4 fold larger (Louis et. al., 2007). MBs exclusively containing large cell histology are rare, instead featuring clusters of large cells surrounded by dense anaplastic cell populations (Louis et. al., 2007). When the anaplastic and large cell MB subtypes are combined into

the LC/A subtype, they account for 16.6% of pediatric MBs with comparable frequency in infant and childhood MBs (Ellison 2010). The histological classification system of MBs provides few prognostic indicators. Within infant populations, desmoplastic tumors show the best prognosis, with typical survival of 60% versus 20-40% for non-desmoplastic MBs (Crawford et. al., 2007). The presence of large cell and anaplastic morphology has been suggested as an indication of aggressive tumors with poor prognosis, although this association has not been consistently supported (Louis et. al., 2007, Zhukova et. al., 2013).

1.3 Hereditary Predisposition Syndromes Contributing to MB Incidence

Observation of the epidemiology of MBs led to the discovery that several hereditary cancer predisposition syndromes were capable of contributing to the incidence of MB. Two of these syndromes, Gorlin Syndrome (or Nevoid Basal Cell Carcinoma Syndrome, NBCCS) and Turcot syndrome, are associated with critical signaling pathways involved in cerebellar development, while the third is Li-Fraumeni syndrome, associated with germline alteration of *TP53* (Rossi et. al., 2008, Louis et. al., 2007, Gajjar and Robinson 2014).

Gorlin Syndrome, initially described in 1960, is an autosomal dominant disorder associated with basal cell carcinomas and MBs, as well as bone cysts in the mandible, macrocephaly, and several other physiological defects (Gorlin and Goltz 1960, Kimonis et. al., 1997). Between 3-5% of Gorlin syndrome patients will be diagnosed with MBs, with the majority arising during infancy (Garré et. al., 2009). Gorlin syndrome has been linked to inactivating mutations of two genes, patched (*PTCH1)* or suppressor of fused (*SUFU)*, thereby leading to activation of Hedgehog signaling pathway (Jiang and Hui 2008). Although mutations in *SUFU* only represent a small fraction of the overall Gorlin's population, the frequency of MBs within these patients is approximately 20 times greater than that seen with *PTCH1* (Smith et. al., 2014). Sporadic mutation of the Hedgehog pathway genes is also often observed within MBs, with approximately 9% of MBs bearing a sporadic mutation in *PTCH1*. The majority of tumors with a sporadic mutation in *PTCH1* are found to not retain the wild type *PTCH1* allele, indicating that

complete loss provides elevated Hedgehog pathway activation, the oncogenic driver in SHH-MBs (Pazzaglia et. al., 2002, Ward et. al., 2009, Read et. al., 2009, Tamayo-Orrego et. al., 2016).

Like Gorlin Syndrome, Turcot syndrome is a well-characterized but rare hereditary condition initially discovered in families displaying an overabundance of intestinal polyps, leading to heightened incidence of colon cancer, as well as increased risk of gliomas and MBs (Huang et. al., 2000). Overall MB incidence in Turcot patients is at least 100 fold greater than the general population, although incidence is still less than 1%. Turcot syndrome is associated with mutations in adenomatous polyposis coli (*APC*), leading to activation of the Wingless (Wnt) pathway (Huang et. al., 2000, Clevers 2006). Wnt is a ligand capable of interacting with a complex comprised of the transmembrane protein Frizzled and LRP5/6, which in turn activates Disheveled to inhibit the APC complex (Clevers 2006). Inhibition of the APC complex allows transport of ß-Catenin to the nucleus, where ß-Catenin then forms a complex with TCF/LEF to allow transcription of the Wnt pathway target genes, including several genes involved in proliferation and inhibition of apoptosis, such as *c-Myc* and *CCND1* (Clevers 2006). Several studies have demonstrated that mutations of *CTNNB1*, the gene associated with ß-catenin, are present in approximately 8% of MBs, accounting for approximately 90% of sporadic Wnt pathway mutations, though mutations to *AXIN1*, the APC complex backbone, and *APC* account for 3% and 2% of Wnt pathway mutations, respectively (Baeza et. al., 2003).

Li-Fraumeni syndrome is a rare autosomal dominant genetic condition characterized by mutations in the p53 pathway, with between 60-80% resulting from mutations in *TP53* (Adesina et. al., 1994). Mutations in *TP53* typically prevent transcription factor activity by interfering with the p53 DNA binding domain, a region of the *TP53* allele associated with 90% of *TP53* mutations, including all six of the mutational hotspots (Joerger and Fersht 2016). Due to the importance of p53 in preventing neoplastic transformation, the lifetime risk of developing cancer in Li-Fraumeni patients is 73% in men and 100% in women (Wu et. al., 2006). Soft-tissue sarcomas are the most frequent tumor associated with Li-Fraumeni, though a wide range of tumor varieties, including myeloid lymphoma, leukemia, non-small cell lung cancer,

breast cancer, astrocytoma, and MB, occur with increased frequency in this population (Wu et. al., 2006). Genetic analysis of MBs found that mutation of *TP53* only occurred within 8-10% of the total cases (Adesina et. al., 1994, Louis et. al., 2007, Tabori et. al., 2010). Curiously, although the majority of tumors containing mutant *TP53* also saw loss of chromosome 17p, the frequency of 17p loss extends far beyond those tumors with mutant *TP53*, indicating that *TP53* may not be the only gene targeted by loss of chromosome 17p (Cho et. al., 2010). The scarcity of *TP53*/*p53* mutations in MBs represents an exception to the observed trend in other cancers that has not been fully explored, but may provide insight into cerebellar development and the cellular origin of MBs (Wetmore et. al., 2001, Tamayo-Orrego et. al., 2016).

1.4 Molecular Subgroups of MB

The clear association between several signaling pathways and MB occurrence suggests that prognosis and expected treatment response could be predicted with a method of molecular categorization of MB. In 2006, a collaborative effort headed by the Gilbertson lab performed expression profiling, using 46 pediatric MB samples, identifying five genetic subtypes (Thompson et. al., 2006, Robinson et. al., 2012, Jones et. al., 2012). Two of these subtypes were found to correspond with developmental pathways of the cerebellum, Hedgehog and Wnt, with the other three subgroups not explicitly matching with any known signaling pathway (Thompson et. al., 2006). This was explored by subsequent studies, which, using a broader range of samples and techniques, condensed the number of subgroups to 4, retaining the SHH and Wnt groups, but also proposing that Group 3 MB were associated most strongly with c-Myc activation (Northcott et. al., 2010). Based on these molecular varieties, new approaches to diagnosis and deeper insight into MB prognosis have become available.

Only 10% of the total diagnosed MBs are characterized as the Wnt subgroup, associated with 90% patient survival, the best overall prognosis amongst MB subtypes (Louis et. al., 2007). Wnt MBs occur primarily in children and young adults, and almost never in infants (Shih et. al., 2014). Several mutations are enriched within the Wnt subgroup, with nearly all MBs of this subtype carrying mutations within *CTNNB1*, the

gene encoding ß-Catenin, as well as several other genes enhancing Wnt pathway activation, such as methyltransferase *KMT2D* and helicase *SMARCA4* (Gajjar and Robinson et. al., 2014). Additionally, these tumors tend to show elevated *c-Myc* expression. Although sporadic *TP53* mutations are associated with 10-15% of Wnt MBs, overall survival does not appear to change between *TP53* wild type and *TP53* mutant tumors (Pfaff et. al., 2010, Jones et. al., 2012). Due to excellent prognosis and reliable treatment response, the Wnt subgroup has not been a typical focus for translational research.

Group 3 (Group C) MBs, accounting for approximately 25% of MB, are regarded as the most aggressive subgroup, with only 50% overall survival in group 3 patients (Northcott et. al., 2010, Korshunov et. al., 2012, Jones et. al., 2012, Zhukova et. al., 2013). Group 3 MBs are highly aggressive, with metastasis in approximately 40% of patients, and occur primarily in infants and young children (Northcott et. al., 2010, Shih et. al., 2014). Group 3 MBs, while not linked to any hereditary syndrome, exhibit increased expression of *MYC* in the majority of samples, as well as amplification of the *MYC* oncogene in approximately 16% of tumors (Cho et. al., 2011, Northcott et. al., 2012). In addition to MYC, *TGF-ß* receptor pathway genes undergo copy number alterations in 20.2% of all Group 3 MBs (Cho et. al., 2011, Northcott et. al., 2012, Gajjar and Robinson et. al., 2014). Other than these alterations, a wide variety of chromatin modifying genes, such as *SMARCA4*, *KMT2D*, *CHD7* and several members of the *KDM* family, are altered in Group 3 MBs (Cho et. al., 2011, Northcott et. al., 2012). Group 3 MBs possessing *MYC* amplification represent the most severe of all MBs, with an overall survival rate of 21%, compared to 75% overall survival in Group 3 MBs without *MYC* amplification (Cho et. al., 2011). Group 3 MBs have been of great interest clinically, as this subtype has some of the worst prognosis, leading to development of *c-Myc* driven mouse models (Pei et. al., 2012, Kawauci et. al., 2012).

Group 4 MBs are the most common subgroup, representing 35% of diagnosed MBs and predominantly occurring in children greater than 3 years of age and adults (Louis et. al., 2007, Gajjar and Robinson 2014). Group 4 MBs typically respond well to therapy, with a 75% overall survival rate (Shih et. al., 2014). Evidence exists that these

tumors are potentially driven by a sex-linked gene, as tumor incidence is three times greater in males, and female patients often show loss of the X-chromosome (Cho et. al., 2011, Gajjar and Robinson 2014). Group 3 and Group 4 MBs possess molecular similarities, as demonstrated by their overlapping expression pattern, and it has been proposed that Group 3 and Group 4 represent a GABAergic and glutamatergic neuron-like subtype, respectively, with some portion of these tumors carrying a mixed expression pattern (Robinson et. al., 2012, Cho et. al., 2011). Likewise, many molecular alterations observed in Group 4 MBs overlap with Group 3 MBs, including alterations to *SMARCA4* and *KMT2D* (Northcott et. al., 2010, Gajjar and Robinson 2014). Mutation of *TP53* is very rare in Group 4 and non-existent in Group 3, although isochrome 17q is a very common phenomenon (Cho et. al., 2011). Due to the lack of a central molecular mechanism, a representative mouse model for Group 4 MBs has yet to be developed.

The best studied of the MB subgroups is the SHH-MB. SHH-MBs, accounting for 25-30% of MBs, are associated with mutations affecting components of the hedgehog pathway. Approximately 30% of these tumors carry mutations in *PTCH1*, while other tumors of this subtype increased Hedgehog pathway signaling by altering other pathway components, including Smoothened (*SMO*) or Suppressor of Fused (*SUFU*), or by amplification of downstream targets, most frequently *Gli1*, *Gli2* or *n-MYC* (Gajjar and Robinson 2014, Shih et. al., 2014). Likewise, loss of chromosome 9q, corresponding with the location of PTCH1, is observed in approximately 45% of SHH-MBs and is enriched in tumors possessing mutation to one allele of *PTCH1*, occurring in approximately 90% of patients with *PTCH1* mutation (Cho et. al., 2011). As a result of the frequency of deregulated hedgehog signaling, one of the key treatment interests for SHH-MBs is the introduction of potent Hedgehog pathway inhibitors, preferably capable of targeting the downstream hedgehog pathway targets.

The potential for targeting the Hedgehog pathway was recognized even before the current molecular categories were discovered. Using the theoretical model of oncogene addiction, it was hypothesized that disruption of the Hedgehog pathway would target a vulnerability in SHH-MBs. Initial trials made use of cyclopamine, a naturally occurring inhibitor of Smo extracted from the corn lily, and were able to demonstrate that hedgehog

pathway blockade was capable of inducing growth arrest in both human cell line and murine models (Berman et. al., 2002, Romer et. al., 2004). Although largely successful, clinical trials with vismodegib, an early Smo inhibitor, showed that a patient with a metastatic SHH-MB developed resistance to the Hedgehog pathway inhibitor within three months of therapy, by acquiring a single point mutation to Smo (Yauch et. al., 2009). Additional Hedgehog pathway inhibitors with the ability to target components further down the Hedgehog pathway, such as Gli1/2, have been developed, which may prove valuable in treating SHH-MBs with amplifications of downstream Hedgehog pathway components (Yauch et. al., 2009, Kim et. al., 2013). While several potential compounds have been discovered that fit this criteria, none have gone beyond clinical trials, although arsenic trioxide, a potent inhibitor of SHH effectors Gli1 and Gli2, shows potent inhibition of MB progression *in vivo* (Kim et. al., 2013).

TP53 alterations are most common in the SHH-MB subgroup (Zhukova et. al., 2013). Approximately 20% of SHH-MBs harbor mutations in *TP53* (Eberhart et. al., 2005, Tabori et. al., 2010, Jones et. al., 2012). Of these mutations, roughly half are germline, representing the majority of those MBs that occur within Li-Fraumeni syndrome patients. Based on molecular characterization of the *TP53* mutant SHH-MBs, distinct mutation and chromosomal alterations become evident. Perhaps the most unexpected observation from these tumors is that less than 1% of MBs possess mutations to both *TP53* and *PTCH1* (Parsons et. al., 2011). The correlation between mutations to these genes was explored using a *Math1*-promoter associated sleeping beauty transposon, thereby leading to insertional mutagenesis within the $Math1^{+}$ granule cell precursor population (Wu et. al., 2012). The sleeping beauty system was used in $Ptch1^{+/-}$ or $p53^{-/-}$ models, and insertion sites associated with decreased tumor latency were assessed (Wu et. al., 2012). Curiously, although the mutation most associated with sleeping beauty in the $p53^{-/-}$ background was *Ptch1*, mice in the $Ptch1^{+/-}$ background never showed mutation in *p53* (Wu et. al., 2012). Likewise, *TP53* mutant tumors frequently undergo chromosome 17p loss, but almost never correspond with loss of chromosome 9q, the location of *PTCH1* (Cho et. al., 2011). Analysis of allele frequency and single nucleotide variant (SNV) accumulation demonstrated that SHH-MBs could be segregated based on

TP53 mutational status, with MBs containing mutant *TP53* typically occurring during late childhood and containing several fold greater SNVs as well as evidence of chromothripsis, widespread chromosomal rearrangement arising from a single event (Rausch et. al., 2012, Jones et. al., 2012). Unlike the Wnt subtype, *TP53* mutations are a prognostic indicator within the SHH-MB subgroup, with a strong association between mutant *TP53* and rapid progression. Initial reports indicated that presence of mutant *TP53* was sufficient to induce complete treatment resistance and rapid lethality, with 100% fatality within 2 years as opposed to 74% survival within p53 wild type, with subsequent reports demonstrating comparable associated risk, albeit with lower overall severity, demonstrating survival in 41% of *TP53* mutant MBs compared to 81% TP53 wild type. Activation of p53 in murine models by treatment with MDM2 inhibitor Nutlin-3 was able to suppress the rate of MB growth in xenograft models, but was insufficient to prevent tumor formation (Künkele et. al., 2012). The correlation between poor prognosis and *TP53* mutation has served to highlight the need for new therapeutic approaches capable of targeting *TP53*-mutant SHH-MB.

1.5 The TP53 Signaling Pathway

TP53 and its associated pathway is one of the most important and well-studied tumor suppressor responses available to regulate abnormal cell populations. First discovered in 1979, p53 was initially believed to be a viral oncogene carried by SV40. (Kress et. al., 1979, Lane and Crawford 1979, Linzer and Levine 1979, [reviewed in Soussi 2010]). It was later theorized that, although TP53 was enriched in cells infected with the SV40 virus, the newly discovered *TP53* was in fact an oncogene, a belief fostered by the frequency of enrichment within tumor cells and the potential of transfected *TP53* along with the *KRAS* oncogene, to induce the formation of tumors within transfected cells (Parada et. al., 1984, Jenkins et. al., 1984, Eliyahu et. al., 1984). Understanding of TP53 took a radical change in 1989, when it was demonstrated that, when non-mutant p53 was cloned, no oncogenic function was detected. Rather, the majority of TP53 detected in tumor was demonstrated to harbor mutations rendering the gene non-functional (Finlay et. al., 1989, Baker et. al., 1989, Takahashi et. al., 1989). This discovery was followed shortly by the discovery of TP53 as the key gene involved

with Li-Fraumeni syndrome, the now well-known hereditary tumor predisposition syndrome associated with *p53* mutation (Malkin et. al., 1990). Since these discoveries, the TP53 protein and the pathway's activators, regulators and effectors have been further investigated.

The TP53 protein is comprised of five key domains, two adjacent trans-activation domains at the n-terminus, the second of which includes a proline-rich region, a DNA binding domain, an oligomerization domain critical for the formation of the p53 tetramer and a C-terminal domain that contains three nuclear localization signal elements (Figure 5A) (Joerger and Fersht 2016). For successful transcription, TP53 must form a tetrameric complex, reliant on the oligomerization domain, which is capable of binding to its effectors at the DNA binding domain (Zauberman et. al., 1993). The transactivation domains influence which effectors are activated by TP53, with loss of the first transactivator domain leading to widespread failure to activate most target genes, including *MDM2* but not *Perp* or *Bax*, thereby permitting tumor suppressive functions via apoptosis but not cell cycle arrest, whereas loss of the second domain had only minor effects on TP53 transcription (Jimenez et. al., 2000, Brady et. al., 2011). The C-terminal domain is a key component of TP53 regulation, containing the ubiquitination site targeted by MDM2, the chief regulator of TP53 activity (Hamard et. al., 2013).

MDM2, as well as its family member MDM4, are the key regulators of p53 transcription (Wang et. al., 2001, Lahav et. al., 2004). MDM2 is a RING-finger e3 ubiquitin ligase capable of inhibiting TP53 by ubiquitinating sites in both the DNA binding domain and the C-terminal domain, whereas the highly similar MDM4 is able to bind but not ubiquitinate TP53 (Xia et. al., 2008, Barboza et. al., 2008). Ubiquitination of TP53 is capable of inhibiting transcription through several mechanisms, including directly preventing transcription, inducing nuclear export, and promoting degradation of cytoplasmic TP53 via the 26S proteasome (O'Keefe et. al., 2003). Failure to regulate TP53 function can be catastrophic, with a null mutation in MDM2 causing embryonic lethality in animal models and even partial inactivation leading to phenotypic abnormalities (Jones et. al., 1995, Pant et. al., 2016). While TP53 is generally tightly regulated by MDM2, in times of cell stress the p53 pathway is activated through two key

responsive elements, $P14^{ARF}$ ($p19^{ARF}$ in mouse), typically activated in response to cellular or oncogenic stress, and ATM/ATR (Figure 1), activated as a result of DNA damage, as might be induced through ionizing radiation (Bouvard et. al., 2000, Suh et. al., 2011). Both of these elements interfere with MDM2 function, with ATM/ATR inducing phosphorylation of TP53 both directly and through CHK1/2, and ARF binding MDM2 and sequestering it in the nucleolus. In either case, inhibition of MDM2 function leads to a temporary accumulation of transcriptionally active TP53 in the nucleus. In the absence of MDM2 to serve as a regulator, TP53 is a potent transcription factor with effectors involved in a myriad array of processes, including cell cycle arrest and apoptosis, as well as DNA repair, senescence, autophagy, ferroptosis and metabolism (Polyak et. al., 1997, Tokino and Nakamura 2000, Riley et. al., 2008, Li et. al., 2012, Jiang et. al., 2015). The TP53-mediated cell cycle arrest response is primarily controlled by tumor suppressor $p21^{CIP1/WAF1}$, encoded by the gene *CDKN1A*, a CDK inhibitor capable of inducing G1 arrest (El-Deiry et. al., 1994, Deng et. al., 1995). The apoptotic activities of TP53 are engaged through multiple effectors, including *NOXA* and *PUMA*, inhibitors of anti-apoptotic gene *BCL2*, and *BAX*, which directly activates the intrinsic apoptotic pathway (Nakano and Vousden 2001, Joerger and Fersht 2016). Which of these effectors activated is regulated through several mechanisms, including promoter binding affinity, protein modification, and epigenetic regulation. In general, promoter binding affinity can be generalized into high and low affinity binding sites , with many of the high affinity binding sites corresponding with cell cycle arrest targets, such as *P21*, and low affinity binding sites with apoptotic targets, such as *Bax* (Ludwig et. al., 1996, Szac et. al., 2001, Inga et. al., 2002). Further, the TP53 protein can be altered in a variety of ways that predispose the transcription factor activity to different binding sites, such as phosphorylation of Ser-46, leading to transcription of *p53AIP1*, and acetylation of Lys-117, required for p53 apoptotic response (Oda et. al., 2000, Li et. al., 2012). This wide array of effectors also contains *MDM2*, thereby forming a negative feedback loop capable of attenuating TP53 signaling following stress.

A variety of p53 mutant alleles have been developed in order to study p53 function in the mouse model. Some of the more well known of these mutant alleles make

use of hotspot mutations, meant to imitate human disease, such as the $p53^{R172H}$ mutant, which resembles the human $p53^{R175H}$ hotspot (Joerger and Fersht 2016). An infrequent mutation to the same hotspot produces the $p53^{R172P}$ mutant, a hypomorph allele identified in only 8 human patients (Edlund et. al., 2012). However, this allele provides a useful experimental system, retaining partial cell cycle arrest activity, chromosomal repair function, and MDM2 feedback regulation while ablating the p53-mediated apoptotic response (Liu et. al., 2004). Using this allele as a homozygous germline mutation, mice develop lymphoma and sarcoma between 7-12 months of age, compared with 4-8 months in p53 null mice, with less evidence of DNA damage in the resultant tumors (Liu et. al., 2004). An additional p53 allele of recent interest is the $p53^{3KR}$ model, which replaces lysine to arginine at three acetylation sites, 117, 161 and 162, thereby producing a p53 with no p53-mediated apoptosis, senescence or cell cycle arrest, but retaining metabolic regulation activity (Li et. al., 2012). These new p53 alleles provide the opportunity to study the effects of p53 transcriptional activity with greater specificity than previous models have allowed.

The role of TP53 in cerebellar development has not been fully explored. Loss of p53 has few associated phenotypes in the murine model, although hGFAP-Cre mediated p53 disruption is capable of inducing MBs in approximately 10% of affected animals (Zhuo et. al., 2001, Wang et. al., 2009). Although no phenotypic alteration is observed in the cerebellum of *p53* null mice, hyperactivity of p53 as induced by MDM2 loss leads to a drastic reduction of cerebellum (Malek et. al., 2011). The effect of MDM2 loss was completely rescued with the loss of p53 and partially rescued by introduction of homozygous $p53^{R172P}$, which resulted in reduced cerebellar size and foliation (Liu et. al., 2007). This demonstrates that the role of p53 during cerebellar development is a highly potent inhibitory effect, but also shows that this role is highly regulated, affecting only developmental cells only rarely.

1.6 The Hedgehog Signaling Pathway

The Hedgehog pathway was initially discovered in Drosophila, where it plays a critical role in embryonic patterning (Nüsslein-Volhard and Wieschaus 1980, Hooper and

Scott 1989). In vertebrates, loss of Sonic hedgehog signaling led to defects in neural plate formation, absence of hind limbs, and cyclopia (Chiang et. al., 1996, Marigo et. al., 1996). Vertebrate hedgehog signaling is maintained in an inactive state without ligand stimulation, wherein the transmembrane receptor protein Patched (PTCH1) inhibits the function of the G-protein coupled receptor-like protein Smoothened (SMO) (Figure 2) (Marigo et. al., 1996, Stone et. al., 1996, Lee et. al., 2006). The GLI family of zinc-finger transcription factors, consisting of GLI1, GLI2 and GLI3, are the key downstream effectors of hedgehog signaling (Fuccillo et. al., 2006). While Smoothened is repressed, trafficking of a SUFU-GLI complex at the primary cilia leads to GLI phosphorylation by the PKA/GSK3ß/CK1 complex prior to being processed into a transcriptional repressor form (Blaess et. al., 2006, Pan et. al., 2009). Binding of hedgehog ligand to PTCH1, in combination with co-receptors BOC, CDON, and GAS1, de-represses SMO, thereby allowing SMO migration to the primary cilia (Wechsler-Reya and Scott 1999, Fuccillo et. al., 2006, Rohatgi et. al., 2007, Corrales et. al., 2009, Izzi et. al., 2011). SMO migration to the primary cilia, facilitating accumulation of SUFU-GLI complex, and permits dissociation of SUFU and GLI, which then bypasses PKA and migrates to the nucleus as the active form of GLI (GliA) (Rohatgi et. al., 2007, Briscoe and Therond 2013) This allows GLI-mediated transcription of numerous downstream effectors, including *Ptch1, Gli1, Gli2, Cyclin-D* and *n-Myc (*Oliver et. al., 2003*)*. Through these effectors, the hedgehog pathway can promote both cell cycle progression and tumor initiation.

1.7 Form, Function and Development of the Cerebellum

The mature cerebellum is the most neuron dense tissue in the brain, accounting for more than 75% of the brain's neurons (Marzban et. al., 2015). The neurons of the cerebellum, through a complex network of excitatory and inhibitory interactions, are able to translate intended movements to match with sensory and spatial inputs, calculating the timing of movements in coordination with other objects (Kandel et. al., 2000). Moreover, the cerebellum responds to the effects of these movements on the overall body, maintaining balance and directing the function of the sensory organs (Kandel et. al., 2000). The coordination that the cerebellum provides arises from its role as a mediator circuit that regulates outgoing motor signaling, receiving sensory and motor input from

the brainstem, spinal cord, and inferior olive and outputting signal through the deep cerebellar nuclei (White and Sillitoe 2013). Much like the cerebral cortex of the forebrain, the cerebellum is a structurally organized tissue, comprised of a three layered cortex over an interior comprised of cerebellar white matter (Figure 3) (Roussel and Hatten 2011). The cerebellar signaling network is comprised of 5 major neuron types, the glutamatergic granule cells, and the GABAergic Purkinje, basket, stellate and Golgi cells, as well as three rare interneuron populations, the glutamatergic unipolar brush cells, and the GABAergic candelabrum and Lugaro cells (Kandel et. al., 2000, Schilling et. al., 2008). Afferent signals are carried to the cerebellum by mossy fibers from the spinal cord and brainstem, which act as excitatory signals on cerebellar granule cells and deep cerebellar nuclei, and climbing fibers from the inferior olive, which directly activate Purkinje cells and deep cerebellar nuclei (Gilbertson and Ellison 2008). Cerebellar granule cells occupy the densely populated granular layer, from which their axons extend into the molecular layer. These axons bifurcate and extend in straight lines through the molecular layer, forming a dense structure comprised of granule cell axons called the parallel fibers, each of which activates multiple Purkinje cells (Kandel et. al., 2000). Between the molecular and granular layer lies the Purkinje layer, comprised primarily of Purkinje cells, large neurons that carry inhibitory signal to the deep cerebellar neurons, and Bergmann glia, cerebellar astrocytes supporting the surrounding neurons (Kandel et. al., 2000). Purkinje cells function as inhibitors of efferent signaling, receiving excitatory impulses from granule cells and climbing fibers that lead to inhibitory signal to deep cerebellar neurons (White and Sillitoe 2012).

During embryonic development, the tissue of the central nervous system arises from the ectodermal germ layer (Figure 4A) (Kandel et. al., 2000). Initial transformation into neuroectodermal cells is a process regulated by interplay in bone morphogenetic protein (BMP) signaling pathway, with BMP4 secreted from the lateral edges of the ectoderm and opposed by BMP antagonists Follistatin, Chordin and Noggin, secreted by the notochord and dorsal mesoderm (Kandel et. al., 2000, Marzban et. al., 2015). High BMP stimulates epidermal transformation whereas low signal leads to neuroectodermal cells forming the neural plate and the intermediary region forming the neural crest, the

source of the peripheral nervous system. Once formed, the neural plate folds inward to form the neural tube, a process reliant on Hedgehog signaling from the notochord and floor plate (Kandel et. al., 2000, Marzban et. al., 2015). Discrete brain structures appear along the anterior-posterior axis of the neural tube, resulting from signaling factor gradients as well as a wide array of Homeobox (Hox) and Hox-like transcription factors, including Engrailed 1 and 2 (En1/En2), Otx2 and Gbx2, genes crucial for proper cerebellar formation and patterning (Wang and Zoghbi et. al., 2001). The isthmus region found between the mesencephalon, the midbrain, and the rhombencephalon, the hindbrain, controls patterning of these regions through FGF8 and Wnt1 paracrine signaling (Yaguchi et. al., 2009, White and Sillitoe 2012, Marzban et. al., 2015). Posterior to the isthmus organizer region, the neural tube forms the hindbrain, itself subdivided into eight rhombomeres, with rhombomeres 1-3 forming the metencephalon, which gives rise to the cerebellum and pons, and 4-8 forming the myelencephalon, which forms the medulla (Kandel et. al., 2000).

Transformation from neural tube to cerebellar primordium begins at embryonic day 8 (E8) from the fourth ventricle at rhombomere 1. The cerebellar primordium continues to develop with the formation of the two distinct germinal zones involved in formation of the cells of the cerebellum, the rhombic lip and roof of the fourth ventricle (Kandel et. al., 2000, Gilbertson and Ellison 2008). The rhombic lip germinal zone produces glutamatergic neurons, including excitatory projection neurons of the deep nuclei from E10-E12, granule cell precursors from E12-16 and unipolar brush cells from E14-18. The fourth ventricle germinal zone, on the other hand, produces GABAergic neurons, including inhibitory deep nuclei neurons also from E10-E12, Purkinje cells from E10.5 to E12.5, and several other interneuron types from E14 to E18. After birth, projection neurons migrate to the rostral end of the cerebellar plate and form the deep cerebellar nuclei. Purkinje cell placement is a critical organizer for the cerebellum, highly regulated by transcription factors Ebf2 and Engrailed 1 and 2 (Kandel et. al., 2000, Gilbertson and Ellison 2008, Marzban et. al., 2015). Embryonic Purkinje cells migrate into clusters at E14 from which they will then form a monolayer in the postnatal cerebellum a process completed by postnatal day 5 in rodents, a process controlled

through Reelin signaling from the nascent EGL (Fatemi 2008). As this process proceeds, granule precursor cells, born in the rhombic lip, begin to migrate along the exterior dorsal surface of the cerebellar anlage, proceeding from posterior to anterior (Figure 4B). Covering the cerebellum by E15, the granule precursors form the external granular layer (EGL), the source of granular neurons (Aruga et. al., 2002, Klein et. al., 2005, Gilbertson and Ellison 2008). Postnatally, granular cell precursors proliferate and expand into several layers in response to paracrine SHH signaling from the Purkinje cells, and the innermost granule cell precursors begin to differentiate into granular neurons into granular neurons (Dahmane and Ruiz i Altaba 1999, Wechsler-Reya and Scott 1999, Behesti and Marino 2009). This differentiation process of the granule cell precursors is controlled by a combination of bFGF, BMP and Notch signaling and downstream targets *Math1* and *Zic1* (Aruga et. al., 2002, Gazit et. al., 2004, Fogarty et. al., 2007, Salero and Hatten 2007). As EGL cells exit the cell cycle, they begin to express $p27^{Kip1}$, a cell cycle inhibitor, and begin to differentiate into neurons. These neurons then migrate inward, following fibers from Bergmann glia, until they reach the inner granule layer, where they differentiate and begin to extend axons into the molecular layer. Granular cell precursors remain proliferative until about P14, after which they will also differentiate and migrate into the granular layer (White and Sillitoe 2013). At this point, the only remaining process in cerebellar development is formation of the cerebellar neural circuitry, an ongoing process that is largely complete by P21, but will continue into adulthood (Reeber et. al., 2013). At P21, the EGL is fully depleted, with all EGL cells having differentiated into neurons or been eliminated.

Hedgehog signaling plays a significant role in cerebellar development, which is reflected in MB initiation. Hedgehog ligands are secreted by Purkinje cells during postnatal cerebellar development, and functions to promote GCP proliferation (Dahmane and Ruiz I Altaba 1999, Fogarty et. al., 2007). Loss of SHH ligand secretion inhibits the ability of the cerebellum to properly develop folia (Dahmane and Ruiz I Altaba 1999, Wechsler-Reya and Scott 2002). On the other hand, activation of the Hedgehog signaling pathway through *Ptch1* inactivation prevents proper differentiation of granular precursor cells, leading to retained EGL following P21 (Oliver et. al., 2005). This function of the

Hedgehog pathway is dose dependent, with the homozygous loss of *Ptch1*, using a conditional knockout specific to Math-1 positive GCPs, during development leading to a greater enlargement of cells of the EGL (Yang et. al., 2008). Although the key mechanism attributed to Hedgehog pathway dysfunction regards maintenance of proliferative GCP-like cells in the cerebellum, an alternate mechanism proposed is a result of crosstalk between the SHH and p53 signaling pathways (Abe et. al., 2008, Po et. al., 2010, Malek et. al., 2011). This regulation is carried through multiple routes, with n-Myc increasing transcription of *MDM2* and Gli1 indirectly causing *MDM2* activation, as demonstrated by the decreased EGL proliferation and size observed in cerebellum without functional MDM2/MDM4 (Malek et. al., 2011).

The growth advantage provided by *Ptch1* homozygous inactivation is supported by the frequent inactivation of Ptch1 noted in the $Ptch1^{+/-}$ mouse model, which has been demonstrated to undergo loss of heterozygosity in 70-100% of the mice (Wetmore et. al., 2000, Yang et. al., 2008, Ward et. al., 2009, Tamayo-Orrego et. al., 2016). It has been proposed that loss of heterozygosity, and by association Hedgehog pathway hyperactivation, is a required early event in the development of SHH-MBs (Tamayo-Orrego et. al., 2016). Several Hedgehog pathway components or downstream targets contribute to the development of MB. Inactivation of *Gli1* by deletion of the zinc finger domain has been shown to reduce the penetrance of MBs in the $Ptch1^{+/-}$ background drastically, from 24% in $Ptch1^{+/-}$ model to 3.4% in $Ptch1^{+/-};Gli1^{-/-}$ model (Weiner et. al., 2002, Kimura et. al., 2005). Although retention of Gli1 provides a potent advantage for tumor development, it was found that deactivation of *Gli1* was fully compensated for by *Gli2* activity (Weiner et. al., 2002, Kimura et. al., 2005). However, activation of downstream target *n-Myc* is a crucial target of SHH signaling in giving rise to MBs (Zindy et. al., 2006, Hatton et. al., 2006, Thomas et. al., 2009). Demonstrated as a key factor in cerebellar development required for proper expansion of the EGL, *n-Myc* loss was shown to completely rescue MB penetrance in the ND2:SmoA1 mutant mouse model (Knoepfler et. al., 2002, Hatton et. al., 2006).

1.8 MB Mouse Models and Cell of Origin

1.8.1 Murine Models of SHH-MB

Thanks to early investigation into molecular biology of MBs through the association with Gorlin and Turcot syndromes, the SHH-associated MB mouse model was established. The earliest transgenic model of SHH-MB was the germline *Ptch1*$^{+/-}$ model developed in 1997 (Goodrich et. al., 1997). As a model meant to mimic Gorlin syndrome, several features were held in common between these animals and patients, including rare limb defects, especially in the digits, an increase in body tumors, and an increase in brain tumors, although basal cell carcinoma was not observed in this background, a reversal from the epidemiology associated with Gorlin syndrome in humans. When backcrossed into the 129SV background, the model produced MBs in 22% of animals examined (Goodrich et. al., 1997). Mouse background was capable of drastically influencing penetrance in the *Ptch1*$^{+/-}$ model, with reported penetrance as low as 6.7% and as high as 55% noted within the literature (Wetmore et. al., 2001, Pazzaglia et. al., 2002, Kimura et. al., 2004, He et. al., 2014, Mille et. al. 2014, Tamayo-Orrego et. al., 2016). In order to improve penetrance, the *Ptch1*$^{+/-}$ model was crossed with mutant alleles of several potential genes of interest, including *Apc*, *p19*^{Arf} and *p53* (Wetmore et. al., 2001). Within these models, only *p53* inactivation was capable of altering penetrance compared to *Ptch1*$^{+/-}$ alone, increasing the penetrance while lowering the median survival, reproducing the germline Li-Fraumeni syndrome within the mouse model (Wetmore et. al., 2001). Because of the scarcity of *TP53* mutations in MBs, several alternative models of MB were developed making use of alterations to the Hedgehog pathway. Constitutively activated Smoothened, *Smo*^{W539L}, induced MBs with higher penetrance in multiple mouse models, including ND2:SmoA1, a germline mutant driven by the cerebellar granule cell specific Neurod2 promoter capable of 50% MB penetrance, and R26SmoM2, a Cre-activated allele capable of inducing MBs with 100% penetrance with hGFAP-Cre (Hallahan et. al., 2004, Mao et. al., 2006, Ahlfeld et. al., 2013). Activation of smoothened in these models An alternate approach to produce MBs with high frequency is to use a Cre driver to target *Ptch1* for homozygous loss, thereby overcoming embryonic lethality (Ellis et. al., 2003, Adolphe et. al., 2006). Introducing this

background with drivers targeting stem and progenitor cells of the cerebellum was capable of generating tumors with nearly complete penetrance (Yang et. al., 2008).

1.8.2 Cell of Origin for SHH-MB

Initial studies using the *Ptch1*$^{+/-}$ model were able to demonstrate a population of abnormally retained cells in the postnatal cerebellum occupying the developmental external granular layer (Kim et. al., 2003, Oliver et. al., 2005). These cells, although retaining markers associated with the normally differentiated population of cerebellar GCPS, remained proliferative and were associated with the location in which MBs developed. By using *Math1-GFP* in the *Ptch1*$^{+/-}$ model to track cells that give rise to MBs, it was demonstrated that the GCP lineage is a source for SHH-MBs (Oliver et. al., 2005). Math1 is required for *Gli2* expression during cerebellar development, and loss of *Math1* reduced proliferation of GCPs (Flora et. al., 2009).. Using the GCP marker Math1 for conditional deletion of Ptch1 in the the *Math1-Cre;Ptch1*$^{flox/flox}$ model, thereby increasing tumor penetrance and median survival as effectively as is seen in the *Ptch1*$^{+/-}$*;p53*$^{-/-}$ model (Yang et. al., 2008). Curiously, Nestin-expressing cells are found amongst the GCPs of the postnatal EGL, and Nestin-expressing cells represent only a rare subpopulation in the postnatal EGL, use of either *Math1-CreER* or *Nestin-CreER* in a *Ptch1*$^{floxflo/x}$ model were capable of inducing MBs (Li et. al., 2013). A survey of the capacity of various cerebellar cells capability to give rise to SHH-MBs made use of a panel of Cre drivers, including *Math1, Tlx3, hGFAP, Olig2* and *Gli-CreER,* to demonstrate that SHH-MB may arise from various stages of EGL development (Schuller et. al., 2008).

One of the characteristic features discovered in the mouse MB model is the presence of abnormally retained pre-neoplastic cells sharing the location and believed to be derived from the external granular layer. In the *Ptch1*$^{+/-}$ model, retained cells were observed in mature cerebellum following the complete migration of the GCP population (Oliver et. al., 2005, Matsuo et. al., 2013). Curiously, the frequency of these lesions was noted to decrease following postnatal day 21, from 84% of animals showing enrichment at 6 weeks to 16% at 10-25 weeks (Oliver et. al., 2005). Cells within MBs also express

stem and progenitor markers, leading to some suggestion that MBs may harbor a stem-like population. Several cerebellar precursor markers, including Nestin and Sox2, have been found in mouse xenograft MBs established from an *GFAP-Cre;Rb$^{x/x}$;p53$^{-/-}$* model (Marino et. al., 2000, Sutter et. al., 2010). By investigating the relation between molecular subgroups and *Sox2* expression, it was found that frequent Sox2 labeling corresponds with the SHH-MB signature, as well as cells of the embryonic rhombic lip germinal zone (Ahlfeld et. al., 2013). Although conditional knockout of *Sox2* had no impact on MB penetrance in the *SmoM2* model, it was shown that loss of *Sox2* in cultured GCPs was capable of decreasing the proliferative population (Ahlfeld et. al., 2013). Characterization of the Sox2-positive cell population found in SHH-MBs revealed that these rare cells were frequently quiescent and molecularly similar to neural stem and granule cell precursors, but apparently were responsible for producing a transient amplifying population of MB cells (Vanner et. al., 2014). Moreover, following chemotherapeutic treatment with either vismodegib, the Smo inhibitor, or Ara-c, an antimitotic agent, it was found that Sox2-positive cells were enriched, demonstrating that these cells have greater treatment resistance compared to the tumor mass. Although it is not certain, some studies have proposed that the presence of stem cell markers in a quiescent cell population indicate the existence of a MB cancer stem cell (Fan and Eberhart 2008, Hambardzumyan et. al., 2008, Vanner et. al., 2014). However, although it seems clear that MB cells may have qualities attributed to stem cells, this direction has not been thoroughly investigated and has not yet been successfully leveraged into developing a therapeutic approach.

1.8.3 MB Models for other Subtypes

Producing mouse models for other models of MBs was a challenging endeavor that initially met with few positive results. The Wnt subtype MB model was unable to provide a model capable of producing tumors, partially due to a misunderstanding of the underlying biology of the Wnt subtype (Lorenz et. al., 2011). While the cell of origin for the SHH-MB subtype was demonstrated as precursor cells of the rhombic lip and EGL, a different cerebellar population, the cells of the lower rhombic lip and embryonic dorsal brainstem are associated with Wnt subtype MB based on gene expression patterns

(Gibson et. al., 2010). This corresponds with the location of these tumors in human patients, where the Wnt subtype often occupies the fourth ventricle and invades the brain stem. Two models for the Group 3 MB subtype were developed in 2012, using either transfection of GCPs from an *CDKN2C/p53* null background with c-Myc expressing retrovirus or transfection of both nonfunctional *p53* and active *c-Myc* (Kawauchi et. al., 2012, Pei et. al., 2012). Unlike human disease, where *p53* mutation is not associated with the Group 3 MB subtype, addition of p53 is required for either of these models to develop tumor. An additional study, making use of *GFI1* and *GFI1b*, was able to induce an oncogenic transformation in neural stem cells by infecting them with *GFI1* or *GFI1b* in conjunction with *c-Myc*, and thereby produce tumors that match Group 3 tumors by molecular characterization (Northcott et. al., 2014).

1.8.4 p53 Mutant MB Models

Incorporation of mutant *p53* within the $Ptch1^{+/-}$ model increased SHH-MB penetrance to 100%, providing clear correlation between p53 activity and suppression of MB (Wetmore et. al., 2001). Although murine MB models were typically developed using genes corresponding to at least one of the specifically mutant subtypes, several models were capable of inducing MBs by targeting tumor suppressor pathways alone. A model featuring deletion of both *p53* and *Rb* following *GFAP-Cre* mediated recombination gave rise to aggressive tumors resembling LCA morphology and expressing high levels of *Gli2* and *n-Myc* (Shakhova et. al., 2006). Making use of the TUNEL assay, it was found that apoptosis was very rarely observed, but that loss of *Rb* was capable of inducing both increased proliferation and apoptosis in cells of the EGL and IGL (Shakhova et. al., 2006). Inactivation of both *Rb* and *p53* was capable of further driving apoptosis in the IGL, but failed to promote additional apoptosis in the developing EGL, indicating that p53 is a key component of a suppressive response within the developing cerebellum, though not of all cells (Shakhova et. al., 2006). Moreover, although loss of *p53* at the germline did not give rise to MBs, conditional loss of *p53* alone was capable of inducing MB formation, as was seen with the $p53^{\Delta E5\text{-}6}$ model, which was capable of inducing MBs, though only in approximately 10% of animals, with the remainder developing glioblastomas (Wang et. al., 2009). The successful induction of

MBs within the $p53^{\Delta E5\text{-}6}$ model provides a potentially advantageous direction compared to previous *p53* conditional knockout models, as the recombined *p53* will form a non-functional protein following pathway activation that will accumulate in stressed cells without inducing transcription. In this way, accumulation of p53 may be used as a marker for stressed cells (Lin et. al., 2004, Wang et. al., 2009).

1.8.5 Irradiation of Granule Cell Precursors and MB

The genetic damage caused by radiation therapy can increase the risk of a patient developing a second cancer after treatment. The incidence of second cancers is increased in both Li-Fraumeni and Gorlin syndrome patients, indicating that inactivation of the p53 or Hedgehog pathways sensitize cells to genetic damage (Hisada et. al., 1998, Pazzaglia et. al., 2002). Within the $Ptch1^{+/-}$ mouse model, irradiation of GCPs increased the frequency of MB formation, although the timing of radiation treatment proved to be a determining factor in this approach's efficacy (Pazzaglia et. al., 2006). Treatment with irradiation at postnatal day 0.5 (P0.5) is capable of inducing MBs in 81% of specimens, compared with only 7% of specimens if untreated or 3% if treated at postnatal day 10 (P10). At a molecular level, this behavior was attributed to a differential radiation response between the cells of the P0.5 and P10 EGL, with neither p53 or apoptosis detected in irradiated P0.5 EGL, while the P10 EGL activated a robust p53 response (Pazzaglia et. al., 2006). This reduced radiation response was also observed in the embryonic rhombic lip, though not in the 4^{th} ventricle germinal zone (Tanori et. al., 2013). Likewise, MB cells located in the perivascular niche are associated with cell survival following radiation in the $Ptch1^{+/-}$ model (Hambardzumyan et. al., 2008). This response was also reliant on p53 activation, with p53 only activating outside of the perivascular niche and corresponding to cell survival in these regions.

1.9 Summary and Significance

In summary, MBs arise from stem and progenitor populations of the developing cerebellum, where elevation of the Hedgehog pathway drives tumor formation. Unlike most tumors, MBs rarely inactivate the p53 pathway, retaining wild type *p53*. One of the

relevant directions in MB research is determining how MBs are capable of forming without inactivating the p53 pathway. I propose that the cell of origin of SHH-MBs may be unable to elevate p53 to a level capable of removing these cells through normal developmental processes, thereby permitting tumor progression even in the presence of wild type *p53*. In order to address this question, I developed mouse models with reduced potential p53 response, making use of $p53^{\Delta E5\text{-}6}$ and $p53^{R172P}$, and then increased p53 response in these models by inducing radiation stress (Liu et. al., 2004, Wang et. al., 2009). In Chapter 2, I will present research related to the initiation and progression of MBs and the role p53 plays in this process, making use of the three tiers of p53 response to demonstrate that discrete functions of p53 play separate roles throughout development. In Chapter 3, I will discuss the effects of elevating p53 activity through the use of radiation therapy, either in PNLs or MBs. The final chapters present the techniques used and a discussion of the implications of the data shown in this study.

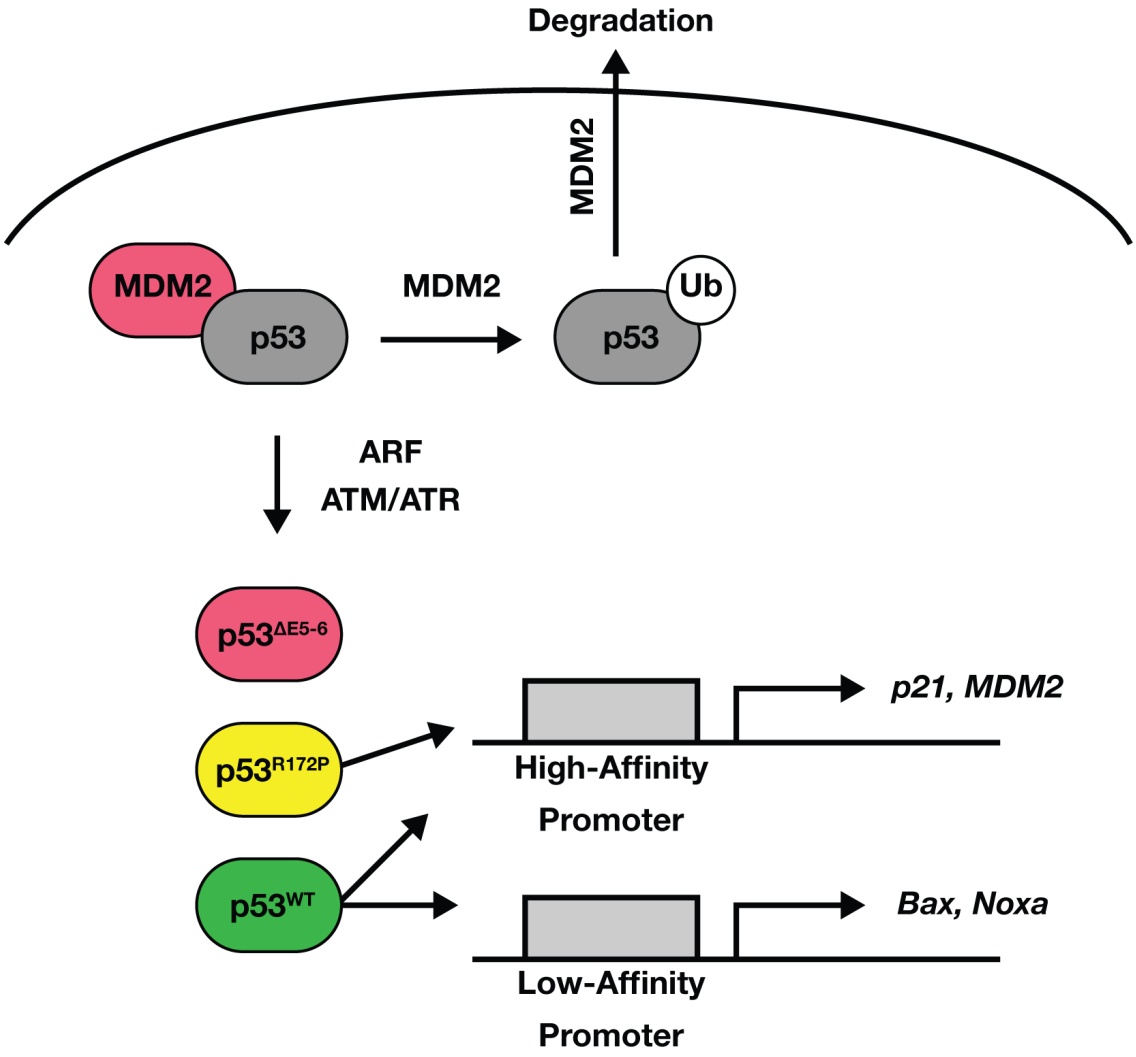
Degradation
MDM2
MDM2
p53
MDM2
Ub
p53
ARF
ATM/ATR
p53ΔE5-6
p53R172P
p53WT
p21, MDM2
High-Affinity
Promoter
Bax, Noxa
Low-Affinity
Promoter

Figure 1: The p53 Signaling Pathway

Cells maintain tumor suppressor TP53/p53 in an inactive state through basal expression of *MDM2*. When MDM2 binds to p53, it regulates p53 transcription activity through several mechanisms, including facilitating nuclear export and ubiquitination that suppresses chromosome interaction and promotes degradation of cytoplasmic p53. Following either oncogenic stress or chromosome damage, upstream targets ARF or ATM/ATR will be activated, respectively. Activation of these proteins enables p53 transcription by either protecting p53 through phosphorylation in the case of ATM/ATR, or through targeting MDM2 in the case of ARF. Once MDM2 repression is alleviated, p53 transcription factor activity is restored. Wild type p53 maintains a range of targets, including negative receptor *MDM2*, apoptotic targets *Bax* and *Noxa*, and cell cycle arrest target *p21*. Different p53 targets are controlled by promoters with varying p53-affinity thereby allowing differential response to p53 activation. High affinity promoters are typically associated with cell cycle arrest targets, like *p21,* whereas low affinity targets tend to correspond with apoptotic genes. The $p53^{R172P}$ protein is a p53 hypomorph with decreased functionality, which fails to activate low-affinity binding while retaining high-affinity promoter binding (Liu et. al., 2004). The $p53^{\Delta E5\text{-}6}$ allele expresses a conditional knockout that, following Cre-mediated recombination, loses a large portion of the DNA binding domain, and therefore loses transcription activity (Wang et. al., 2009).

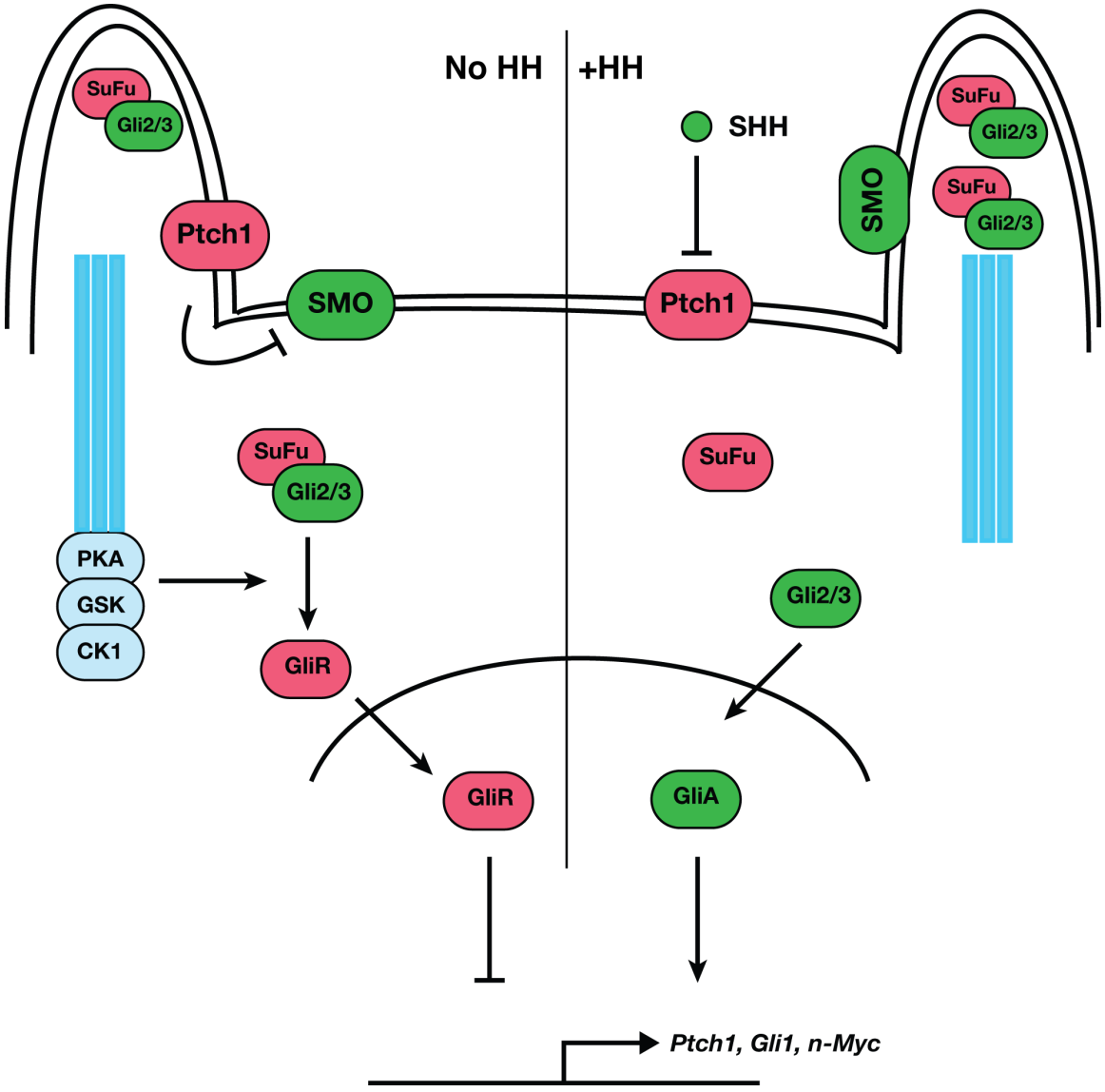
No HH
+HH
SHH
SuFu
Gli2/3
Ptch1
SMO
PKA
GSK
CK1
GliR
GliA
Ptch1, Gli1, n-Myc

Figure 2: The Sonic Hedgehog Pathway

The hedgehog pathway, without ligand activity, remains in a repressed state as trans-membrane protein Patched (Ptch1) inhibits the activity of Smoothened (Smo). Without Smo, the GLI2 and GLI3 transcription factors form a complex with SUFU, which is moved to the primary cilia at low levels and are targeted by the PKA/GSK/CK1 complex for phosphorylation while leaving the primary cilia. Phosphorylated GLI2/3 are subject to proteolytic conversion into the GLI repressor form, which migrates to the nucleus and inhibits SHH signaling. Following SHH ligand binding to Ptch1, Smo migrates to the primary cilia where it facilitates accumulation of GLI-SUFU complex. Active HH pathway then permits dissociation of SUFU and GLI, which then bypasses PKA and migrates to the nucleus as the active form of GLI (GliA), activating downstream transcription targets, including *Ptch1*, *Gli1* and *n-Myc*.

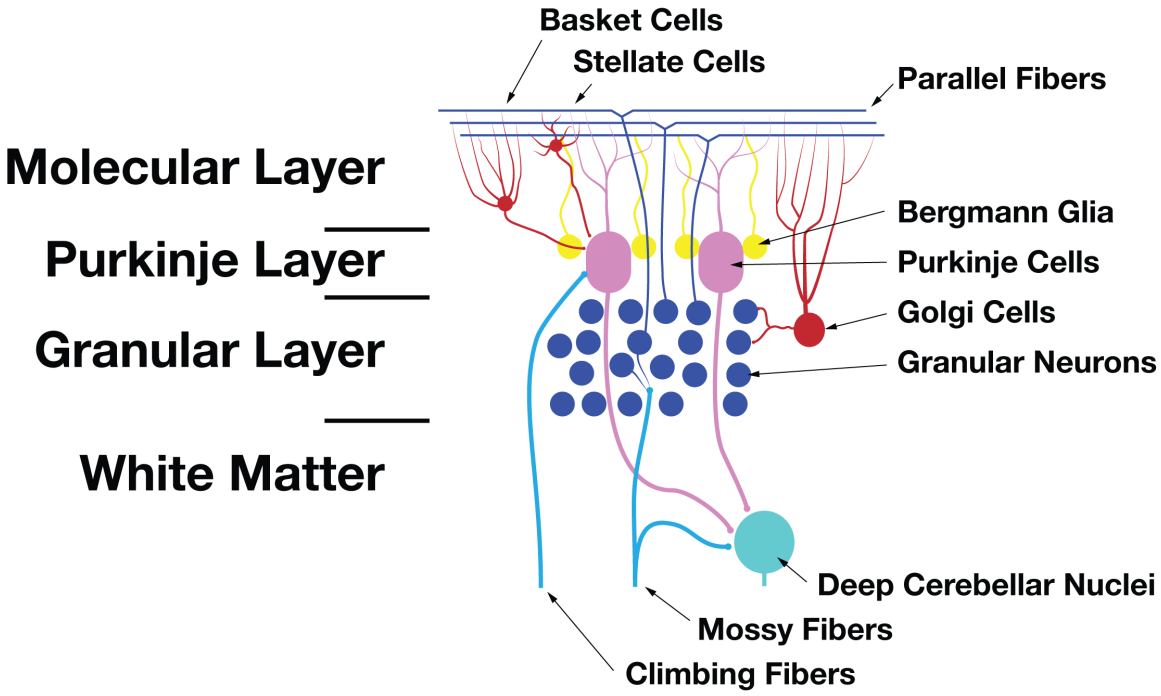

Figure 3: Cerebellar Organization

The cerebellum is comprised of a three-layered cortex overlying a white matter core. Mossy and climbing fibers carry signal to the cerebellar neurons, where, through a complex interaction between the glutamatergic and GABAergic interneurons of the cerebellum, an efferent signal is carried by the cerebellar deep nuclei. The initial neurons targeted by the mossy fibers are granular neurons, the most common neuron of the cerebellum, located in the granular layer, which matches with the developmental inner granular layer. Each granular cell extends a lengthy axonal process into the molecular layer, forming a compact network of axonal processes called the parallel fibers. These fibers carry signal to the dendrites of Purkinje cells, occupying the aptly named Purkinje layer, in turn directly inhibiting outgoing signal at the deep nuclei. Several varieties of GABAergic interneurons, including the Golgi cells of the granular layer, which target Granular Neurons, and Mossy and Basket cells of the molecular layer, inhibiting Purkinje cells. Bergamann Glia, located in the Purkinje layer, are crucial support cells for the processes of the molecular layer, and also involved in neuronal migration during development.

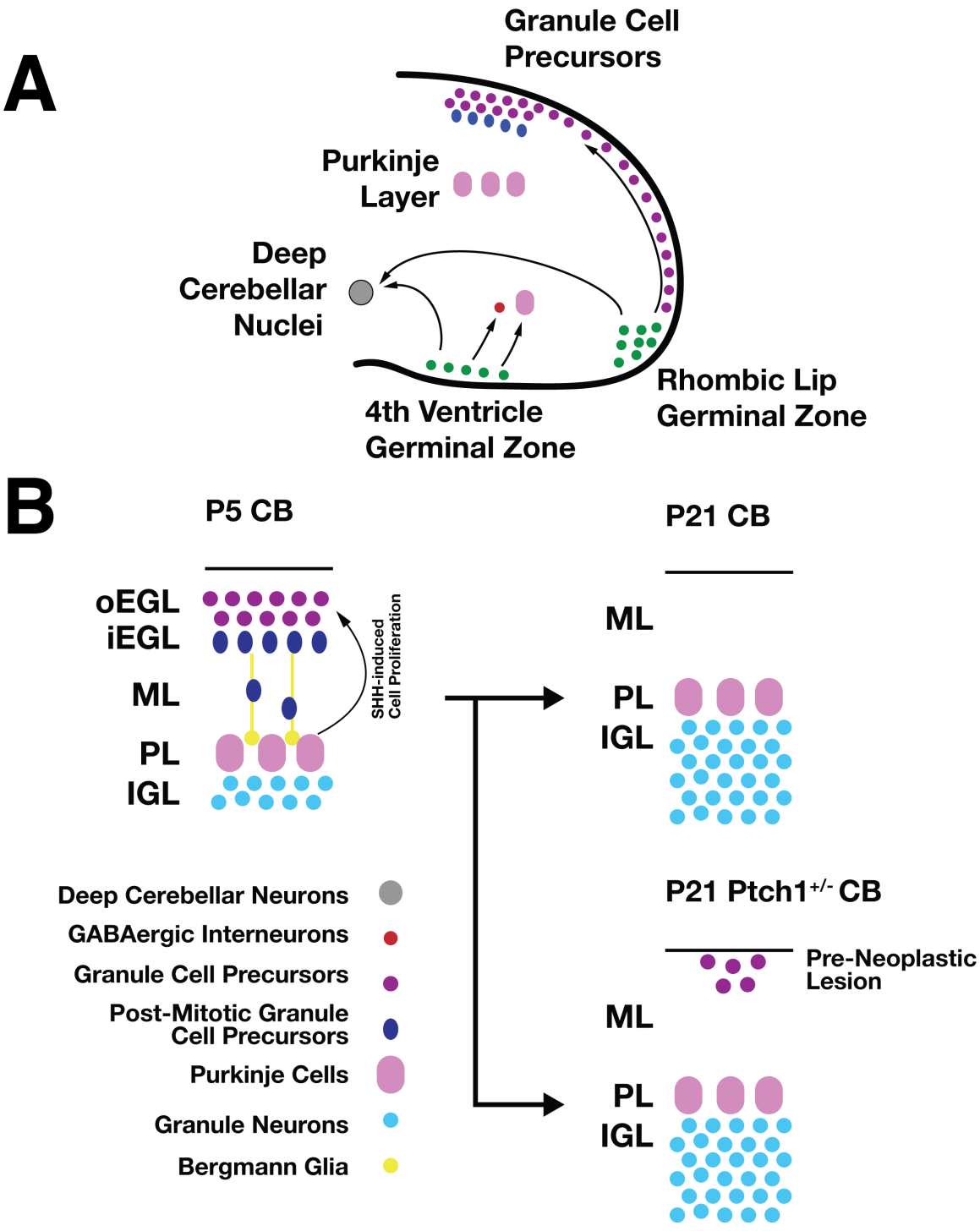
A
Granule Cell Precursors
Purkinje Layer
Deep Cerebellar Nuclei
4th Ventricle Germinal Zone
Rhombic Lip Germinal Zone
B
P5 CB
oEGL
iEGL
ML
PL
IGL
SHH-induced Cell Proliferation
P21 CB
ML
PL
IGL
Deep Cerebellar Neurons
GABAergic Interneurons
Granule Cell Precursors
Post-Mitotic Granule Cell Precursors
Purkinje Cells
Granule Neurons
Bergmann Glia
P21 Ptch1+/- CB
Pre-Neoplastic Lesion
ML
PL
IGL

Figure 4: Cerebellar Development and MB initiation

(A) During embryonic cerebellar development, two germinal zones arise in the cerebellum, the rhombic lip and the 4th ventricular zone. The rhombic lip gives rise to glutamatergic cells, including deep cerebellar neurons, the excitatory efferent signaling apparatus of the cerebellum, arising from the upper rhombic lip and granule cell precursors from the lower rhombic lip. The 4th ventricle germinal zone gives rise to GABAergic neurons, including inhibitory deep cerebellar neurons, Purkinje cells and most cerebellar interneurons. During embryonic development, the rhombic lip births the cells of the deep nuclei and a population of Granule Cell Precursors, which form a thin layer occupying the exterior surface of the cerebellum. Meanwhile, Purkinje cells migrate from the 4th ventricle into clusters, which will expand into the Purkinje layer postnatally in response to Reelin signaling as well as other factors.

(B) Postnatally, the Granule cell precursors expand in response to SHH secreted by the Purkinje cells. Proliferative Granular Cell Precursors form the outer external granular layer. As the layer expands, cells begin to differentiate into a neuronal population, forming the inner external granular layer, in response to FGF and BMP signaling. These differentiating granule cells migrate along processes extending from the Bergmann glia toward the internal granular layer, where they will fully differentiate. In general, granule cell precursors stop proliferating around postnatal day 15 in mice, and the external granular layer is completely absent by postnatal day 21. In mice with abnormal Hedgehog pathway activity, a population of GCP-like cells remains in the EGL even after P21, and are thought to represent the cell of origin for SHH-MBs.

Chapter II: p53-mediated Apoptosis Targets Granule Cell Precursors during Cerebellar Developmental thereby Suppressing medulloblastoma

2.1 Introduction

TP53 tumor suppressor gene is the most frequently mutated gene in human cancer, with 50% of tumors featuring a mutation in the *TP53* allele and many other tumors showing p53 pathway inactivation. Medulloblastoma (MB) is an exception to this tendency, with only 10% of tumors demonstrating loss of p53 function (Louis et. al., 2007). The presence of mutant p53 is of prognostic significance in only one of the MB subgroups, the Sonic Hedgehog (SHH) pathway associated MBs (Zhukova et. al., 2013). Further, MBs arising in Li-Fraumeni patients, harboring germline loss-of-function mutations in the *TP53* tumor suppressor gene, have been molecularly characterized as the SHH-MB subgroup (Kool et. al., 2014). However, p53 mutations are increased following standard therapy, indicating that p53 activation is crucial for the treatment response of SHH-MBs (Morrissy et. al., 2016). The role that p53 plays during cerebellar development and how this contributes to MB formation is not well understood.

The cell of origin for SHH-MBs has been established as part of the GCP lineage, proliferative cells located in the postnatal EGL, as demonstrated by the formation of SHH-MBs after targeting either Math1+ or hGFAP+ cells of the ventricular zone located on the lower rhombic lip (Schuller et. al., 2008, Yang et. al., 2008, White and Sillitoe 2013). Loss of heterozygosity in the *Ptch1* heterozygous mice ($Ptch1^{+/-}$) triggers the generation of $Ptch1^{-/-}$ pre-neoplastic lesions (PNLs) in the developing EGL, a small number of which can eventually progress and form MBs (Tamayo-Orrego et. al., 2016). The tumor suppressive mechanism that eliminates the majority of Ptch1-deficient PNLs remains unknown, but the cells of the EGL are sensitive to p53 hyper-activation

following *MDM2/MDM4* disruption (Malek et. al., 2011). This leads to my hypothesis that the p53 response is activated in rare cells of the postnatal cerebellum to eliminate granule cell precursors (GCPs) undergoing oncogenic stress.

In this chapter, I have employed a combination of mutant p53 alleles within the Ptch1-deficient MB model, Ptch1p53^{WT} (*Ptch1*$^{+/-}$*;p53*$^{\Delta E5\text{-}6/\Delta E5\text{-}6}$). The Zhu lab has developed a combination of mouse models, making use of a Cre-mediated p53 exon 5 and 6 in-frame deletion, targeting the p53 DNA binding domain and preventing p53 transcription following recombination, to produce the Ptch1p53$^{\Delta E5\text{-}6}$ model (*hGFAP-Cre;Ptch1*$^{+/-}$*;p53*$^{\Delta E5\text{-}6/\Delta E5\text{-}6}$). I also developed the germline *p53*^{R172P} mutant, a hypomorph p53 that retains partial cell cycle arrest activity while completely losing p53-mediated apoptotic activity (Ptch1p53$^{\Delta/R172P}$: *hGFAP-Cre;Ptch1*$^{+/-}$*;p53*$^{R172P/\Delta E5\text{-}6}$) (Liu et. al., 2004, Wang et. al., 2009). These results show that activation of p53 occurs throughout Ptch1-deficient MB development, revealing the potentially earliest MB precursor cells in the inner layer of the developing EGL. While p53-mediated apoptosis is the crucial p53-mediated response to eliminate PNLs in the Ptch1 model, p53-mediated cell cycle arrest only delays MB progression without impacting penetrance. By making use of p53$^{\Delta E5\text{-}6}$ as a marker within the PNLs, I found that two varieties of PNL were formed from GCPs and that these may represent two models of MB.

2.2 Results

2.2.1 Tumor suppressor p53 marks normal and neoplastic cells under oncogenic stress

Previous effort by the Zhu lab made use of the *hGFAP-Cre;p53*$^{\Delta E5\text{-}6/\Delta E5\text{-}6}$ model to induce the formation of glioblastomas and MBs, and found that p53 accumulation was detected by immunohistochemistry within these tumors (Wang et. al., 2009). To demonstrate whether p53 accumulation could serve as a marker for abnormal cells in addition to tumor cells, lab member Yinghua Li conducted a series of experiments showing the molecular activity of p53$^{\Delta E5\text{-}6}$. In order to demonstrate that the mutant protein was retained in spite of the loss of two exons of the functional DNA binding domain

(Figure 5A), I performed a western blot using the p53 antibody, demonstrating that $p53^{\Delta E5\text{-}6}$ was detected with fidelity equivalent to wild type p53, and that blocking p53 translation by two independent *p53*-specific siRNAs, but not the mismatched *p53* siRNA, lead to a complete loss of p53 detection (Figure 5B). Further, I demonstrated that in both murine (Figure 5C) and human (Figure 5D-F) cell lines, activation of MDM2 was capable of targeting $TP53^{\Delta E5\text{-}6}$/$p53^{\Delta E5\text{-}6}$ for degradation in the same manner as is observed with wild type TP53/p53. These data demonstrate that mutant $p53^{\Delta E5\text{-}6}$ is both produced and regulated in the same way as wild type p53, but, in losing the DNA binding domain and thus p53 transcription, no longer up-regulates the MDM2/Mdm2 negative feedback loop. Therefore, in addition to marking tumor populations, accumulation of mutant $p53^{\Delta E5\text{-}6}$ is a marker for normal and neoplastic cell populations under oncogenic stress.

2.2.2 Tumor suppressor p53 is activated during cerebellar development

In order to investigate p53 activation during cerebellar development, I isolated control and mutant brains at postnatal day 8 (P8) from each of my mouse models, ascertaining that all mice were maintained on a mixed background and utilizing littermates to control for variation due to background (Figure 6A). I found that the p53 protein was not stabilized in the EGL of control models, including both $p53^{WT}$ (*p53*$^{E5\text{-}6/E5\text{-}6}$) (n = 6) and $Ptch1p53^{WT}$ (*Ptch1*$^{+/-}$;*p53*$^{E5\text{-}6/E5\text{-}6}$) (n = 5), but was fully capable of accumulating in a subset of cells in the $p53^{\Delta E5\text{-}6}$ (*hGFAP-Cre;p53*$^{E5\text{-}6/E5\text{-}6}$) (n = 5) mutant. In $Ptch1p53^{\Delta E5\text{-}6}$ (*Ptch1*$^{+/-}$;*hGFAP-Cre;p53*$^{E5\text{-}6/E5\text{-}6}$) (n = 9), PNLs, indicated by clustered p53-positive cells, were readily detectable in the EGL of 56% of the samples observed (Figure 6B). This phenomenon was largely rescued when p53-mediated cell cycle arrest activity was restored in the $Ptch1p53^{\Delta R172P}$ (*Ptch1*$^{+/-}$;*hGFAP-Cre;p53*$^{E5\text{-}6/R172P}$) (n = 4) model, leading to a reduction in p53 positive cells, specifically in the EGL, as well as an absence of discernable PNLs (Figure 6C). Curiously, p53-positive cells were located within the other cerebellar layers, including the molecular layer (ML) and internal granular layer (IGL), where the same pattern of p53 activity was observed within all mutant p53 models, regardless of *Ptch1* status or the mutant *p53* allele (Figure 6D). Of note, the frequency of p53-positive cells was not statistically different between the $Ptch1p53^{\Delta E5\text{-}6}$ and $Ptch1p53^{\Delta E5\text{-}6}$ models for any cerebellar layer, demonstrating that the

presence of a mutant allele of *Ptch1* was not sufficient to lead to p53 activation within the developing CB. Surprisingly, the cells of the Ptch1p53$^{\Delta/R172P}$ model, while not rescuing from p53 expression within the IGL or ML, were able to produce a significant reduction in p53 positive cells within the EGL. These data demonstrate that the p53 response is temporarily activated in a rare population of cells during development, a process only detectable with the mutant *p53*$^{\Delta E5\text{-}6}$, and that even partial function of p53 is sufficient to remove the majority of these stressed cells.

2.2.3 p53 inactivation permits accumulation of abnormal cells with stem cell markers

Clusters of p53 positive cells within the p53 mutant cerebella are an abnormal cell population, which might represent an early pre-neoplastic population. I next tried to characterize the behavior of these cells, in an effort to determine whether they represented a pre-neoplastic population, a task made difficult by the widespread proliferation of the GCP population, affecting 80-90% of the cells of the outer EGL at this developmental time-point (Figure 7A-7B). Proliferation within these p53 positive clusters was comparable to the outer EGL, with approximately 90% of the cells of the clusters in the cell cycle, unlike p53 labeled cells located within the EGL but outside of the clusters, where only 50-60% are proliferative (Figure 7C). These data demonstrate that the p53$^{\Delta E5\text{-}6}$ marker labels stressed GCPs, and that the cells of the p53 positive clusters are an abnormal, pre-neoplastic population overriding the p53 response. As would be predicted from the theory that the cluster is a PNL, p53 positive cell clusters were associated with reduced thickness of the iEGL and depleted the population of differentiating cells that would be seen in this layer, demonstrating these cells are able to already overcome developmental processes (Figure 7D). Previous studies have found that Sox2, an early marker of stem cells in the cerebellum normally not found after P5 is sustained within the *Ptch1*$^{+/-}$ model EGL (Ahlfeld et. al., 2013). Whereas both control and mutant P8 EGL was found to contain few or no Sox2-positive cells, I found that the majority of P8 p53-positive clusters found in the p53$^{\Delta E5\text{-}6}$ model contained widespread proliferative Sox2-positive cells (60%), with the remaining clusters only containing infrequent Sox2-positive cells (Figure 8A-B). Only Sox2 was widely expressed in these

clusters, with none of the clusters expressing brain lipid-binding protein (BLBP), a marker for the Sox2-positive Bergmann glial cells, and only one p53 positive cluster featuring any Nestin expression, a marker of committed granule neuron precursors in the CB that have been indicated as one of the cells of origin for SHH-MBs (Figure 8C-D) (Li et. al., 2013). *Sox2* expression has been associated with hyperactive SHH signaling, which suggests that loss of the wild type *Ptch1* allele likely occurs and triggers de-differentiation of *Ptch1*-deficient GCPs to stem-like cells, initiating MB formation (Ahlfeld et. al., 2013). These results demonstrate that, similar to malignant glioma (Wang et al., 2009), the $p53^{\Delta E5\text{-}6}$ marker detects the earliest identified MB precursor cells in an otherwise morphologically normal EGL and cerebellum in the $Ptch1^{+/-}$ MB model. Further, the restoration of even partial p53 activity, as is the case with the Ptch1p53$^{\Delta/R172P}$ model, was sufficient to rescue the observed phenotype, suggesting that the developing brain is highly sensitive to p53 activation.

2.2.4 Loss of p53-mediated apoptosis is sufficient to promote PNLs

The widespread proliferation of the developing cerebellum has the potential to mask pre-neoplastic cells within the proliferative granule precursor cells present in the developing EGL. In order to observe the effects of partial p53 activity on formation of PNLs, I next investigated the accumulation of PNLs following the process of postnatal cerebellar development, at postnatal day 21 (Figure 9A). It has been demonstrated previously that within the $Ptch1^{+/-}$ murine MB model, the EGL fails to fully differentiate and PNLs remain where the EGL was located (Pazzaglia et. al., 2006, Yang et. al., 2008). To further investigate the function of p53 in regulating the developing EGL, mutant brains were collected at P22, and exhibit retained PNLs (Figure 9A). PNL size (Figure 9A') and lesion frequency (Figure 9A'') were increased in the Ptch1p53$^{\Delta E5\text{-}6}$ model (n = 8) compared to Ptch1p53^{WT} control (n = 10), although the Ptch1p53^{WT} model, on rare occasion, contained larger lesions of size and proliferative frequency comparable to the lesions seen in the Ptch1p53 mutant models. In spite of the lack of observed p53-positive lesions at P8, the frequency and area of PNLs in the Ptch1p53$^{\Delta/R172P}$ model (n = 9) was comparable to that observed in the Ptch1p53$^{\Delta E5\text{-}6}$ model, indicating that the absence of a functional p53-mediated apoptotic response is the key factor for PNL penetrance. I next

investigated the behavior of the cells of these PNLs, focusing on apoptosis and cell cycle. The frequency of apoptotic cells, as represented by cleaved Caspase-3 (C-Casp3), varied within PNLs based on the presence of mutant p53, with 4% of cells in the Ptch1p53^{WT} PNL expressing cleaved Caspase-3, but less than 2% in the samples from both p53 mutant models, thereby demonstrating that p53-mediated apoptosis is playing a role in the suppression of PNLs remaining after cerebellar maturation (Figure 9B-B'). The similarity between the Ptch1p53$^{\Delta E5-6}$ and the Ptch1p53$^{\Delta/R172P}$ models was further demonstrated by the proliferative frequency of the cells of PNLs from both the p53 mutant models, where, in spite of the partial cell cycle arrest activity that the Ptch1p53$^{\Delta/R172P}$ mutant retains, no difference in proliferative frequency was demonstrated (Figure 9C-C''). Curiously, both p53 wild type and mutant PNLs contained a rare subpopulation of Sox2-positive cells at P22, indicating that Sox2-positive cell retention is independent of p53. Unlike the Sox2-positive cells located within p53 positive clusters identified at P8, co-localization of Sox2 with either p53 or Ki67 was infrequent in PNLs at P22 (Figure 9D). Overall, my results from the P22 cerebellum demonstrate that activation of wild type p53, but not activation of the p53^{R172P} hypomorph, eliminates most PNLs driven by *Ptch1* loss, clear evidence that p53-mediated apoptosis is critical for eliminating retained GCPs following maturation of the cerebellum.

2.2.5 Retention of p53-mediated cell cycle arrest delayed MB formation and prolonged survival

Having established a clear mechanism for p53 regulation of PNL, I began to investigate what consequence p53 activity has on the progression of PNL into MB. Age-matched samples collected at postnatal day 46 (P46), were collected for Ptch1p53$^{\Delta E5-6}$, Ptch1p53$^{\Delta/R172P}$ and Ptch1p53^{WT} (n = 8, 7, and 8, respectively) (Figure 10A-B'). The cerebellum of the Ptch1p53$^{\Delta E5-6}$ model was visibly enlarged at this early time-point, with the average scale of PNLs in the model 10 fold larger than those observed in the Ptch1p53$^{\Delta/R172P}$ model, although mice collected at this age did not demonstrate behavioral symptoms (Figure 10B-B'). This increase in cerebellar size corresponded to the development of early MBs in the Ptch1p53$^{\Delta E5-6}$ model, which stands in stark contrast to the Ptch1p53$^{\Delta/R172P}$ model, which showed limited expansion of the PNL, and to

Ptch1p53^{WT} model which showed reduced penetrance and severity of PNLs in the Ptch1p53^{WT} lesion were reduced when compared to the PNLs observed immediately following cerebellar development (Figure 10C). These results suggest that p53 response, including both apoptotic and cell cycle arrest components, remain active in the GCP cells of the cerebellum, targeting PNLs driven by *Ptch1* loss for removal, as indicated by the reduced penetrance observed in the Ptch1p53^{WT} model. However, while p53-mediated cell cycle arrest reduces the rate of MB progression in the Ptch1p53$^{\Delta/R172P}$ model, it is insufficient to eliminate PNLs and instead merely curtails their growth.

In order to better understand the effect loss of p53 function has on cellular behavior of PNLs, I investigated the proliferation and differentiation rate, using Ki67 and P27 (Figure 10D). I found that within the Ptch1p53$^{\Delta E5-6}$ model, the frequency of proliferative cells was increased to approximately 58% at P46, a substantial increase compared to the observed frequency at P22 of 44% ($p = 0.019$) (Figure 10D'). Partial p53 function, as is present in the Ptch1p53$^{\Delta/R172P}$ model, was sufficient to prevent accumulation of proliferative cells, and the frequency of proliferation remained similar from P22, at 45%, to P45, at 42% ($p = 0.116$). On the other hand, full p53 function, in addition to leading to a lower penetrance of proliferative PNLs, dropping from 60% of P22 samples to 37.5% at P45, also demonstrated a reduction in proliferative frequency, from 20% at P22 down to 5% at P45 ($p = 0.046$). With regards to non-proliferative cells of the PNL, the majority of these cells, in all three models, were marked by p27, a protein associated with cerebellar granule neuron differentiation during CB development (Zindy et. al., 2006; Miyazawa et. al., 2000). Inversely reflecting the change in Ki67, the frequency of P27 positive cells showed that as p53 functionality was lost, P27 frequency decreased, demonstrating that cell cycle arrest and differentiation were mechanistically linked to p53, although p53 was not the sole requirement for this process, as demonstrated by the fairly high (50%) frequency of p27 positivity within the Ptch1p53$^{\Delta E5-6}$ model (Figure 10D''). Curiously, cells positive for both p27 and Ki67 were found within both the Ptch1p53$^{\Delta E5-6}$ and Ptch1p53$^{\Delta/R172P}$ models, indicating that without fully functional p53 regulation, it is possible for cells in the PNL to remain proliferative in spite of the differentiation process. These results demonstrate that the p53-mediated cell

cycle arrest response targets proliferating cells of both the Ptch1p53$^{\Delta/R172P}$ and Ptch1p53^{WT} PNLs, pushing pre-neoplastic cells into cerebellar granular neuron differentiation.

2.2.6 Identification of a variant of PNLs that do not activate p53

Having identified the roles that p53 played during cerebellar development, the mechanism by which PNLs were able to evade the p53 response remained unclear. Surprisingly, I found that, by making use of *p53*$^{\Delta E5-6}$ as a marker, a variant of PNL could be identified in postnatal P22 cerebellum from both Ptch1p53$^{\Delta E5-6}$ and Ptch1p53$^{\Delta /R172P}$ models where no accumulation of p53 was observed, in spite of the lack of potential *p53* transcription (Figure 11A-C). These clusters, much like the clusters observed in the Ptch1p53^{WT} model, showed less than 10% of the cells as p53 positive (Figure 11C). Curiously, it was evident that the p53^{R172P} allele remained functional, accounting for a reduction in the number of clusters with high frequency of p53 positive cells (Figure 11B). Based on the mean number of PNLs observed between models (Figure 9A''), it seems likely that the increased number of PNLs observed in the Ptch1p53$^{\Delta E5-6}$ and Ptch1p53$^{\Delta/R172P}$ models compared to Ptch1p53^{WT} is explained by the increased number of PNLs with stabilized p53. Thus, each of the cerebella observed contained, on average, a similar number of p53 negative PNLs at P22. This theory is supported by the observation at P46, where it was demonstrated that, within both mutant brains, there was a decline in the frequency of p53 negative clusters relative to the frequency observed at P22 (Figure 11D-F). This again corresponds with the decline in penetrance of PNLs in the Ptch1p53^{WT} model (Figure 10C). Thus, I show two variants of PNLs, one of which is a p53 negative cluster found in all of the *Ptch1*$^{+/-}$ models, and the other as a p53 positive cluster only observed in the context of mutant *p53*. These observations are most consistent with a model in which a subset of PNLs arise from a p53 resistant GCPs population, with all other PNLs requiring mutant p53 to form.

2.2.7 Loss of p53-mediated apoptotic activity is the crucial barrier to MB formation

Following the investigation of developing tumors, I then sought to investigate the repercussions of p53 function on MB formation. It has been well established that loss of a single allele of *Ptch1*$^{+/-}$ is sufficient to induce MBs, although with less than complete penetrance, varying in the literature between 8% and 55%, principally varying by background, but increasing to nearly 100% with the inclusion of mutant p53 (Wetmore et. al., 2001, Mille et. al., 2014). I found the Ptch1p53^{WT} model had median survival of 159 days and 34% penetrance, within the range of previously reported *Ptch1*$^{+/-}$ models (Figure 12A-C). No significant change in penetrance or survival was observed when one allele of p53 was replaced with either a germline knockout p53, *p53*^{KO} (Jacks et. al., 1994), or the p53^{R172P} allele, indicating minimal carrier effect associated with mouse background (Figure 12D). Homozygous loss of p53 in the Ptch1p53$^{\Delta E5\text{-}6}$ model reduced median survival to 64 days and increased SHH-MB penetrance to 98%. Within the Ptch1p53$^{\Delta/R172P}$ model, I found a 39% increase in life span as compared to Ptch1p53$^{\Delta E5\text{-}6}$, with a mean survival of 89 days and a penetrance of 95% (Figure 12A). Due to the presence of germline *p53*^{R172P} allele, the incidence of body tumors was elevated, although these mice were most often sacrificed as a result of neurological symptoms (95%) (Figure 12B). Although these MBs arise at different rates, the MBs that arise within each model are not histologically or molecularly distinct. Upon dissection, I found that each MB model produced tumors in the same locations, most typically occupying the fourth ventricle (Figure 12C). Further, the tumors from each model featured similar histological characteristics, including nuclear molding and mitotic figures (Figure 12E). I characterized both proliferation and apoptosis within these MBs, and found that widespread proliferation was consistent through each model, with all three models showing mean proliferation greater than 80%, though proliferation was heterogeneous, with some regions showing a lower rate, and apoptosis was uncommon in all three models (Figure 12F-F''). I characterized the resultant MB in order to determine whether tumors arising from the Ptch1p53^{WT} model formed with any distinctive molecular characteristics compared to the rapid onset tumors found in the Ptch1p53$^{\Delta E5\text{-}6}$ model, but

found that within all three models, the tumors had comparable labeling with Synaptophysin, GFAP, Nestin, and Olig2, markers used to label neural, glial, progenitor and oligodendrocyte populations, respectively, for pathological assessment of human brain tumors (Figure 12G).

Several publications have indicated that *Ptch1* loss of heterozygosity (LOH) is an early step in the formation of MBs within the Ptch1 background (Read et. al., 2009, Tamayo-Orrego et. al., 2016). To investigate whether Hedgehog pathway activity might play a role in differential penetrance, I investigated the frequency of *Ptch1* LOH in SHH-MBs, and found that it did not vary between models, with the majority of samples showing *Ptch1* LOH, but with approximately 10% of samples from each model retaining one allele of *Ptch1* (Figure 13A-B). Expression of downstream targets of the hedgehog pathway, including *Gli1, Gli2 and N-Myc*, were increased in every tumor model, regardless of the status of *Ptch1* LOH (Figure 13C). Curiously, expression of *Gli1, Gli2 and N-Myc* was elevated in all samples, regardless of the status of *Ptch1* LOH, indicating that the Hedgehog pathway is targeted at alternate locations. PGM sequencing using 4 of the non-LOH samples failed to find clonal mutations to the *Ptch1* allele, demonstrating that the pathway was not targeted at *Ptch1*. Based on the elevated expression of SHH targets in all MBs tested, I demonstrated that, whether through LOH or an alternate mechanism, elevated activation of the Hedgehog pathway is a common trait of the SHH-MB group.

Previous studies have indicated that genomic instability is a common feature of SHH-MBs with mutant TP53, but the initial characterization of $p53^{R172P}$ showed retention of p53-associated chromosomal stabilization, as well as cell cycle arrest activity (Liu et. al., 2004, Jones et. al., 2012). I sought to understand the role genomic stability might play in MB formation, and therefore founded primary cell lines from Ptch1$p53^{\Delta E5\text{-}6}$ and Ptch1$p53^{\Delta/R172P}$ (Figure 14A). Karyotyping of these cell lines indicated that the chromosome of murine *Ptch1*$^{+/-}$ SHH-MBs, regardless of p53 status, had minimal genomic alterations and did not give evidence of chromosomal alterations, indicating that the potential role of $p53^{R172P}$ with regards to chromosomal stability is unlikely to be the source of the observed rescue (Figure 14B-C). Although chromosomal alteration was

observed in cell lines, incidence of aneuploidy was equivalent between both Ptch1p53$^{\Delta E5\text{-}6}$ and Ptch1p53$^{\Delta/R172P}$. Based on these data, I reject the *p53^{R172P}* function of increased genomic stability as the mechanism explaining delayed MB progression and propose that partial activation of p53's cell-cycle arrest function is the primary mechanism responsible for the decreased rate of tumor onset in the Ptch1p53$^{\Delta/R172P}$ models.

2.3 Summary

To summarize these results, my major findings in this chapter are the demonstration of p53's role in limiting a rare population of stressed GCPs during cerebellar development and the capacity for p53-mediated apoptosis to target retained SHH-MB during tumor initiation, thereby preventing the formation of MB in the presence of wild type *p53*. Using the *p53$^{\Delta E5\text{-}6}$* mutant allele, I was able to mark stressed cells that would normally not be visible due to the p53-Mdm2 negative feedback loop. Introduction of even a single functional allele of p53 was sufficient to drastically reduce the frequency of this p53$^{\Delta E5\text{-}6}$-positive cell population in the EGL. However, this population of p53-positive cells did not expand, and appeared to be driven out of the cell cycle by p53-independent mechanisms. Only after the *Ptch1$^{+/-}$* allele was introduced to this model was it possible for p53-positive cells to expand into p53-positive clusters, suggesting that Hedgehog pathway hyper-activation was capable of driving growth in a population of p53-activation sensitive GCPs. These clusters were capable of disrupting normal differentiation in the EGL, indicative of an oncogenic transformation in p53-sensitive GCPs in response to Hedgehog pathway disruption. Characterization of these p53-positive clusters revealed that the majority of clusters were labeled by stem cell marker Sox2. These results show that the Hedgehog pathway is partially responsible for maintenance or dedifferentiation of stem-like cells in the EGL, although the process is not clear from these results, and that p53 is responsible for eliminating those cells if they exist outside of a brief window.

Following cerebellar maturation, PNLs were visible in cerebella from all three models, but the frequency of PNL formation was approximately 4 times greater in Ptch1p53$^{\Delta E5\text{-}6}$ and Ptch1p53$^{\Delta/R172P}$ models compared to the Ptch1p53^{WT} model. Further, the

average size of clusters observed in the Ptch1p53$^{\Delta E5\text{-}6}$ and Ptch1p53$^{\Delta/R172P}$ models was greater than the Ptch1p53^{WT} model. In attempting to define a mechanism for these differences after development, I investigated the behavior of PNLs from each model, and demonstrated that increased apoptosis was detected in PNLs in the Ptch1p53^{WT} model, supporting the role of apoptosis in preventing SHH-MB formation. Further, complete penetrance of Ptch1p53$^{\Delta/R172P}$ model revealed that retained cell cycle arrest function was insufficient to prevent the formation of SHH-MBs, showing nearly 100% tumor penetrance. These results demonstrate that only in the case of wild type p53 function was it possible for abnormally retained EGL cells to be effectively targeted, and that p53-mediated apoptosis was the mechanism by which p53 prevents SHH-MB formation.

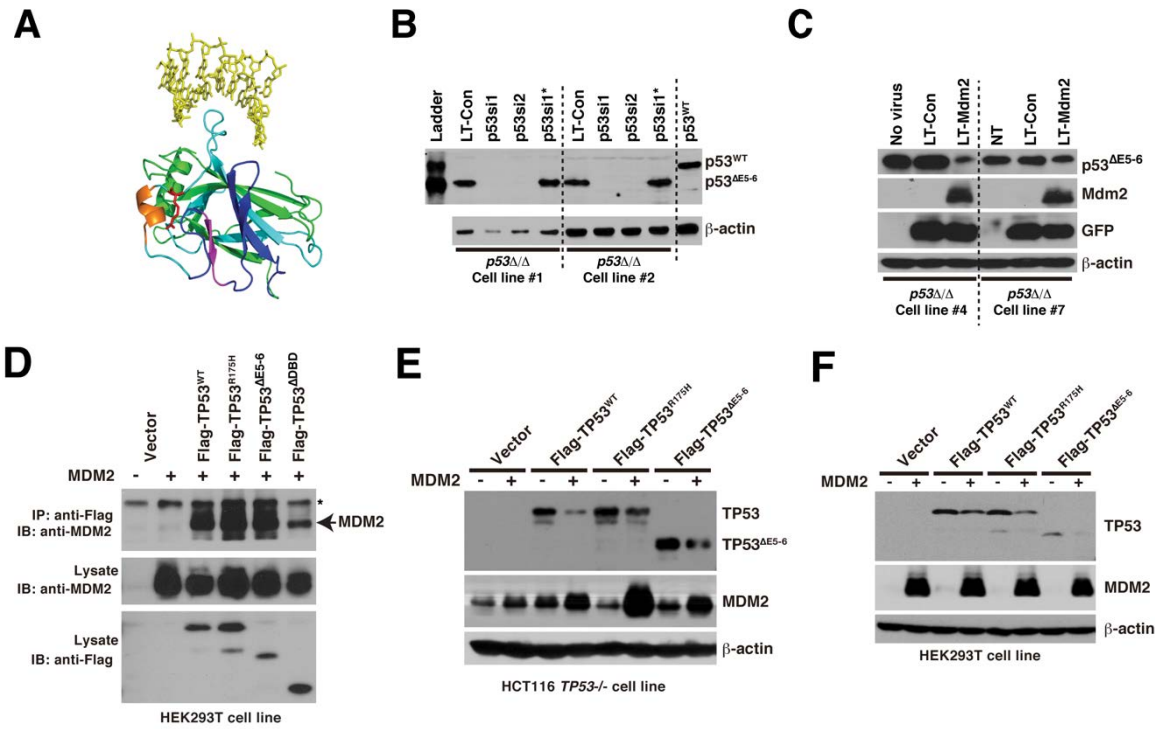
A
B
Ladder
LT-Con
p53si1
p53si2
p53si1*
LT-Con
p53si1
p53si2
p53si1*
p53WT
p53WT
p53ΔE5-6
β-actin
p53Δ/Δ
Cell line #1
p53Δ/Δ
Cell line #2
C
No virus
LT-Con
LT-Mdm2
NT
LT-Con
LT-Mdm2
p53ΔE5-6
Mdm2
GFP
β-actin
p53Δ/Δ
Cell line #4
p53Δ/Δ
Cell line #7
D
Vector
Flag-TP53WT
Flag-TP53R175H
Flag-TP53ΔE5-6
Flag-TP53ΔDBD
MDM2
IP: anti-Flag
IB: anti-MDM2
MDM2
Lysate
IB: anti-MDM2
Lysate
IB: anti-Flag
HEK293T cell line
E
Vector
Flag-TP53WT
Flag-TP53R175H
Flag-TP53ΔE5-6
MDM2
TP53
TP53ΔE5-6
MDM2
β-actin
HCT116 TP53-/- cell line
F
Vector
Flag-TP53WT
Flag-TP53R175H
Flag-TP53ΔE5-6
MDM2
TP53
MDM2
β-actin
HEK293T cell line

Figure 5: The $p53^{\Delta E5\text{-}6}$ protein is accumulated in tumors

(A) Structure of the $TP53^{DBD}$-DNA complex. *TP53*-exon 5 is colored in cyan; exon 6 is colored in blue; two small in-frame deletions observed in human GBMs are colored in orange and purple, respectively; and a hot-spot residue R175 in exon 5 is colored in red. DNA is shown in yellow.

(B) $p53^{\Delta E5\text{-}6/\Delta E5\text{-}6}$ glioma cell lines were infected with *p53*-specific siRNAs (*p53*si1 and *p53*si2) or mismatched siRNA (*p53*si1*) containing lentiviruses or control lentivirus (LT-Con). Western blot analysis was performed using the cell lysates with the indicated antibodies. Irradiated p53WT spleen was used as positive control for p53 protein.

(C) $p53^{\Delta E5\text{-}6/\Delta E5\text{-}6}$ mouse glioma cell lines were infected with Mdm2-overexpressing GFP-lentivirus (LT-Mdm2) or control GFP-virus (LT-Con). Cell lysates were analyzed by western blot analysis with the indicated antibodies.

(D) Co-immunoprecipitation assay of MDM2 and Flag-tagged TP53 WT or mutant-TP53 proteins ($TP53^{R175H}$, $TP53^{\Delta E5\text{-}6}$, $TP53^{\Delta DBD}$). HEK293T cells were co-transfected with the indicated plasmids. Cell lysates were immunoprecipitated with anti-Flag antibody, and probed with anti-MDM2 antibody. * Non-specific band.

(E-F). Flag-tagged wt-*TP53* and mutant-*TP53* constructs were co-transfected with or without MDM2 plasmid in human cell lines, HEK293T cells (E) or HCT116 $TP53^{-/-}$ cells (F). Cell lysates were subjected to western blotting analysis with the indicated antibodies.

DBD, DNA-binding domain; WT, wild type; ML: molecular layer, IGL: internal granular layer.

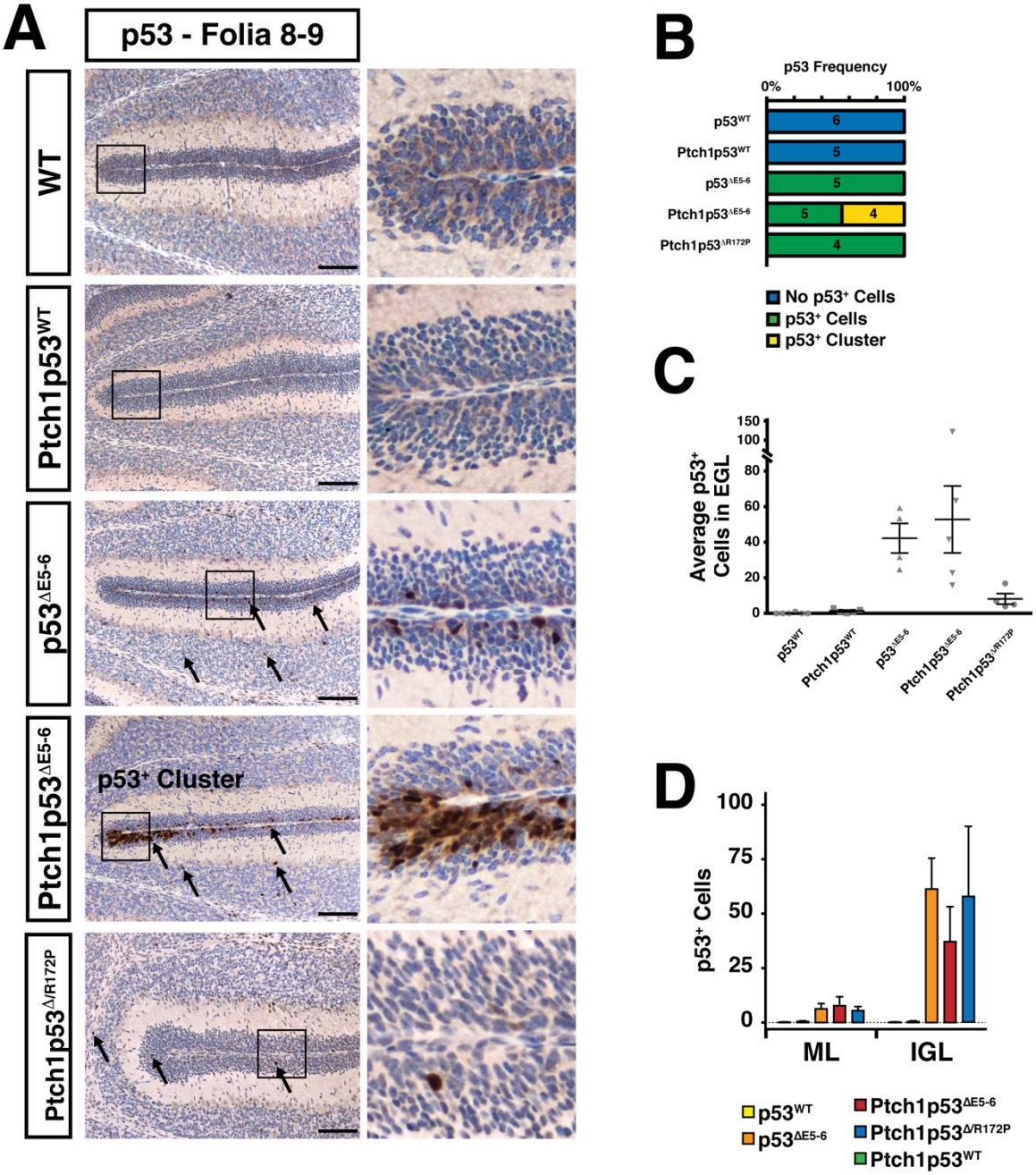
A
p53 - Folia 8-9
WT
Ptch1p53WT
p53ΔE5-6
Ptch1p53ΔE5-6
Ptch1p53Δ/R172P
p53+ Cluster
B
p53 Frequency
0%
100%
p53WT
Ptch1p53WT
p53ΔE5-6
Ptch1p53ΔE5-6
Ptch1p53Δ/R172P
6
5
5
5
4
4
No p53+ Cells
p53+ Cells
p53+ Cluster
C
Average p53+ Cells in EGL
150
100
80
60
40
20
0
p53WT
Ptch1p53WT
p53ΔE5-6
Ptch1p53ΔE5-6
Ptch1p53Δ/R172P
D
p53+ Cells
100
75
50
25
0
ML
IGL
p53WT
p53ΔE5-6
Ptch1p53ΔE5-6
Ptch1p53Δ/R172P
Ptch1p53WT

Figure 6: Abnormal cells are observed in developing cerebellum

(A) Immunohistochemistry of P8 cerebella, showing EGL at folia 8/9, indicates $p53^{+}$ cells. Hi magnification of boxed region shown to the right. Arrows indicate p53 positive cells indicated by arrows, and p53 positive cell cluster is labeled.

(B) Penetrance of $p53^{+}$ cells and clusters in postnatal cerebellum.

(C) Quantification of $p53^{+}$ cells in control and mutant EGL. Each point represents a separate sample, with bars indicating Mean + SEM.

(D) Quantification of $p53^{+}$ cells in the ML and IGL of $p53^{WT}$, $p53^{\Delta E5\text{-}6}$ $Ptch1p53^{\Delta E5\text{-}6}$, $Ptch1p53^{\Delta/R172P}$ and $Ptch1p53^{WT}$ models.

EGL: External Granular Layer, ML: molecular layer, IGL: internal granular layer. Hematoxylin was used as a counterstain. Scale bars represent Mean ± SEM. Scale, 100 um.

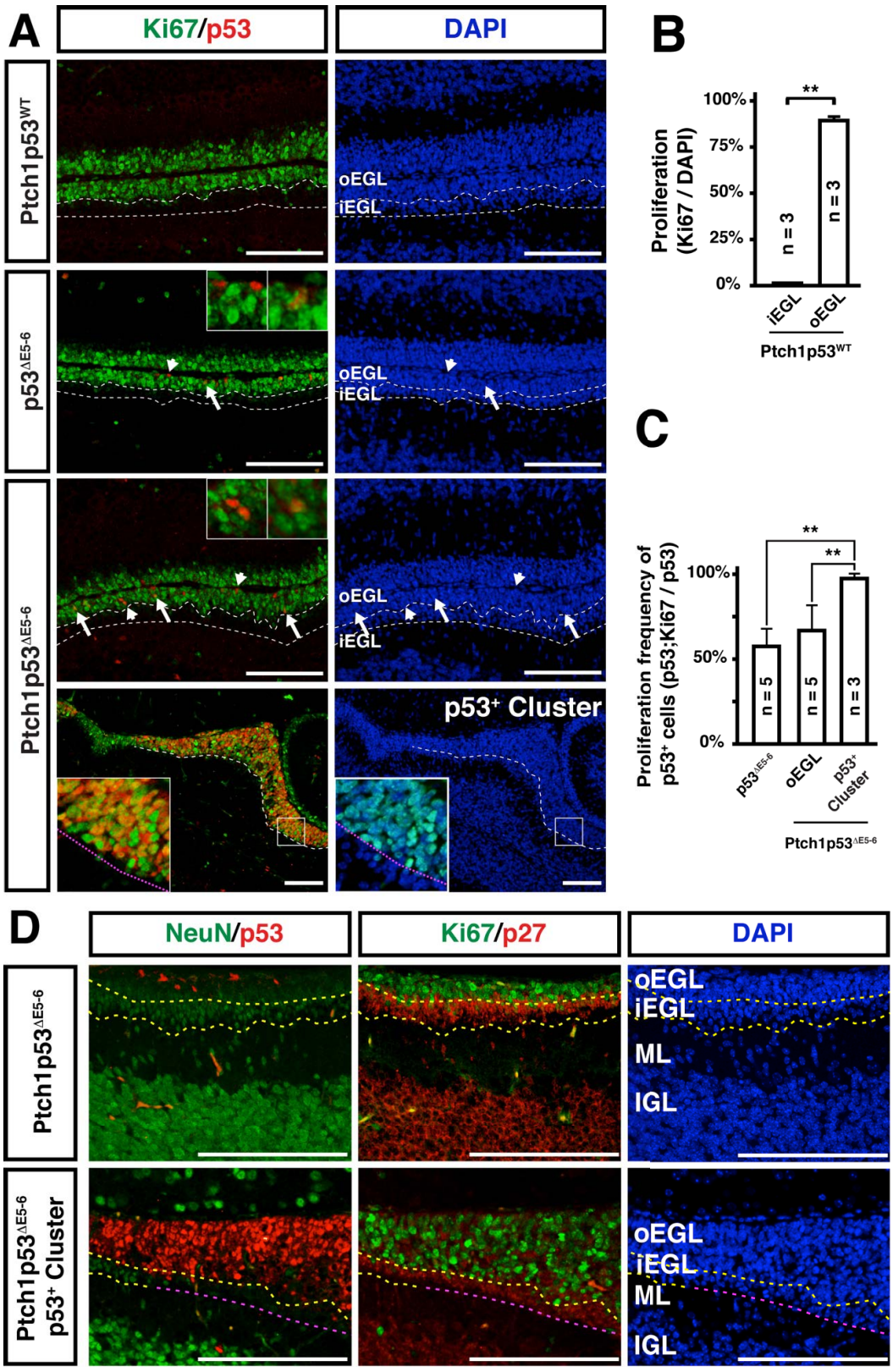
A
Ki67/p53
DAPI
Ptch1p53WT
p53ΔE5-6
Ptch1p53ΔE5-6
oEGL
iEGL
p53+ Cluster
B
Proliferation (Ki67 / DAPI)
100%
75%
50%
25%
0%
n = 3
n = 3
**
iEGL
oEGL
Ptch1p53WT
C
Proliferation frequency of p53+ cells (p53;Ki67 / p53)
100%
50%
0%
n = 5
n = 5
n = 3
**
**
p53ΔE5-6
oEGL
p53+ Cluster
Ptch1p53ΔE5-6
D
NeuN/p53
Ki67/p27
DAPI
Ptch1p53ΔE5-6
Ptch1p53ΔE5-6 p53+ Cluster
oEGL
iEGL
ML
IGL

Figure 7: Clusters of abnormal cells are observed in the p53 mutant

(A) Co-localization of Ki67 and p53 in P8 EGL (upper three images) and $p53^+$ cell cluster (bottom image). Arrows indicate co-localized cells, arrowheads indicate $p53^+$;$Ki67^-$ cells, and the white dotted line highlights to boundary of oEGL to iEGL. Insets show a $p53^+$ and a co-localized cell within the oEGL. Insets at bottom show co-localization in a $p53^+$ cell cluster.

(B-C) Quantification of proliferative cells in control iEGL and oEGL (B) and proliferative frequency in the p53+ cell population of EGL and $p53^+$ cell clusters (C).

(D) Co-localization of NeuN and p53 as well as Ki67 and p27 from adjacent sections of EGL and $p53^+$ cell cluster. Dotted yellow lines demonstrate normal iEGL and oEGL layers. Purple dotted line indicates iEGL layer without NeuN expression.

DAPI was used as a counterstain. Scale bars represent Mean ± SEM. Scale, 100 um. **, $p< 0.01$.

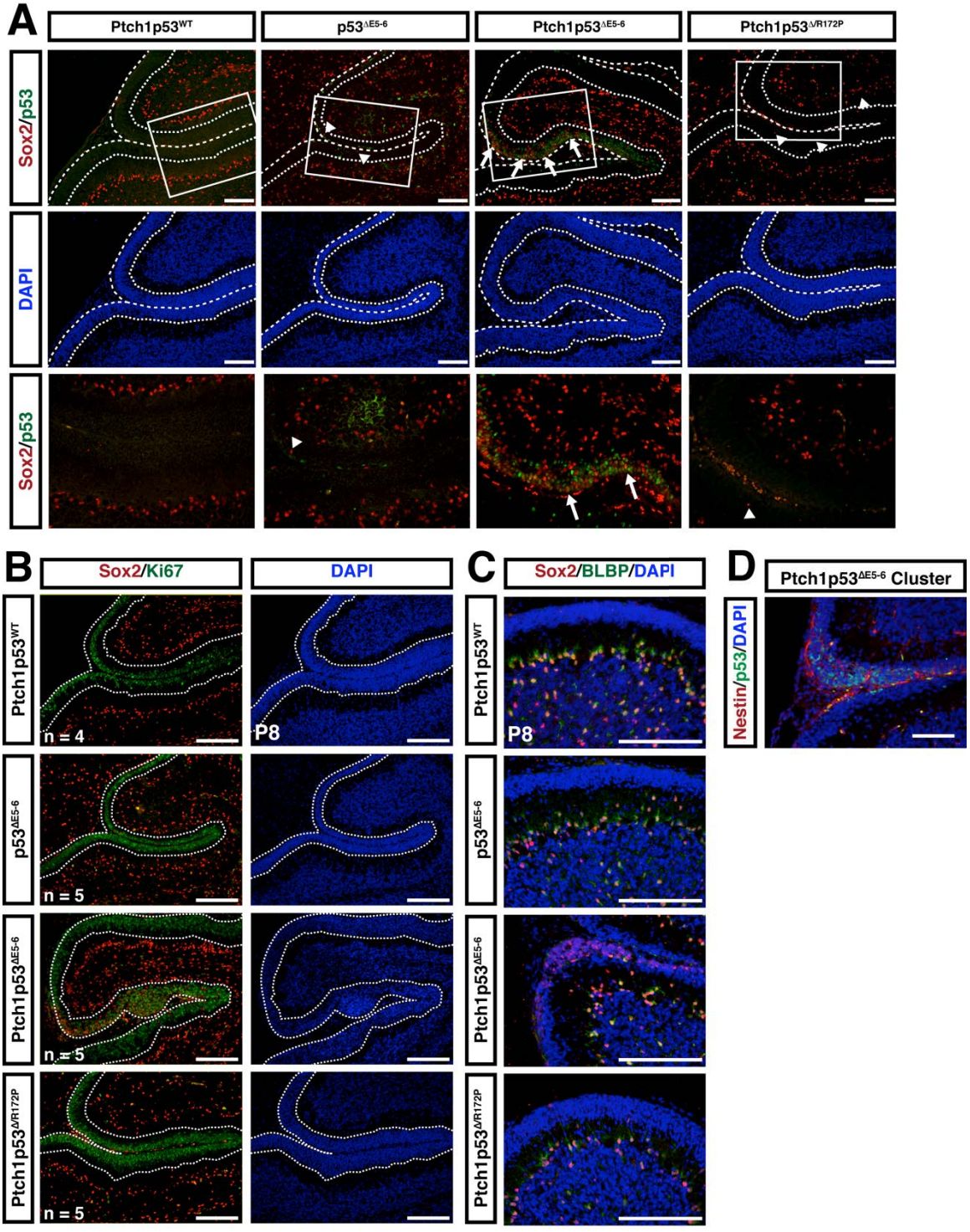
A
Ptch1p53WT
p53ΔE5-6
Ptch1p53ΔE5-6
Ptch1p53ΔVR172P
Sox2/p53
DAPI
Sox2/p53
B
Sox2/Ki67
DAPI
Ptch1p53WT
n = 4
P8
p53ΔE5-6
n = 5
Ptch1p53ΔE5-6
n = 5
Ptch1p53ΔVR172P
n = 5
C
Sox2/BLBP/DAPI
Ptch1p53WT
P8
p53ΔE5-6
Ptch1p53ΔE5-6
Ptch1p53ΔVR172P
D
Ptch1p53ΔE5-6 Cluster
Nestin/p53/DAPI

Figure 8: Abnormal cells discovered in developing cerebellum bear stem cell marker Sox2

(A) Co-localization of Sox2 and p53. Arrows indicate co-localization, arrowheads indicate Sox2-positive; $p53^-$ cells, and the dotted line highlights the EGL. Boxed region shown at high magnification below.

(B) Immunofluorescent co-labeling of Sox2 and Ki67 within P8 CB. Note that adjacent sections reveal that the Sox2-positive cluster in the Ptch1p53$^{\Delta E5\text{-}6}$ model correspond with a p53-positive cell cluster. Dotted line indicates the boundary of the EGL, as defined by DAPI.

(C) Immunofluorescent co-labeling of Sox2 and BLBP as well as Sox2 and NeuN within P8 CB. The Sox2-positive cluster in the Ptch1p53$^{\Delta E5\text{-}6}$ model correspond with a p53-positive cell cluster.

(D) Immunofluorescent co-labeling of p53 and Nestin within a p53-positive cell cluster from the Ptch1p53$^{\Delta E5\text{-}6}$ model.

DAPI was used as a counterstain. Scale bars represent Mean ± SEM. Scale, 100 um.

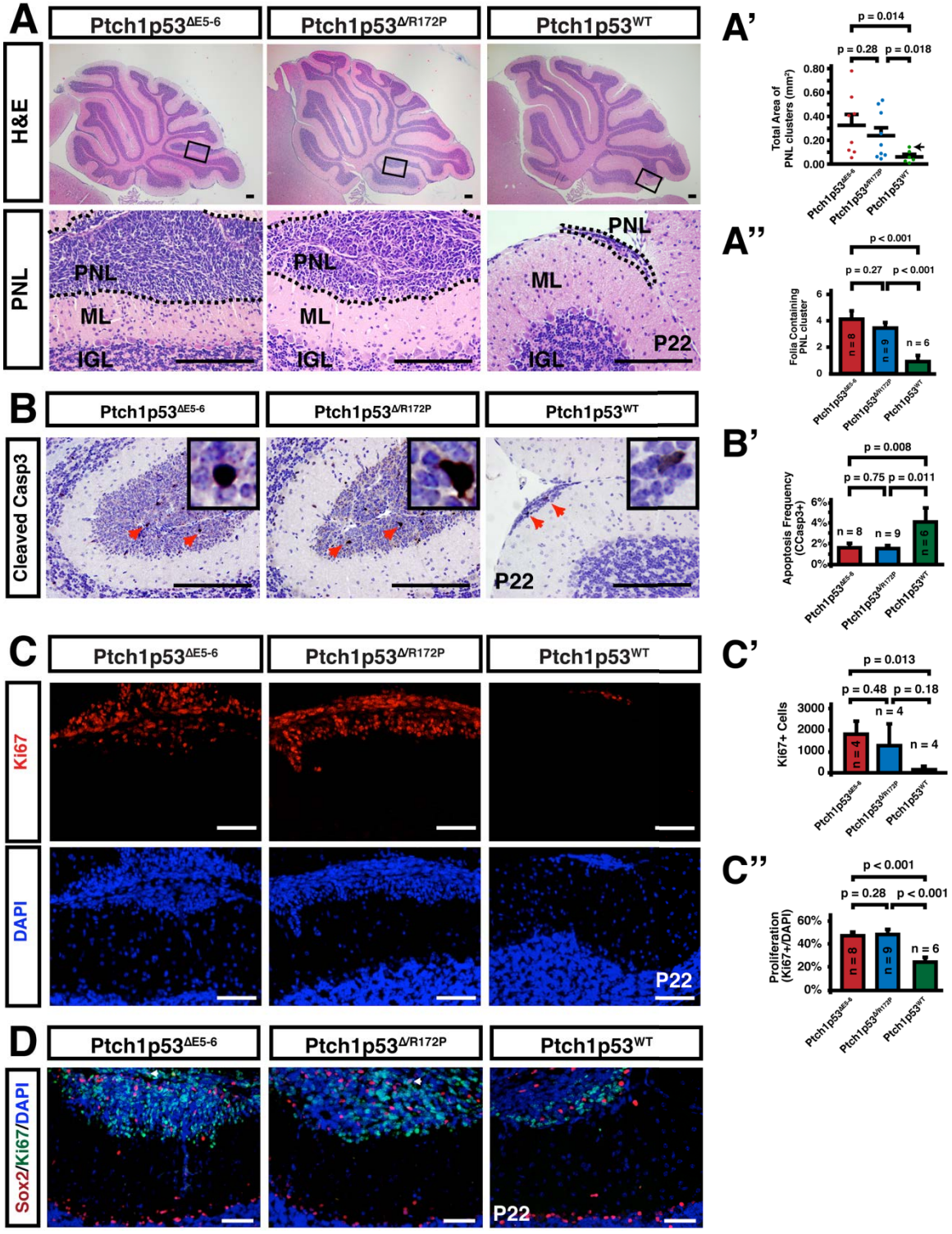
A
Ptch1p53ΔE5-6
Ptch1p53Δ/R172P
Ptch1p53WT
H&E
PNL
PNL
ML
IGL
PNL
ML
IGL
PNL
ML
IGL
P22
A'
p = 0.014
p = 0.28
p = 0.018
Total Area of PNL clusters (mm²)
0.80
0.60
0.40
0.20
0.00
A''
p < 0.001
p = 0.27
p < 0.001
Folia Containing PNL cluster
n = 8
n = 9
n = 6
B
Cleaved Casp3
P22
B'
p = 0.008
p = 0.75
p = 0.011
Apoptosis Frequency (CCasp3+)
6%
4%
2%
0%
n = 8
n = 9
n = 6
C
Ki67
DAPI
P22
C'
p = 0.013
p = 0.48
p = 0.18
n = 4
n = 4
n = 4
Ki67+ Cells
3000
2000
1000
0
C''
p < 0.001
p = 0.28
p < 0.001
Proliferation (Ki67+/DAPI)
60%
40%
20%
0%
n = 8
n = 9
n = 6
D
Sox2/Ki67/DAPI
P22

Figure 9: Pre-neoplastic lesions are eliminated by p53-mediated apoptosis

(A) H&E staining of representative P22 cerebella. Boxed regions are shown magnified below. Dotted lines indicate boundary of preneoplastic lesions.

(A') Quantification of total PNL area (mm^2). Each point represents an individual sample. Area was assessed in two matched locations for each mutant.

(A'') Number of discrete PNL observed per sample.

(B) Representative immunohistochemistry images of cleaved Caspase-3 in P22 PNLs. Arrowheads indicate positive cells. Insets show positive cells at high magnification.

(B') Quantification of the frequency of cleaved Caspase-3.

(C) Immunofluorescenct labeling of Ki67 in postnatal day 22 (P22) Ptch1p53$^{\Delta E5\text{-}6}$, Ptch1p53$^{\Delta/R172P}$ and Ptch1p53^{WT} PNL.

(C'-C'') Quantification of absolute number of proliferative cells (C') as well as frequency of proliferation (C'').

(D) Immunofluorescenct co-labeling of Sox2 and Ki67 in postnatal day 22 (P22) Ptch1p53$^{\Delta E5\text{-}6}$, Ptch1p53$^{\Delta/R172P}$ and Ptch1p53^{WT} PNL.

PNL: Pre-neoplastic Lesion, DAPI was used as a fluorescent nuclear counterstain. Scale 100 um. Error bars represent Mean ± SEM. Unpaired, two-tailed students T-Tests were used to determine p-values.

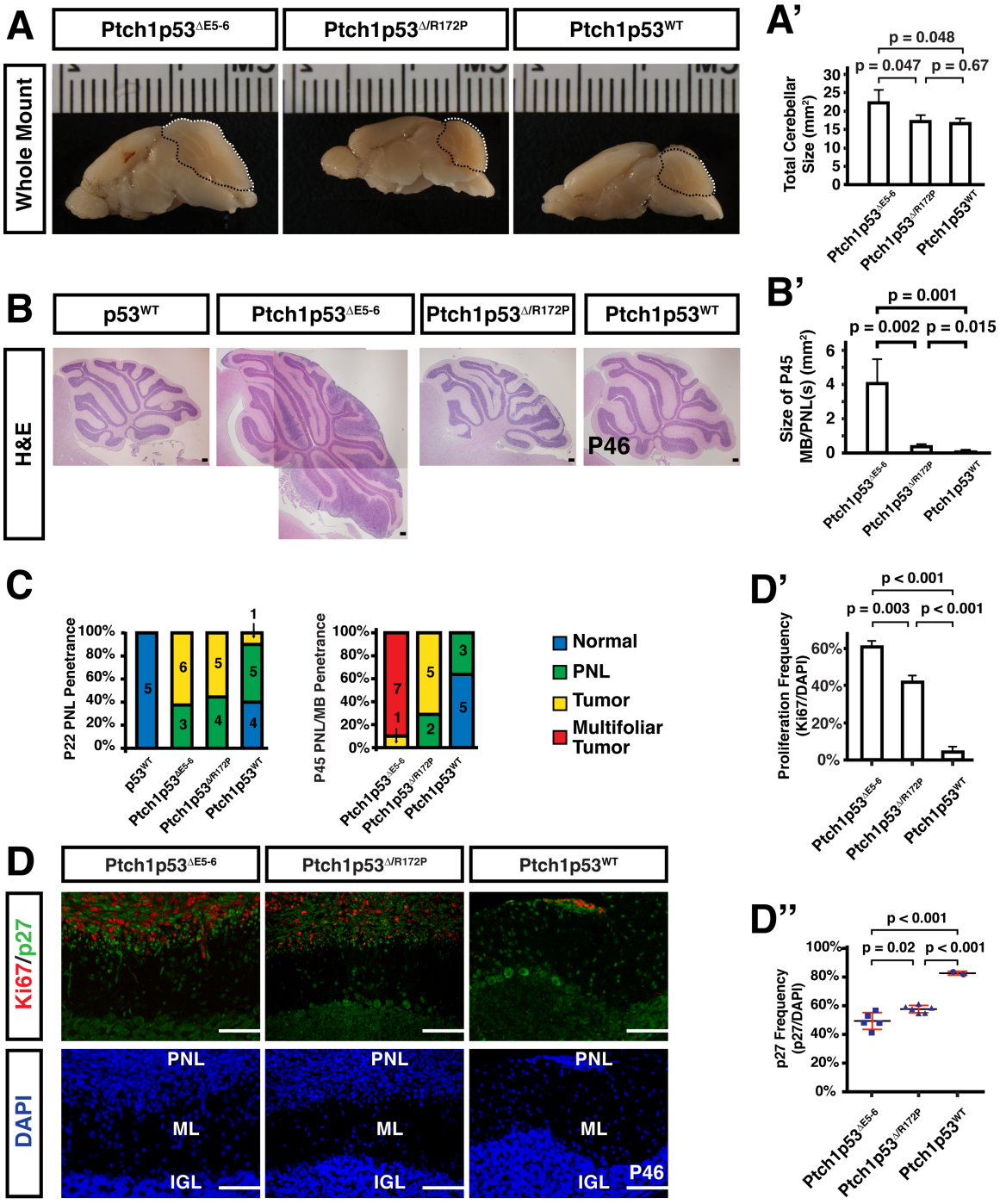
A
Ptch1p53ΔE5-6
Ptch1p53Δ/R172P
Ptch1p53WT
Whole Mount
A'
p = 0.048
p = 0.047
p = 0.67
Total Cerebellar Size (mm²)
B
p53WT
Ptch1p53ΔE5-6
Ptch1p53Δ/R172P
Ptch1p53WT
H&E
P46
B'
p = 0.001
p = 0.002
p = 0.015
Size of P45 MB/PNL(s) (mm²)
C
P22 PNL Penetrance
P45 PNL/MB Penetrance
Normal
PNL
Tumor
Multifoliar Tumor
D'
p < 0.001
p = 0.003
p < 0.001
Proliferation Frequency (Ki67/DAPI)
D
Ki67/p27
DAPI
PNL
ML
IGL
P46
D''
p < 0.001
p = 0.02
p < 0.001
p27 Frequency (p27/DAPI)

Figure 10: p53-mediated cell cycle arrest delays MB progression

(A) Whole mount and (B) H&E images were taken from representative brains of Ptch1p53$^{\Delta E5\text{-}6}$, Ptch1p53$^{\Delta/R172P}$, and Ptch1p53^{WT} models at P46. (B) Images shown represent multiple images for the Ptch1$^{+/-}$p53$^{\Delta E5\text{-}6}$ model.

(A') Quantification of the mean cerebellar area of each model at midline.

(B') Quantification of the total size of PNLs and MBs from each brain.

(C) Penetrance of PNLs and MBs at P22 and P46 for each mutant model.

(D-D'') Representative images of co-labeling of Ki67 and p27, a marker of cell cycle arrest and differentiation during cerebellar development, in P46 PNL and/or MB. Quantification of the frequency of proliferation (D') and frequency of cell cycle arrest/differentiation (D'').

PNL: Pre-neoplastic Lesion, ML: molecular layer, IGL: internal granular layer. DAPI was used as a counterstain. Scale bars represent Mean ± SEM. Scale, 100 um.

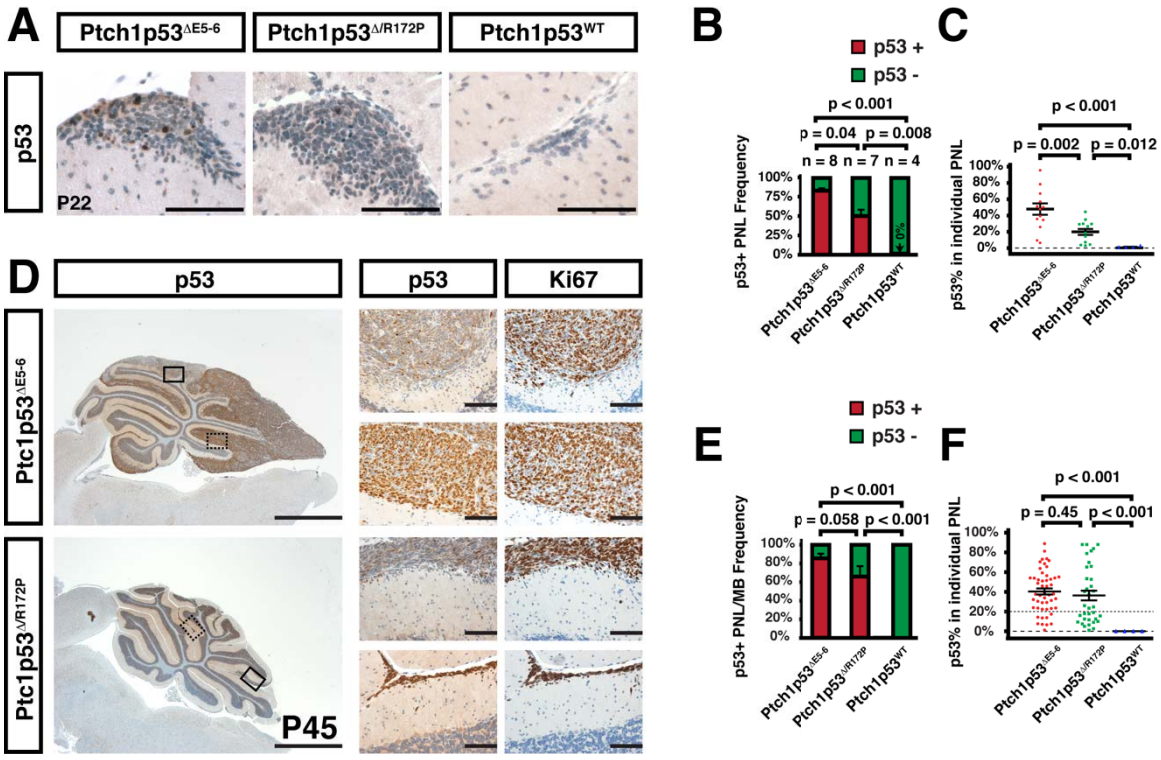
A
Ptch1p53ΔE5-6
Ptch1p53Δ/R172P
Ptch1p53WT
p53
P22
B
p53 +
p53 -
p < 0.001
p = 0.04
p = 0.008
n = 8
n = 7
n = 4
p53+ PNL Frequency
100%
75%
50%
25%
0%
0%
Ptch1p53ΔE5-6
Ptch1p53Δ/R172P
Ptch1p53WT
C
p < 0.001
p = 0.002
p = 0.012
p53% in individual PNL
100%
80%
60%
40%
20%
0%
Ptch1p53ΔE5-6
Ptch1p53Δ/R172P
Ptch1p53WT
D
p53
p53
Ki67
Ptc1p53ΔE5-6
Ptc1p53Δ/R172P
P45
E
p53 +
p53 -
p < 0.001
p = 0.058
p < 0.001
p53+ PNL/MB Frequency
100%
80%
60%
40%
20%
0%
Ptch1p53ΔE5-6
Ptch1p53Δ/R172P
Ptch1p53WT
F
p < 0.001
p = 0.45
p < 0.001
p53% in individual PNL
100%
80%
60%
40%
20%
0%
Ptch1p53ΔE5-6
Ptch1p53Δ/R172P
Ptch1p53WT

Figure 11: Pre-neoplastic lesions are capable of progressing without p53 activation

(A, D) Immunohistochemistry of p53 identified negative PNL found in P22 (A) and P46 (D) mutants. Adjacent sections were labeled for Ki67 to demonstrate proliferative activity in PNLs and MBs.

(B, E) Frequency of p53 positive and p53 negative clusters were qualitatively assessed for p22 (B) and P46 (E).

(C, F) Frequency of $p53^{+}$ cells in P22 PNL (C) and P46 PNL and/or MBs (F). Each point represents a discrete lesion.

Scale, 200 um, Error bars represent Mean + SEM. Fishers exact test was used to determine p-value in B and E. Unpaired, two-tailed students t-tests were used to determine p-values in C and F.

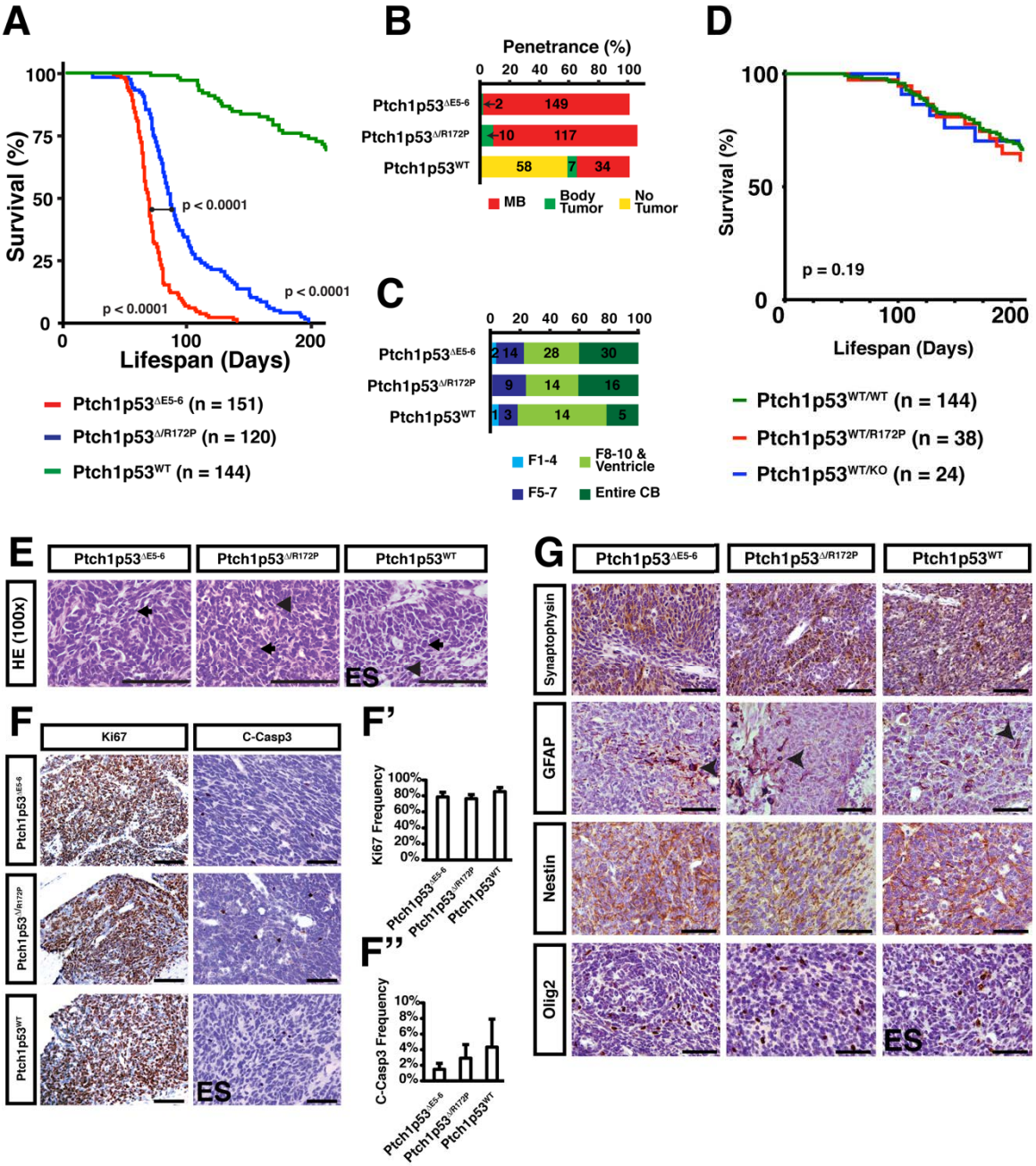
A
Survival (%)
Lifespan (Days)
p < 0.0001
p < 0.0001
p < 0.0001
Ptch1p53ΔE5-6 (n = 151)
Ptch1p53Δ/R172P (n = 120)
Ptch1p53WT (n = 144)
B
Penetrance (%)
Ptch1p53ΔE5-6
Ptch1p53Δ/R172P
Ptch1p53WT
MB
Body Tumor
No Tumor
C
F1-4
F5-7
F8-10 & Ventricle
Entire CB
D
Survival (%)
p = 0.19
Lifespan (Days)
Ptch1p53WT/WT (n = 144)
Ptch1p53WT/R172P (n = 38)
Ptch1p53WT/KO (n = 24)
E
HE (100x)
ES
F
Ki67
C-Casp3
ES
F'
Ki67 Frequency
F''
C-Casp3 Frequency
G
Synaptophysin
GFAP
Nestin
Olig2
ES

Figure 12: p53-mediated apoptosis is required to prevent MB

(A) MB-free curve of Ptch1p53$^{\Delta E5\text{-}6}$, Ptch1p53$^{\Delta/R172P}$, and Ptch1p53^{WT} models. (p, Log-rank (Mantel-Cox) test)

(B) Tumor Penetrance in the Ptch1p53$^{\Delta E5\text{-}6}$, Ptch1p53$^{\Delta/R172P}$ and Ptch1p53^{WT}. Asymptomatic mice were kept for a minimum of 1-year prior to sacrifice.

(C) Anatomical location of MBs arising in mutant models.

(D) Kaplan-Meier survival curve of Ptch1p53$^{WT/WT}$, Ptch1p53$^{WT/\Delta E5\text{-}6}$ and Ptch1p53$^{WT/R172P}$ models following the long-term IR treatment scheme. Log Rank test (Mantel-Cox) was used to determine p-value.

(E) Representative H&E images of MBs from each Ptch1 model, showing dense, purple tumors characterized by frequent mitotic figures (Arrowheads) and nuclear molding (Arrows).

(F) Immunohistochemistry images of Ki67 and Cleaved Caspase-3 taken from Ptch1p53$^{\Delta E5\text{-}6}$, Ptch1p53$^{\Delta/R172P}$ and Ptch1p53^{WT} MBs. Quantification of Ki67 (F') and Cleaved Caspase-3 (F'') frequency in MBs, showing no significant difference in proliferative or apoptotic cells between MB models. Scale bar, Ki67 200 um, CCasp3,100 um.

(G) Representative immunohistochemistry images taken from Ptch1p53$^{\Delta E5\text{-}6}$, Ptch1p53$^{\Delta/R172P}$ and Ptch1p53^{WT} MBs, demonstrating presence of Synaptohpysin, GFAP, Nestin, and Olig2. Arrowheads indicate tumor cells associated with GFAP. Scale bars, 100um

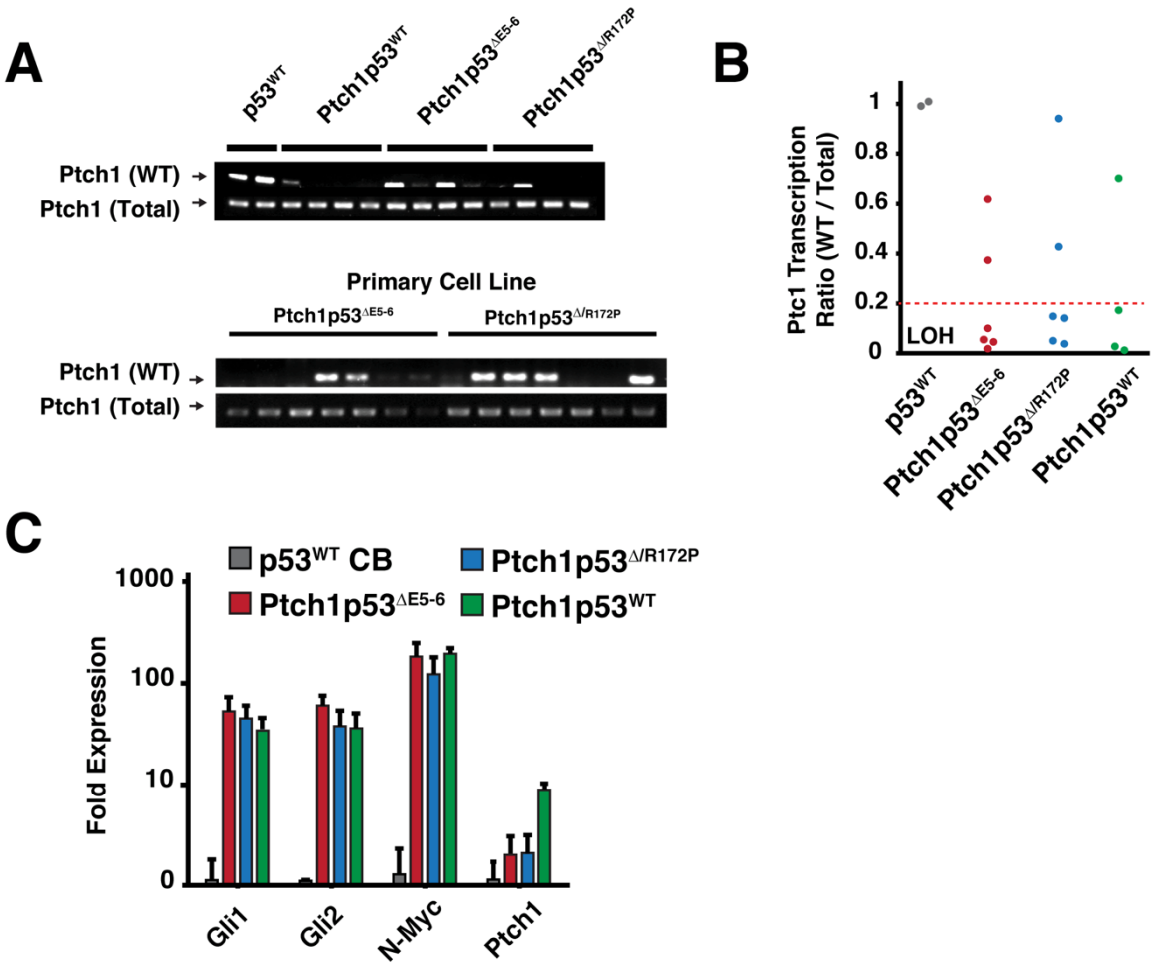
A
p53WT
Ptch1p53WT
Ptch1p53ΔE5-6
Ptch1p53Δ/R172P
Ptch1 (WT)
Ptch1 (Total)
Primary Cell Line
Ptch1p53ΔE5-6
Ptch1p53Δ/R172P
Ptch1 (WT)
Ptch1 (Total)
B
Ptc1 Transcription Ratio (WT / Total)
1
0.8
0.6
0.4
0.2
0
LOH
p53WT
Ptch1p53ΔE5-6
Ptch1p53Δ/R172P
Ptch1p53WT
C
p53WT CB
Ptch1p53Δ/R172P
Ptch1p53ΔE5-6
Ptch1p53WT
Fold Expression
1000
100
10
0
Gli1
Gli2
N-Myc
Ptch1

Figure 13: Activation of the hedgehog pathway is independent of p53 function

(A) Genotyping MB samples from Ptch1p53$^{\Delta E5\text{-}6}$, Ptch1p53$^{\Delta/R172P}$ and Ptch1p53^{WT} mice, as well as primary cell lines from Ptch1p53$^{\Delta E5\text{-}6}$ and Ptch1p53$^{\Delta/R172P}$, to determine the presence of wild type *Ptch1*, using probes covering exons 2-3 or exons 7-9. Exon 2-3 is lost in the germ-line null *Ptch1*. Normal brain tissues of p53^{WT} mice were used as a positive control.

(B) Quantitative PCR was used to determine the ratio of *Ptch1* wild type to total, using probes covering exons 2-3 or exons 7-9. Exon 2-3 is lost in the germ-line null *Ptch1*. Samples with ratios below 0.2 matched samples qualitatively assessed as LOH. Negative control, represented by a ratio of 1.0, was provided by tissue from p53^{WT} model CB.

(C) Quantitative RT-PCR of Hedgehog pathway targets *Gli1*, *Gli2*, *N-Myc* and *Ptch1*, using MBs from Ptch1p53$^{\Delta E5\text{-}6}$, Ptch1p53$^{\Delta/R172P}$ and Ptch1p53^{WT} mice, and normalized against adult CB from p53^{WT} littermates. No difference was detected in downstream target expression between LOH and non-LOH samples.

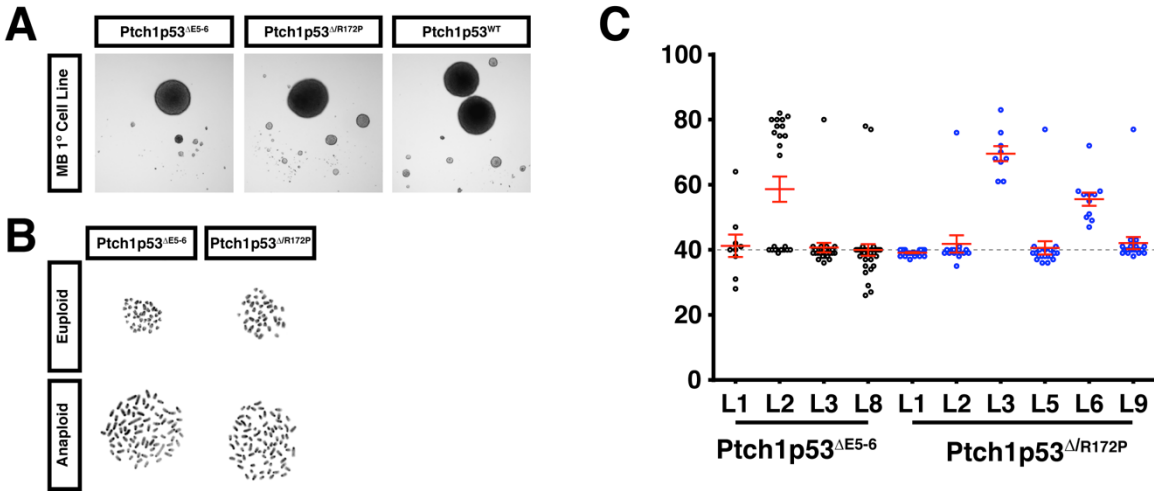

Figure 14: Acquisition of chromosomal defects does not directly correspond to p53 status

(A) Primary cell lines were developed using MBs from Ptch1p53$^{\Delta/\Delta E5\text{-}6}$, Ptch1p53$^{\Delta/R172P}$ and Ptch1p53^{WT} mice and grown in serum free, non-adherent conditions prior to light microscopy imaging.

(B-C) Cell lines were used to demonstrate chromosome number from Ptch1p53$^{\Delta E5\text{-}6}$ and Ptch1p53$^{\Delta/R172P}$ models using (B) metaphase spread techniques. (C) Quantification of chromosome number from multiple low passage (< 2) cell lines from the Ptch1p53$^{\Delta E5\text{-}6}$ and Ptch1p53$^{\Delta/R172P}$ models. Each point represents a single cell.

Chapter III: Radiation Activates p53 Above a Threshold Required to Target p53 wild type MB

3.1 Introduction

Despite relying on the same developmental pathway to drive tumor growth, SHH-MBs with wild type and mutant *TP53* are fundamentally different (Jones et. al., 2012, Zhukova et. al., 2013). SHH-MBs arise from granule cell precursors (GCPs), which depend on Hedgehog signaling for rapid proliferation and expansion during the development of the cerebellum (Oliver et. al., 2005, Yang et. al., 2008). In contrast to *TP53* wild type SHH-MBs, which frequently carry *PTCH1* or *SUFU* mutations, *TP53*-mutant SHH-MBs often harbor amplification of downstream targets of the Hedgehog pathway, such as *N-Myc* and *Gli2*, potentially rendering these tumors resistant to inhibitors of Smoothened (Smo) receptor (Schuller et. al., 2008, Yang et. al., 2008, Northcott et. al., 2010, Kool et. al, 2014). Furthermore, *TP53*-mutant SHH-MBs are frequently associated with large cell/anaplastic histology and exhibit an increased chance of gaining secondary mutations, as well as an increased chance of chromothripsis (Rausch et. al., 2012, Jones et. al., 2012). These observations suggest SHH-MBs form along two distinct paths depending on the p53 response of the GCP population.

Upon oncogenic activation of SHH signaling, the cell response is controlled in a temporal manner, with a limited window during which cells do not respond to stress by activating p53 (Pazzaglia et. al., 2006, Tanori et. al., 2013). Embryonic stem and granule cell precursors (GCP) do not activate the p53 response following radiation-induced DNA damage, but GCP p53 activation increases during postnatal development, displaying widespread p53 activation and associated apoptosis in postnatal day 10, thereby preventing SHH-MB formation (Pazzaglia et. al., 2006). Therefore, in order for MBs to arise with a sporadic p53 mutation, p53 inactivation must occur in the germline or during

embryonic development, providing a permissive context that allows the survival of highly aggressive tumor cells with high levels of genomic instability. On the other hand, p53 wild type GCPs maintaining the p53 response of embryonic cells fail to activate the p53 response above a threshold sufficient to require disruption of *TP53* form without disrupting the p53 response(s), which can be activated in response to radiation and chemotherapy. It remains unknown which p53-mediated responses, cell-cycle arrest, senescence or apoptosis, eliminate tumor susceptible GCPs during the initiation and progression of *TP53*-mutant SHH-MB formation. During cerebellar development, Sox2-positive stem cells of the rhombic lip give rise to Math1+ granule cell precursors migrating from the rhombic lip into the EGL, losing Sox2 expression as they differentiate (Yang et. al., 2008, Pazzaglia et. al., 2013). Recent evidence has implicated that Sox2 also marks a quiescent stem-like population located in SHH-MBs, and these cells have been implicated as a population responsible for MB treatment resistance and recurrence (Ahlfeld et. al., 2013, Vanner et. al., 2014). A rare and quiescent cancer stem cell-like population in SHH-MBs, characterized using early lineage markers, such as Sox2, are resistant to chemotherapy and can generate recurrent tumors both in vitro and in vivo. It remains unknown whether the resistance to chemotherapy of Sox2-positive MB-stem cells is caused by insufficient activation of p53-mediated responses upon radiation and chemotherapy, leading to tumor recurrence.

In this chapter, I demonstrated that p53 remains a viable therapeutic target in MBs and PNLs that form within the Ptch1p53^{WT} model. Making use of ionizing radiation to put stress on MBs, I showed that p53 wild type MBs activated p53 response and thereby induced p53-mediated apoptosis. By characterizing the cells of the deficient regions, I identified a Sox2-positive subpopulation present in the wild type p53 SHH-MB able to avoid p53-mediated apoptosis. Having determined that the reactivation of p53 is capable of targeting mature SHH-MBs, I next sought to understand whether the developing PNLs were able to bypass p53 during development by maintaining p53 signal below a critical threshold. Treating developing lesions with a clinically relevant radiation dose, I revealed a reduction in p53 wild type and heterozygous SHH-MB penetrance in response to p53-mediated apoptosis, and also demonstrated that p53-mediated cell cycle arrest is

insufficient to effectively target Sox2-positive cells, although it induces differentiation response in other PNL cells. Finally, I found that IR treatment is capable of inducing alterations to the p53 pathway, leading to loss of heterozygosity within Ptch1p53 heterozygous mutants. This chapter serves to demonstrate that p53 activation is a viable target within those SHH-MBs that arise with the majority of the p53 pathway intact, and elucidates the role the distinct p53 pathway responses play in MB cells.

3.2 Results

3.2.1 MB formed in the Ptch1 background do not require p53 pathway inactivation

In order to explore the possibility of tumors forming without requiring mutation to p53 or inactivation of the p53 pathway, I began by collecting samples from Ptch1p53$^{\Delta E5\text{-}6}$ (*hGFAP-Cre;Ptch1*$^{+/-}$*;p53*$^{E5\text{-}6/E5\text{-}6}$), Ptch1p53$^{\Delta/R172P}$ (*hGFAP-Cre;Ptch1*$^{+/-}$*;p53*$^{R172P/E5\text{-}6}$) and Ptch1p53^{WT} (Ptch1$^{+/-}$;p53$^{E5\text{-}6/E5\text{-}6}$) MBs, in order to confirm the retention of the p53 allele in SHH-MBs (Figure 15A-B). Due to impurities within the collected tissue samples, recombination efficiency was unclear (Figure 15B), so I also created primary MB cell lines, and used these cell lines to confirm the complete recombination of *p53*$^{\Delta E5\text{-}6}$ in the Ptch1p53$^{\Delta E5\text{-}6}$ (n = 7/7) and Ptch1p53$^{\Delta/R172P}$ (n = 7/7) MBs (Figure 15C). Tissue cultured from Ptch1p53^{WT} was unable to form primary cell lines that remained viable after 3-5 weeks (n = 0/6). Having eliminated the possibility of chromosomal loss as a potential mechanism by which these tumors were capable of forming without p53 stabilization, I next investigated the question of whether additional mutations may have occurred within the p53 alleles and thereby allowed MB progression. Sanger sequencing carried out by a third party source failed to find any additional mutations within 7 Ptch1p53^{WT} tumors, as well as finding no novel mutations within 5 Ptch1p53$^{WT/R172P}$ (*Ptch1*$^{+/-}$*;p53*$^{R172P/E5\text{-}6}$) and 6 Ptch1p53$^{\Delta/R172P}$ MBs, though the expected G515C mutation was detected (Figure 15D-D'). Deep sequencing conducted by collaborator Chaoyang Li found that in 1 of the 7 Ptch1p53^{WT} tumors, a p53 mutant subpopulation existed, and accounted for 15.6% of total cell population (data not shown). The presence of accumulated p53 was confirmed both on tissue and through western blot, with elevated p53 detected in both Ptch1p53$^{\Delta E5\text{-}6}$

and Ptch1p53$^{\Delta/R172P}$ (Figure 15E-F). In spite of elevated levels of p53^{R127P} in the Ptch1p53$^{\Delta/R172P}$ model, only 1 of 17 samples showed accumulation of p53 target p21 (Figure 15F). Curiously, although the p53 antibody was demonstrated to have affinity for both wild type and mutant p53 (Figure 5B), detected level of p53^{R172P} was notably higher in the Ptch1p53$^{\Delta/R172P}$ models, indicating that p53^{R172P} might be preferentially stabilized (Figure 15F). These results demonstrate that p53 is not targeted during the formation of MBs, and remains a viable therapeutic target.

3.2.2 Radiation-induced stress on MB activates the p53 pathway

Having observed that PNLs are fully capable of progressing to MBs without inducing p53, I next sought to determine the differential therapeutic effect observed between SHH-MBs in the context of wild type and mutant p53. In order to elevate p53 activation, animals exhibiting hydrocephalus and brain tumor associated neurological symptoms were treated with 20 Gray of radiation to the head and neck, and chased for 4 hours prior to tissue collection. Within the Ptch1p53^{WT} model, widespread apoptosis, as represented by cleaved caspase-3, and reduced proliferation, as assessed by Ki67, were observed 4 hours after treatment (Figure 16A). Within the Ptch1p53$^{\Delta/R172P}$ model, apoptotic cell frequency was not increased compared to Ptch1p53$^{\Delta E5-6}$, but a limited p53-independent apoptotic effect was observed in both models (Figure 16A-A'). Curiously, radiation was capable of inducing a limited cell cycle arrest response, showing reduced proliferation in non-apoptotic cells of both Ptch1p53$^{\Delta/R172P}$ and Ptch1p53^{WT} (Figure 16A''). Protein was extracted from these tissue and it was demonstrated that, where p53 was expressed in the Ptch1p53$^{\Delta E5-6}$ and Ptch1p53$^{\Delta/R172P}$ models even without radiation, it was only with the elevated level of p53 activation following radiation that p53^{R172P} was able to promote it's downstream targets, including the cell cycle arrest protein p21 (Figure 15F'). This matched with results obtained using quantitative RT-PCR, demonstrating that after radiation therapy, both apoptotic target *Puma* and cell cycle arrest target *p21* were elevated (Figure 16B). Although differential proliferation and apoptosis was not demonstrated in the Ptch1p53$^{\Delta E5-6}$ model at 4 hours after radiation, a response was seen 24-hours after treatment with 4 centigray (cGy) radiation, resulting in decreased proliferation in both Ptch1p53$^{\Delta E5-6}$ and Ptch1p53$^{\Delta/R172P}$ (Figure 17A-B).

Curiously, although the p21 response was only visible by western blot 4 hours after IR, p21 was stabilized in many cells of the Ptch1p53$^{\Delta/R172P}$ model 24 hours after radiation. Based on these data, it is evident that elevated p53 activation is sufficient to induce a potent p53 response, but that without the presence of wild type p53, the radiation response will be insufficient to effectively treat MB.

3.2.3 The Sox2-positive subpopulation of MB cells is treatment-resistant

As I have demonstrated that Sox2-positive cells were present even at early stages of MB development (Figure 9D), I next attempted to determine the p53 response of the Sox2-positive MB population. Similar to the behavior of Sox2-positive cells found in PNLs, I demonstrated that Sox2-positive cells within MBs were rarely labeled with p53, and while the frequency of p53 positivity was marginally higher within both the Ptch1p53$^{\Delta E5\text{-}6}$ and Ptch1p53$^{\Delta/R172P}$ models, the presence of mutant p53 did not lead to a drastic increase in p53 frequency (Figure 18B). However, following 20 cGy radiation dose followed by a 4-hour chase, many Sox2-positive cells express p53. The frequency with which p53 and Sox2 colocalized following a low dose, 4 gray radiation treatment was significantly elevated compared to , and showed a widespread induction of p53 in all groups, but most prominently within the Ptch1p53^{WT} model, where 88% of Sox2-positive cells would activate p53 at high levels following radiation (Figure 18A). Surprisingly, many Sox2-positive cells remained p53 negative following stimulation in both the Ptch1p53$^{\Delta E5\text{-}6}$ and Ptch1p53$^{\Delta/R172P}$ models, indicating that the p53 response of Sox2-positive cells is not a homogenous response, and likewise that Sox2-positive cells are able to at least partially avoid p53 activation in times of stress (Figure 18B). Although my previous observations indicated that overall proliferation decreased following the activation of p53 (Figure 17A-B), I found that the proliferation frequency of Sox2-positive cells remained unchanged following radiation treatment, although proliferative Sox2-positive cells in the Ptch1p53^{WT} model were rare regardless of treatment, limiting the potential effect of any p53 response (Figure 19A-C). Likewise, in the Ptch1p53$^{\Delta/R172P}$ model, but not Ptch1p53$^{\Delta E5\text{-}6}$ or Ptch1p53^{WT}, p27 positive cells were present following radiation, but the p27 positive cells did not colocalize with Sox2, once again indicating that Sox2 is likely a treatment-resistant population lacking a complete p53 response

(Figure 19C). These results show that although the majority of MB cells are p53-activation sensitive in the presence of wild type *p53*, the Sox2-positive cell population is a privileged stem-like population, frequently quiescent throughout MB progression and resistant to activation of p53-mediated apoptosis.

3.2.4 Irradiation of PNLs reduces tumor burden in p53^{WT} SHH-MB

By treating MBs arising in symptomatic animals, I was able to elicit a strong p53-mediated apoptotic response, demonstrating that therapeutic value of p53 in developed tumors. To determine whether p53 activation was below a critical threshold within the retained GCPs of the Ptch1p53^{WT} PNL, I administered a clinically relevant course of radiation at the rate of 2 centiGray (cGy) per day, beginning the week after postnatal cerebellar development (P22-P24) and continuing for two 5-day courses, before specimens were collected at one of three times, either at 24 hours after the final radiation dose, to demonstrate an acute radiation response, at postnatal day 46, thereby demonstrating the impact on MB progression compared to untreated samples, and in SHH-MBs, determining differential survival in mutant models (Figure 20A). I analyzed specimens taken 24 hours post radiation treatment and found that PNLs within specimens from each of the aforementioned models were smaller than those observed at P22 (Figure 20B-C). However, while all three models were reduced in PNL area, though not in the number of PNLs compared to what was observed at P22, the number of proliferative cells in PNL of both Ptch1p53$^{\Delta/R172P}$ (n = 5) and Ptch1p53^{WT} (n = 5) was reduced, with most PNLs featuring less than 10 proliferative cells, whereas the Ptch1p53$^{\Delta E5\text{-}6}$ model retained a proliferative population (Figure 20B, 21C). Further, unlike Ptch1p53$^{\Delta/R172P}$ PNLs at P22, where a mixture of high and low p53 lesions were observed (Figure 11A), all PNLs within the P35 treated cerebella lacked p53 stabilization (Figure 20B, 20B'). While cells with the dense, rounded bodies characteristic of granular neurons are not found in untreated PNL from both Ptch1p53$^{\Delta E5\text{-}6}$ and Ptch1p53$^{\Delta/R172P}$, although occasionally present in untreated Ptch1p53^{WT} PNL, I found that cells with the morphology of granular neurons was heightened in all three models following radiation, with the majority of cells adopting this morphology in almost all p35 PNLs from the Ptch1p53$^{\Delta/R172P}$ and Ptch1p53^{WT} models (Figure 20C-C'). Even within proliferative PNL from the

Ptch1p53$^{\Delta E5\text{-}6}$ model, I identified small clusters of non-proliferative cells with IGL-like morphology (Figure 20B, 20C'). These observations demonstrate that irradiation of PNLs is capable of inducing a potent inhibitory effect on pre-neoplastic lesions, inducing a cell cycle arrest and differentiation response even in the presence of reduced p53 activity, as demonstrated by Ptch1p53^{R172P}. Curiously, a potent p53-independent radiation response was observed in the Ptch1p53$^{\Delta E5\text{-}6}$ model, effectively debulking the lesion without effectively eliminating the proliferative cell population.

I next investigated the role cell cycle arrest and differentiation played on the PNLs, and found that while cells of PNL from the Ptch1p53$^{\Delta E5\text{-}6}$ model were often p27 positive, indicative of cell cycle arrest, they were rarely NeuN positive, with only a handful of NeuN positive cells in or adjacent to the ML (Figure 21A). Within the Ptch1p53$^{\Delta/R172P}$ and Ptch1p53^{WT} models, almost all p27 cells found in PNLs co-labeled with NeuN, indicative of differentiated neurons, a process reminiscent of GCP differentiation and migration as would be observed during cerebellar development. Moreover, within Ptch1p53$^{\Delta/R172P}$, a large number of P27/NeuN positive cells were located within the molecular layer, demonstrating that cells not only converted into granular neurons, but also migrating toward the IGL in response to p53 activation. However, in spite of the success in reducing PNL size and proliferation, the Sox2-positive population only responded to radiation treatment within the Ptch1p53^{WT} model (Figure 21B, 21D-D'). This demonstrated that Sox2-positive cells, in addition to resisting p53-mediated apoptosis at end stage, are also capable of avoiding the p53-mediated cell cycle arrest response. Although there was little evidence of Sox2-positive cell differentiation, Sox2-positive cells remained largely quiescent (Figure 21E). These observations, taken together, indicate that, within the SHH-MB model, p53-stimulation was capable of inducing a p53-mediated response capable of both removing abnormal cells, as indicated by reduced PNL size, and causing initiation of a differentiation process, as shown through the transformed morphology of the PNL cells.

3.2.5 Sox2-positive cells in PNLs are targeted by p53-mediated apoptosis but not cell cycle arrest

I next sought to understand the long-term reaction of PNL to radiation treatment, and therefore collected PNLs found within treated CB at postnatal day 46, and inspected the size of the cerebella. I found that within all three models, the area of PNLs was reduced compared to untreated P46 (Figure 22A). I used each of the models to demonstrate different facets of radiation response, both through p53-dependent and independent mechanisms, to fully explore the PNL treatment response. I found that the greatest reduction in PNL area (85%) was observed within the Ptch1p53$^{\Delta E5\text{-}6}$ model, demonstrating a strong p53-independent radiation response (Figure 22B, B'). Likewise, there was a 65% reduction in PNL area in untreated Ptch1p53$^{\Delta/R172P}$, demonstrating the p53-mediated cell cycle arrest activity response when stimulated (Figure 22B''). Within the Ptch1p53^{WT} model, only a marginal reduction following the prolonged treatment was observed, indicating that the p53-mediated apoptotic response is already capable eliminating many of the PNLs, however, small proliferative lesions were still observed in the Ptch1p53^{WT} model following the therapeutic course (Figure 22B'''). With these three models, a stepwise response to radiation-induced stress was identified, both in a p53 dependent and independent fashion. Based on the observed reduction in size, I sought to demonstrate whether proliferation was likewise reduced compared to untreated specimens (Figure 22D-E). Surprisingly, I found that in both Ptch1p53$^{\Delta E5\text{-}6}$ and Ptch1p53$^{\Delta/R172P}$ models, the proliferation rate was radically increased in PNLs after treatment, whereas proliferation remained infrequent in the Ptch1p53^{WT} model (Figure 22E). These results show an unexpected tumor purification process within the treated p53 mutant tumors, showing a drastically enriched proliferative population.

Based on the reduced PNL size and increased proliferation, as well as my observations from the acute treatment response, I proposed a model in which radiation-induced stress was sufficient to selectively remove non-proliferative cells from the tumor mass but fails to target the quiescent Sox2-positive niche, which is capable of reforming into highly proliferative PNLs, mimicking the proposed recurrence of MBs following treatment. I found that proliferative Sox2-positive cells were drastically enriched within

the Ptch1p53$^{\Delta/R172P}$ model, unlike the Ptch1p53$^{\Delta E5\text{-}6}$ model, unchanged by treatment, or the Ptch1p53^{WT} model, where Sox2-positive cells remained quiescent (Figure 23A-B). I next determined that p53 was not a prominent label in these Sox2-positive cells, indicating that, in spite of the more frequent proliferation, these cells more resembled the Sox2-positive population observed in PNLs and MBs, not those previously described as existing during cerebellar development (Figure 23C-D). Curiously, the enriched proliferation observed in Sox2-positive cells of the treated PNL did not persist into SHH-MBs, where Sox2-positive cells were once again quiescent (Figure 24E). Similar to PNL, apoptosis was a rare process though apoptotic cells were observed in all models, regardless of *p53* mutation (Figure 22C). These observations indicate that radiation treatment efficacy is largely determined by the status of p53 in the MB models, but that only when p53 activation surpasses a critical threshold is it possible to efficiently target all cell populations. Otherwise, a p53-activation resistant population, including Sox2-positive stem-like cells, will remain, evading treatment and potentially leading to tumor recurrence.

3.2.6 Radiation treatment of MB requires wild type p53

Based on these results, I next sought to determine whether the radiation treatment was successfully preventing tumor formation. I began by collecting samples that had been given the same treatment described, but allowed mice to progress until they demonstrated neural symptoms (Figure 24A, 24C). Unsurprisingly, I found that within the Ptch1p53^{WT} model, tumor penetrance was reduced from 38% to 12% as a result of the treatment protocol, as well as increasing median survival by 28 days, and a similar response within the Ptch1p53$^{WT/R172P}$ model, which sees a decline from 44% to 10% penetrance (Figure 24A-B). On the other hand, I observed minimal alterations to the Ptch1p53$^{\Delta E5\text{-}6}$ and Ptch1p53$^{\Delta/R172P}$ models, with no change in penetrance and an eleven and two day increase in median life, respectively. Each model produced MBs featuring histological hallmarks of human MB, and these tumors were aggressive with high frequency of proliferation, much like MBs forming without treatment (Figure 24C-E). Unlike recent publications that suggested frequent mutation to p53 can be found in recurrent SHH-MBs (Hill et. al., 2015, Tamayo-Orrego et. al., 2016), I found that p53

protein was not detectable within irradiated Ptch1p53^{WT} model, although it was present at high frequency in tumors arising from Ptch1p53$^{WT/R172P}$ (Figure 25A). In order to further explore this question, I isolated p53 from the Ptch1p53$^{\Delta/R172P}$, Ptch1p53^{WT} and Ptch1p53$^{WT/R172P}$ models, and submitted the isolated p53 for Sanger sequencing, which found no additional mutations within the *p53^{WT}* allele. While I was unable to find mutations to the p53 allele, I did demonstrate that, in both instances of MBs arising within Ptch1p53$^{WT/R172P}$, p53 underwent loss of heterozygosity following treatment, thereby providing a model mimicking recurrent SHH-MBs (Figure 25B). These result provide evidence that p53 signaling is eliminated following selective pressure in SHH-MBs, and suggests that wild type p53 SHH-MBs do not activate p53 in response to oncogenic stress during tumor progression.

3.3 Summary

In this chapter, I have investigated the response of MBs and PNLs to p53 activation, attempting to elevate p53 response sufficiently to impede SHH-MB formation in the presence of wild type *p53*. The majority of SHH-MBs in humans arise without mutation to *TP53* (Zhukova et. al., 2013), indicating they originate from a TP53-activation resistant cell population, thereby remaining below the level of activation capable of responding to oncogenic stress. However, it was possible to increase the frequency of p53 activation within MBs, thereby activating a potent apoptotic response within those tumors retaining wild type *p53*. Further, treatment of PNLs was able to activate p53, eliciting a strong cell cycle arrest response and blocking SHH-MB formation, in this case sufficient to reduce MB penetrance to one-third of the frequency observed without treatment.

These results provide a clear message regarding the rationale and efficacy of treatment in humans, demonstrating that the radiation response in SHH-MBs is mediated by p53. This stands in contrast to the mechanistic basis of radiation therapy in most other tumors, where radiation effects function in spite of inactivation of the p53 pathway, typically by inducing genetic damage that leads to mitotic collapse (Brachmann et. al., 1993). The effective decline in tumor penetrance following clinically relevant doses of

radiation indicate that activation of the p53 response may be an effective target in SHH-MBs, and should be investigated as soon as a viable therapeutic agent capable of activating p53 in the brain is developed. Surprisingly, I found that, although an p53-independent decline in lesion size was observed following treatment, without the retention of wild type *p53*, the PNLs were only temporarily inhibited by radiation. In fact, treated lesions produced SHH-MBs with equivalent penetrance and little to no change in median survival in both the *p53* mutant models. Further, treatment of PNLs within both the *p53* mutant models resulted in the enrichment of proliferating cells, indicating a differential response to genotoxic stress amongst the cells of the PNLs, with some portion of non-proliferative cells removed and the remaining cells entering the cell cycle. This suggests that radiation treatment may in fact be detrimental within *p53* mutant SHH-MBs, inducing a debulking effect but not successfully targeting proliferative cells capable of tumor recurrence.

My examination of the behavior of the Sox2 population of treated PNLs indicate that this differential response may arise in part as a result of the stem-like population, which appears to be capable of resisting partial p53 activation, as demonstrated with the retention of Sox2-positive cells in the $Ptch1^{+/-}p53^{\Delta/R172P}$ model. This concept is reinforced by the minimal response to radiation observed in both the treated p53 models, which, in spite of receiving radiation dose equivalent to the wild type p53 tumor, saw no change in penetrance. These data suggest reduced p53 activity as a mechanism for resistance to therapy in Sox2-positive cells (Vanner et. al., 2014). As a quiescent population, it has been proposed that Sox2-positive cells are responsible for the recurrence of MB. Based on my data, I have shown that Sox2-positive cells are capable of surviving extreme radiation dose without activating the apoptotic response, and that these cells survive early treatment only to later reenter the cell cycle, indicating that Sox2-positive cells represent a means for SHH-MB recurrence. Sox2 specific therapy may be able to target the quiescent Sox2 population, but my data suggests that the Sox2 population may become vulnerable following radiation therapy, as an increased number of Sox2-positive cells enter the cell cycle following treatment. Further investigation into the Sox2 stress

response, which appears able to drive cells into the cell cycle, may provide insight into methods of treating this cell population.

Taken together, this chapter demonstrates that the activation of wild type p53 above a threshold is capable of eliminating disease. Activation of the p53 response resulted in widespread apoptosis and elimination of almost all proliferative cells in the presence of functional p53, with almost no response when *p53* was lost. This p53 activation was so potent that within p53 heterozygous tumors, the remaining *p53* allele was lost, generating a p53 mutant tumor following radiation. This loss of *p53* is reminiscent of the frequency of *p53* mutation in recurrent human MBs, where the majority of recurrent MBs arise with inactivation of the p53 pathway (Morrissey et. al., 2016). These data suggest that recurrent MBs should be approached using the same treatment methods that are applied to SHH-MBs with mutant *p53*, and further demonstrate the need to develop a robust treatment for MBs arising with mutant *p53*.

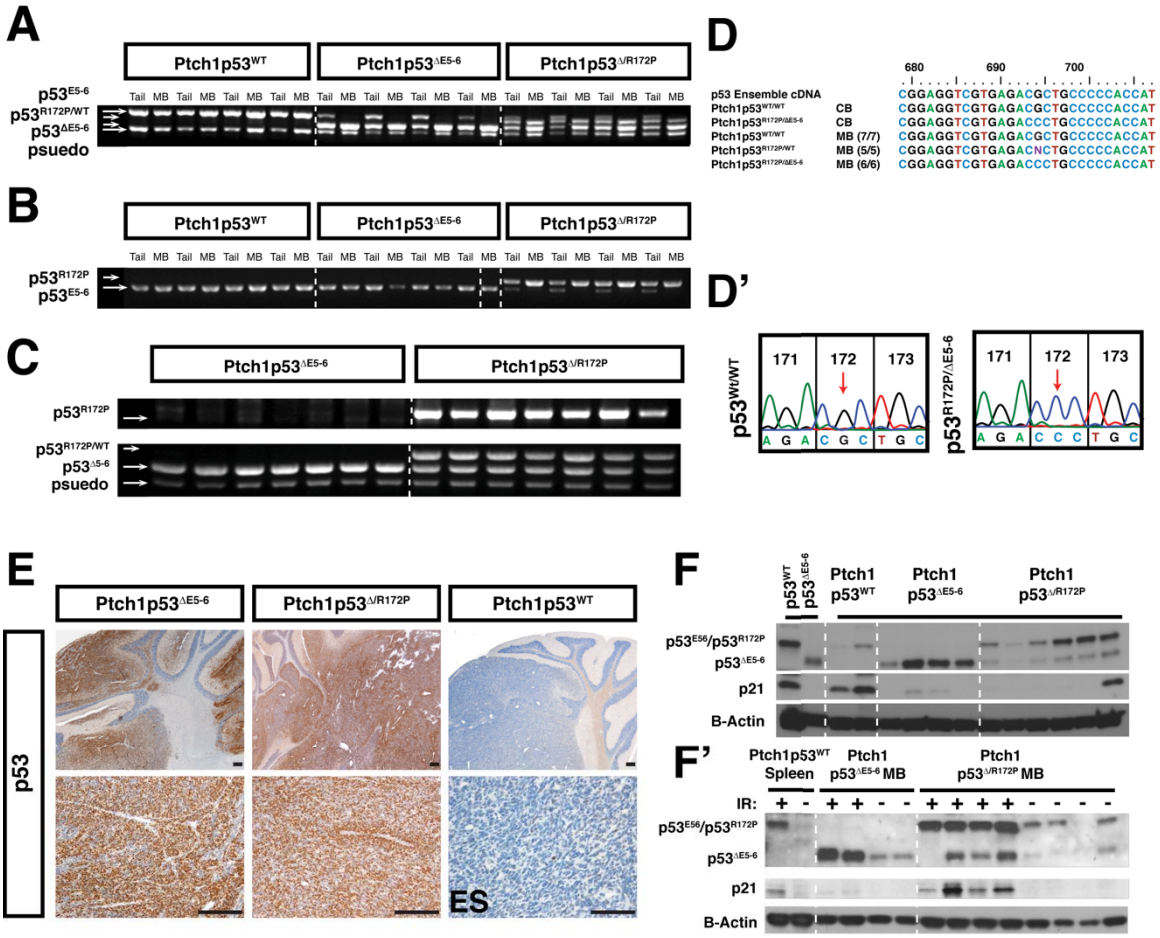
A
Ptch1p53WT
Ptch1p53ΔE5-6
Ptch1p53Δ/R172P
p53E5-6
p53R172P/WT
p53ΔE5-6
psuedo
Tail MB
B
p53R172P
p53E5-6
C
Ptch1p53ΔE5-6
Ptch1p53Δ/R172P
p53R172P
p53R172P/WT
p53Δ5-6
psuedo
D
680 690 700
p53 Ensemble cDNA
Ptch1p53WT/WT CB
Ptch1p53R172P/ΔE5-6 CB
Ptch1p53WT/WT MB (7/7)
Ptch1p53R172P/WT MB (5/5)
Ptch1p53R172P/ΔE5-6 MB (6/6)
CGGAGGTCGTGAGACGCTGCCCCCACCAT
CGGAGGTCGTGAGACCCTGCCCCCACCAT
CGGAGGTCGTGAGACNCTGCCCCCACCAT
D'
p53Wt/WT
p53R172P/ΔE5-6
171 172 173
A G A C G C T G C
A G A C C C T G C
E
Ptch1p53ΔE5-6
Ptch1p53Δ/R172P
Ptch1p53WT
p53
ES
F
p53WT
p53ΔE5-6
Ptch1 p53WT
Ptch1 p53ΔE5-6
Ptch1 p53Δ/R172P
p53E56/p53R172P
p53ΔE5-6
p21
B-Actin
F'
Ptch1p53WT Spleen
Ptch1 p53ΔE5-6 MB
Ptch1 p53Δ/R172P MB
IR:
+ - + + - - + + + + - - - -
p53E56/p53R172P
p53ΔE5-6
p21
B-Actin

Figure 15: Inactivation of p53 is not Required for MB Formation

(A-C) PCR using tail snip and mutant DNA confirms recombination of $p53^{\Delta E5\text{-}6}$ within p53 mutant tumors (A), presence of $p53^{R172P}$ within p53 mutant tumors (B) and $p53^{\Delta E5\text{-}6}$ and confirms presence of $p53^{R172P}$ within primary cell lines (C).

(D-D') Sequencing of tissue from Ptch1p53$^{\Delta/R172P}$ confirms presence of $p53^{R172P}$ and no additional mutations to p53 (D). Sequencing of Ptch1p53^{WT} fails to find any acquired p53 mutation (N = 7, data not shown). Schematic showing the location of the p53R172P mutation, caused by G515C (D').

(E) Low and high magnification images of MBs from Ptch1p53$^{\Delta E5\text{-}6}$, Ptch1p53$^{\Delta/R172P}$ and Ptch1p53^{WT} model labeled with anti-p53 antibody, with hematoxylin counterstain. Scale bars represent 100 um.

(F-F') Immunoblotting of p53 and p21 protein levels in untreated MBs (F) and MBs collected 4 hours after treatment with 20 Gray (F'). B-Actin was used as a loading control.

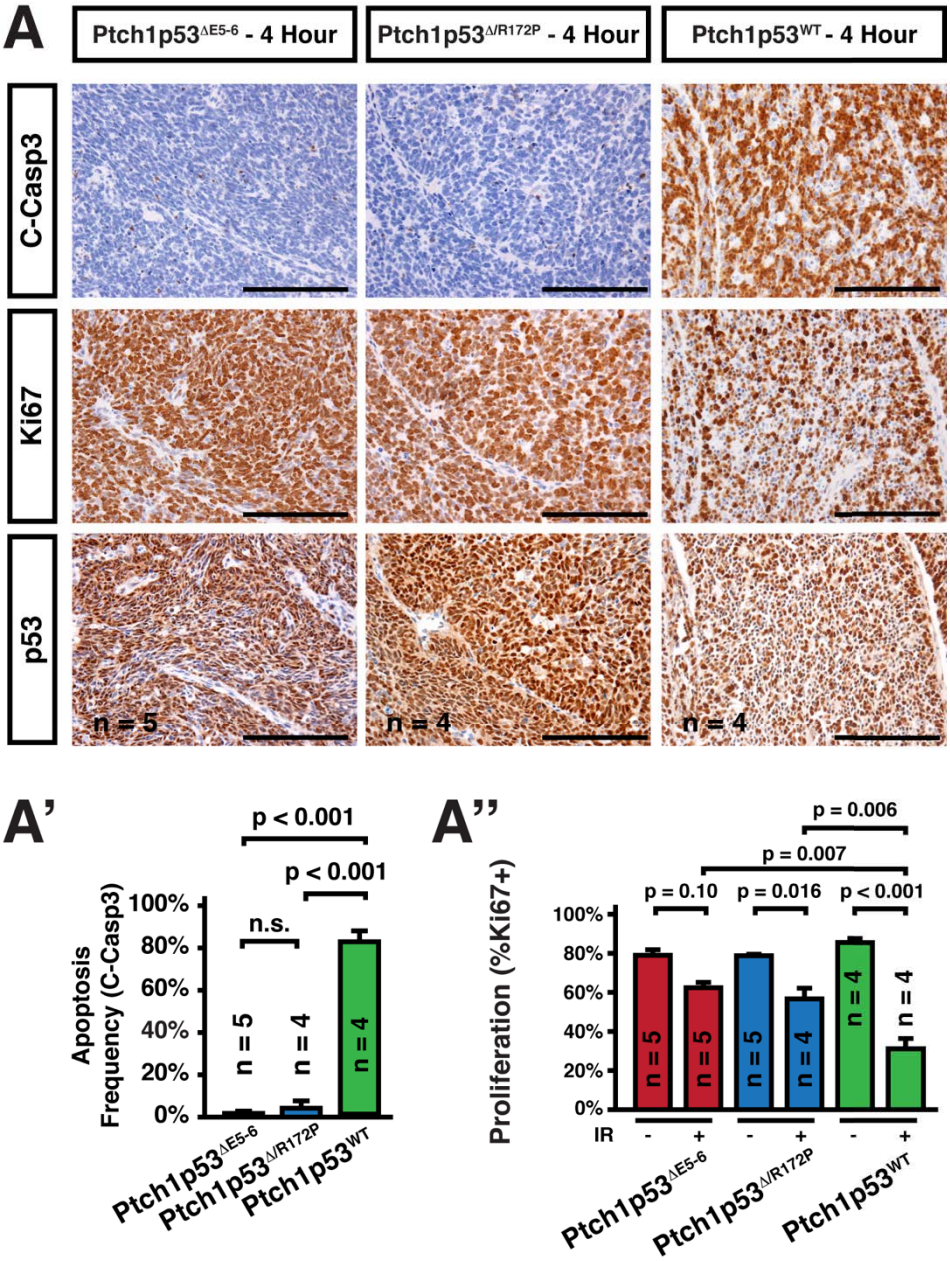
A
Ptch1p53ΔE5-6 - 4 Hour
Ptch1p53Δ/R172P - 4 Hour
Ptch1p53WT - 4 Hour
C-Casp3
Ki67
p53
n = 5
n = 4
n = 4
A'
p < 0.001
p < 0.001
n.s.
Apoptosis Frequency (C-Casp3)
100%
80%
60%
40%
20%
0%
n = 5
n = 4
n = 4
Ptch1p53ΔE5-6
Ptch1p53Δ/R172P
Ptch1p53WT
A''
p = 0.006
p = 0.007
p = 0.10
p = 0.016
p < 0.001
Proliferation (%Ki67+)
100%
80%
60%
40%
20%
0%
n = 5
n = 5
n = 5
n = 4
n = 4
n = 4
IR
- + - + - +
Ptch1p53ΔE5-6
Ptch1p53Δ/R172P
Ptch1p53WT
B
p = 0.01
p = 0.006
p = 0.02
p = 0.09
p = 0.011
Ptch1p53ΔE5-6
Ptch1p53Δ/R172P
Ptch1p53WT
Expression of p53 targets
800%
600%
400%
200%
0%
IR: - + - + - + - + - + - + - + - + - + - +
Puma
P21
MDM2

Figure 16: Radiation is Capable of Activating p53 in MB

(A) Immunohistochemistry images of cleaved caspase-3, Ki67, and p53 in MBs collected 4 hours after treatment with 20 Gray radiation.

(A') Quantification of apoptotic frequency, as assessed by Cleaved Caspase-3 in MBs from the Ptch1p53$^{\Delta E5\text{-}6}$, Ptch1p53$^{\Delta/R172P}$, and Ptch1p53^{WT} models following radiation.

(A'') Quantification of proliferation frequency, as demonstrated by Ki67 staining of treated animals and littermate controls.

(B) Quantitative RT-PCR determined expression of p53 targets PUMA, p21, and MDM2 in untreated MBs and MBs collected 4 hours after treatment with 20 Gray. Fold change was normalized against untreated Ptch1p53^{WT} MBs, and GAPDH was used as a control.

Scale, 100 um. Error bars represent Mean ± SEM. Unpaired, two-tailed students T-Tests were used to determine p-values.

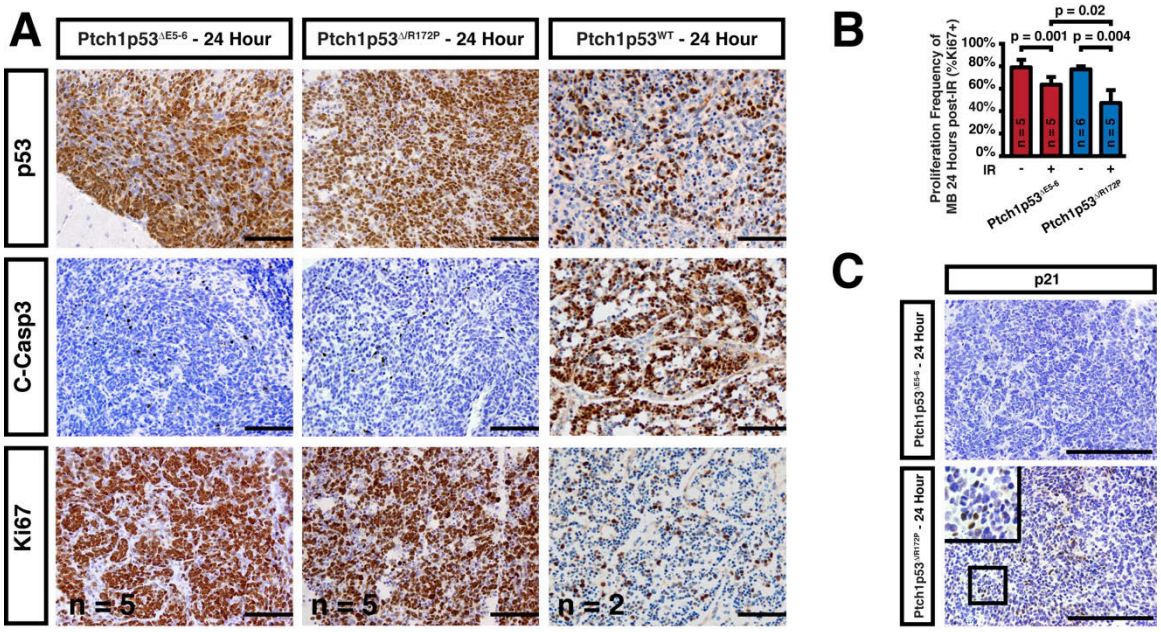

Figure 17: Radiation Activates both Apoptotic and Cell Cycle Arrest Responses

(A) Histopathological analysis of MBs collected 24 hours following a 4 Gray radiation dose, labeling p53, Cleaved Caspase-3 and Ki67 in the Ptch1p53$^{\Delta E5\text{-}6}$, Ptch1p53$^{\Delta/R172P}$ and Ptch1p53^{WT} models.

(B) Quantification of proliferation frequency from Ptch1p53$^{\Delta E5\text{-}6}$ and Ptch1p53$^{\Delta/R172P}$ littermates, comparing proliferation between untreated MBs and MBs collected 24 hours after a 4 Gray treatment.

(C) Histopathological analysis of MBs collected 24 hours following a 4 Gray radiation dose, labeling p21 in the Ptch1p53$^{\Delta E5\text{-}6}$ and Ptch1p53$^{\Delta/R172P}$ models. The boxed region is shown enlarged in the inset.

Scale bars represent 100 um.

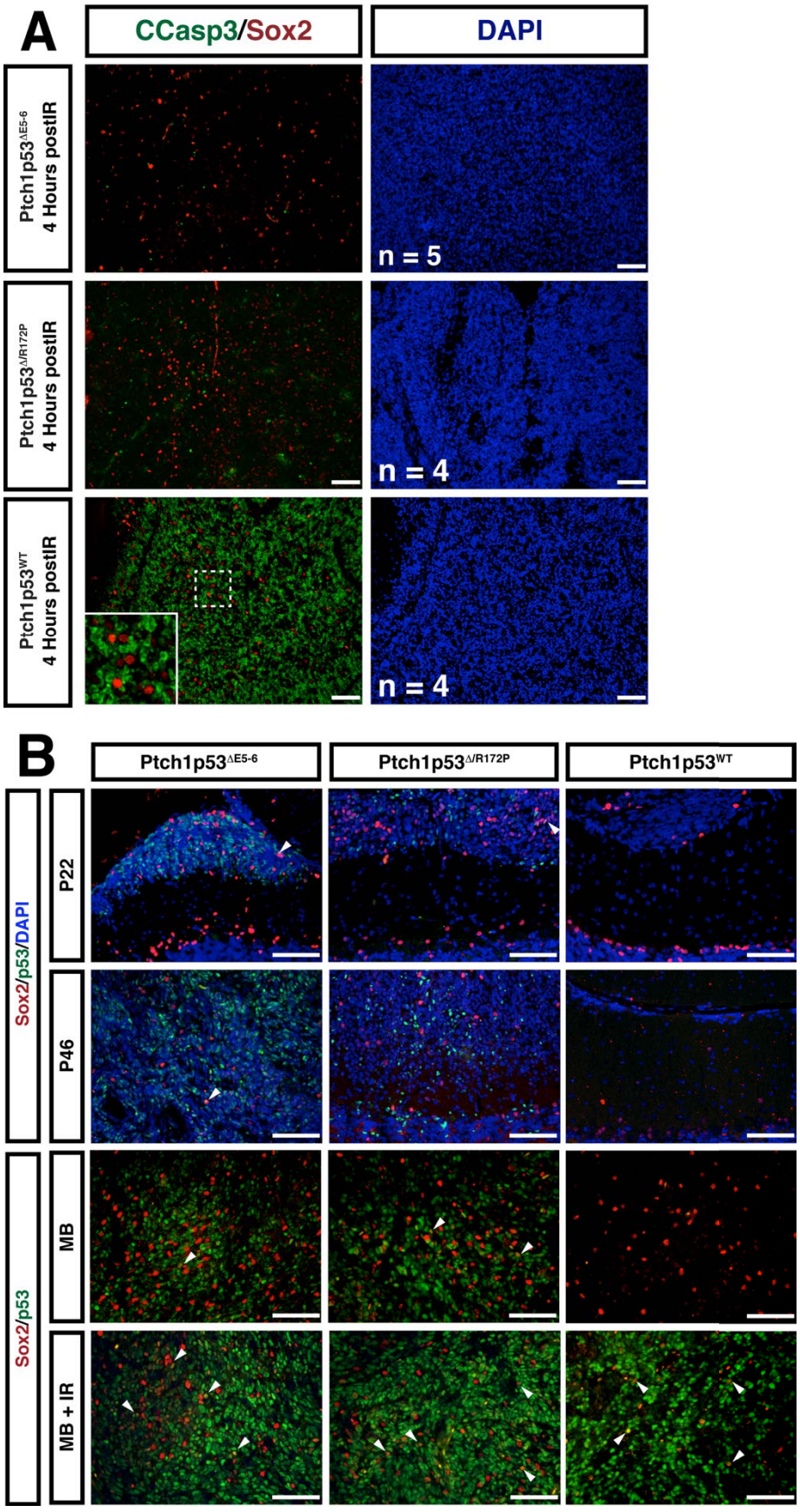
A
CCasp3/Sox2
DAPI
Ptch1p53ΔE5-6 4 Hours postIR
Ptch1p53Δ/R172P 4 Hours postIR
Ptch1p53WT 4 Hours postIR
n = 5
n = 4
n = 4
B
Ptch1p53ΔE5-6
Ptch1p53Δ/R172P
Ptch1p53WT
Sox2/p53/DAPI
P22
P46
Sox2/p53
MB
MB + IR

Figure 18: Sox2 Positive Cells evade Radiation via Decreased p53 Response

(A) Co-localization of cleaved Caspase-3 and Sox2 in MBs collected 4 hours after treatment with 20 centigray from the Ptch1p53$^{\Delta E5\text{-}6}$, Ptch1p53$^{\Delta/R172P}$ and Ptch1p53^{WT} models. Note that, in all three models, Sox2 rarely colabels with cleaved Caspase-3. Inset shows high magnification of boxed region.

(B) Co-localization of p53 and Sox2 in representative images of P22 and P46 PNL, untreated MBs and treated MBs from the Ptch1p53$^{\Delta E5\text{-}6}$, Ptch1p53$^{\Delta/R172P}$ and Ptch1p53^{WT} models. DAPI counterstain is shown in P22 and P46 to delineate the boundary of the PNLs, whereas tumor images were all taken within the tumor mass. Arrowheads indicate colocalized cells.

Scale bar depicts 100 uM.

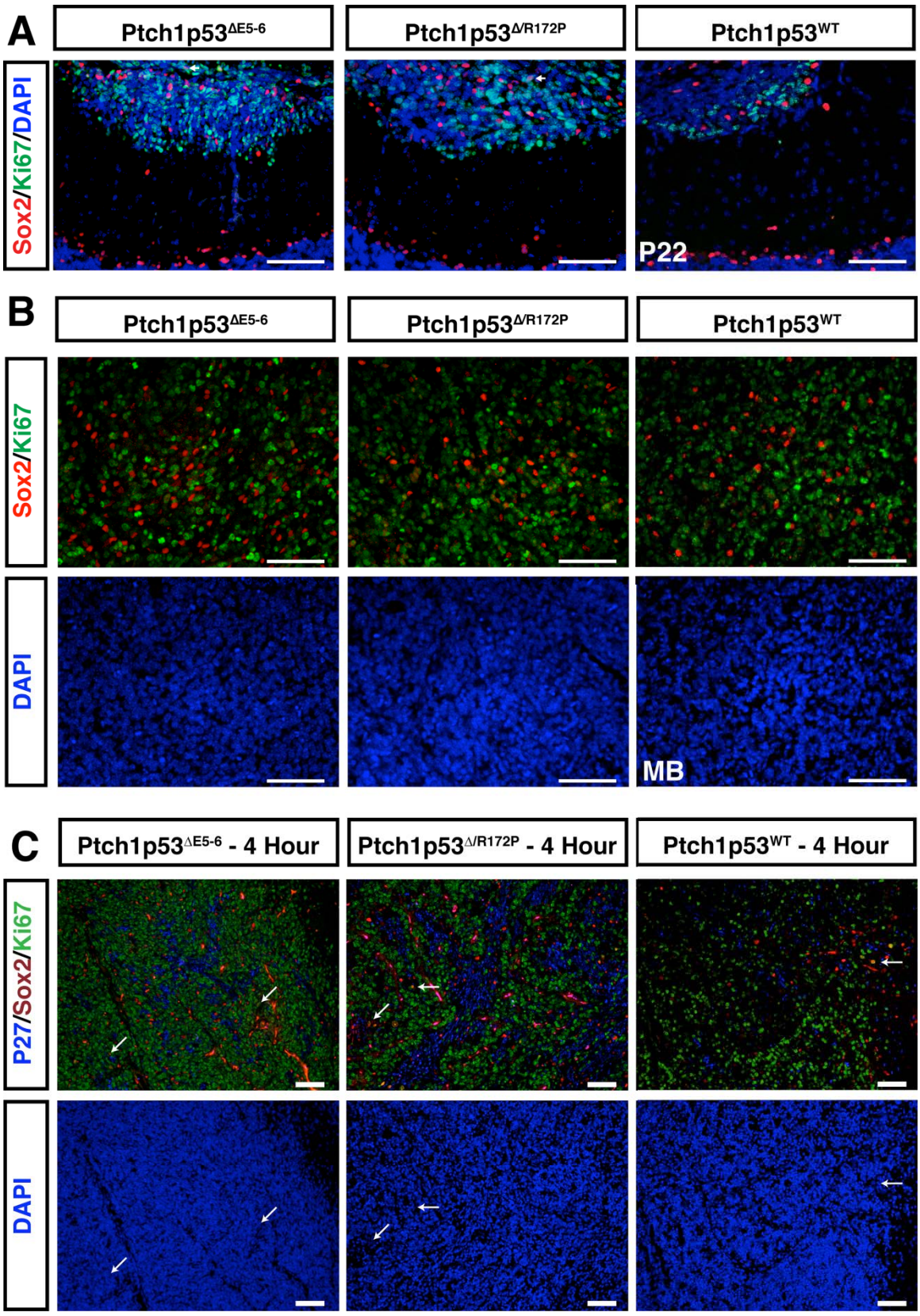
A
Ptch1p53ΔE5-6
Ptch1p53Δ/R172P
Ptch1p53WT
Sox2/Ki67/DAPI
P22
B
Ptch1p53ΔE5-6
Ptch1p53Δ/R172P
Ptch1p53WT
Sox2/Ki67
DAPI
MB
C
Ptch1p53ΔE5-6 - 4 Hour
Ptch1p53Δ/R172P - 4 Hour
Ptch1p53WT - 4 Hour
P27/Sox2/Ki67
DAPI

Figure 19: Sox2-positive cells maintain Quiescence through a p53-mediated Response

(A) Co-labeling of Sox2 and Ki67 in P22 PNL from the Ptch1p53$^{\Delta E5\text{-}6}$, Ptch1p53$^{\Delta/R172P}$ and Ptch1p53^{WT} models. Note that co-localization is uncommon in all models.
(B) Co-labeling of Sox2 and Ki67 in MBs from the Ptch1p53$^{\Delta E5\text{-}6}$, Ptch1p53$^{\Delta/R172P}$ and Ptch1p53^{WT} models.
(C) Co-labeling of p27, Sox2 and Ki67 in MBs from the Ptch1p53$^{\Delta E5\text{-}6}$, Ptch1p53$^{\Delta/R172P}$ and Ptch1p53^{WT} models 4 hours after receiving 20 centigray irradiation. Arrows indicate co-localization of Ki67 and Sox2.
DAPI was used as a nuclear counterstain. Scale bar depicts 100 uM.

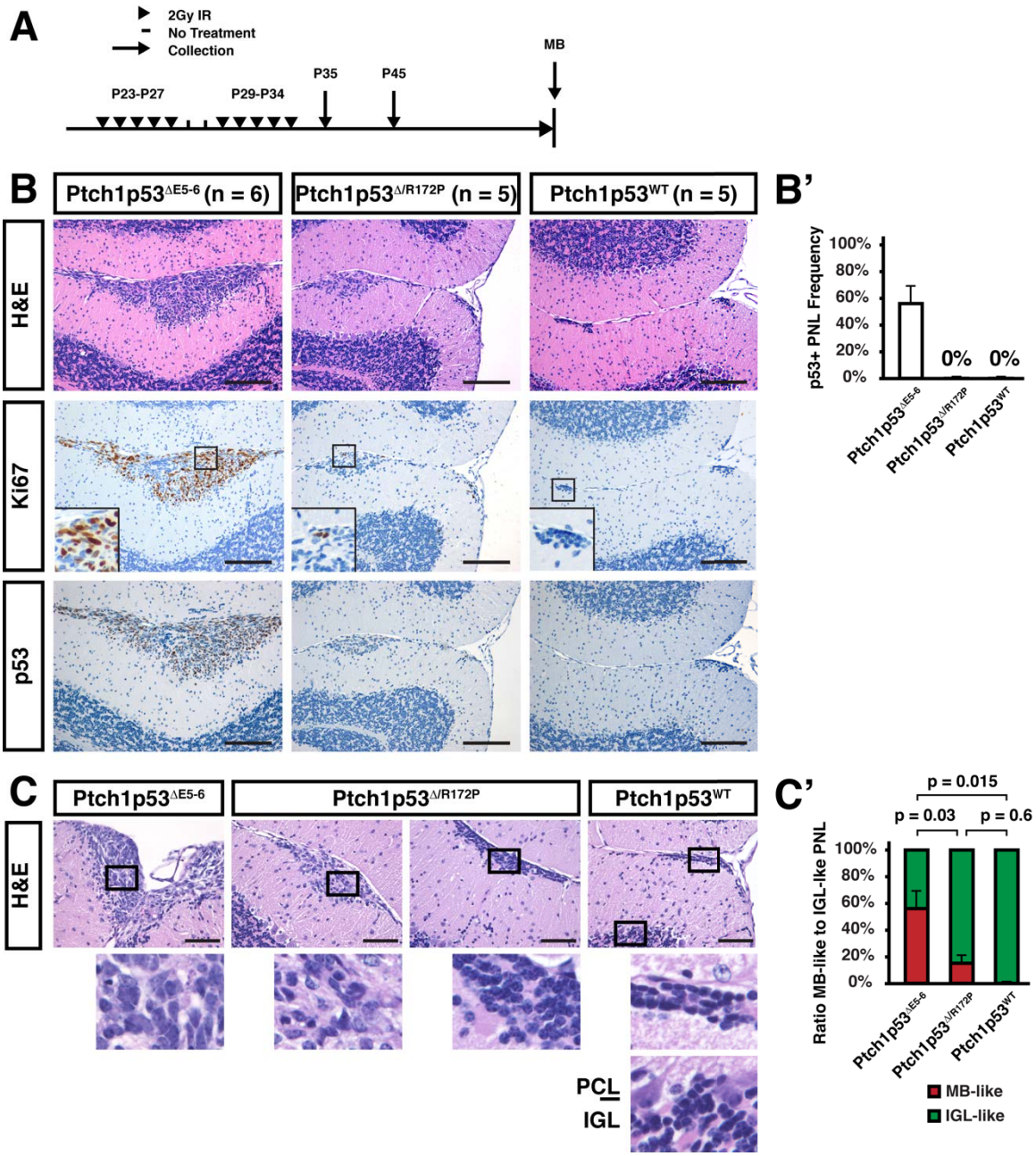
A
2Gy IR
No Treatment
Collection
P23-P27
P29-P34
P35
P45
MB
B
Ptch1p53ΔE5-6 (n = 6)
Ptch1p53Δ/R172P (n = 5)
Ptch1p53WT (n = 5)
H&E
Ki67
p53
B'
p53+ PNL Frequency
100%
80%
60%
40%
20%
0%
0%
0%
Ptch1p53ΔE5-6
Ptch1p53Δ/R172P
Ptch1p53WT
C
Ptch1p53ΔE5-6
Ptch1p53Δ/R172P
Ptch1p53WT
H&E
PCL
IGL
C'
p = 0.015
p = 0.03
p = 0.6
Ratio MB-like to IGL-like PNL
100%
80%
60%
40%
20%
0%
Ptch1p53ΔE5-6
Ptch1p53Δ/R172P
Ptch1p53WT
MB-like
IGL-like

Figure 20: Radiation Treatment of Pre-neoplastic Lesions Activates a potent p53 response, inducing cell cycle arrest and differentiation

(A) Graphical representation of long term treatment scheme, wherein mice were irradiated for 5 days given 2 rest days, and then irradiated 5 days more, beginning at P21-23, and then mice were collected at one of three indicated time points, P35, P46, or upon MB associated neurological symptoms.

(B) Images taken of H&E, anti-Ki67, and anti-p53 mutants from the Ptch1p53$^{\Delta E5\text{-}6}$, Ptch1p53$^{\Delta/R172P}$ and Ptch1p53^{WT} models collected 24 hours after the completion of long-term IR treatment scheme, in which mice were subjected to a 2 Gray per day dose ionizing radiation for a total of 10 days beginning at P22-P23 and ending at P34-P35. Insets show high magnification of boxed regions. Scale bars show 200 um.

(B') Calculation of the frequency of p53 positivity in P35 treated PNLs, as calculated based on histology.

(C) High magnification H&E images show cellular morphology, with the boxed region(s) shown below at increased magnification, demonstrate that cells of the IR treated PNL acquire dense rounded cell bodies, reminiscent of granular neurons, in the Ptch1p53$^{\Delta E5\text{-}6}$, Ptch1p53$^{\Delta/R172P}$ and Ptch1p53^{WT} models. Scale bars show 100 um.

(C') A qualitative analysis of PNL containing a majority of cells that morphologically resemble granular neurons, characterized by small, dense rounded nuclei.

Error bars represent Mean + SEM. Unpaired, two-tailed students t-tests were used to determine p-values.

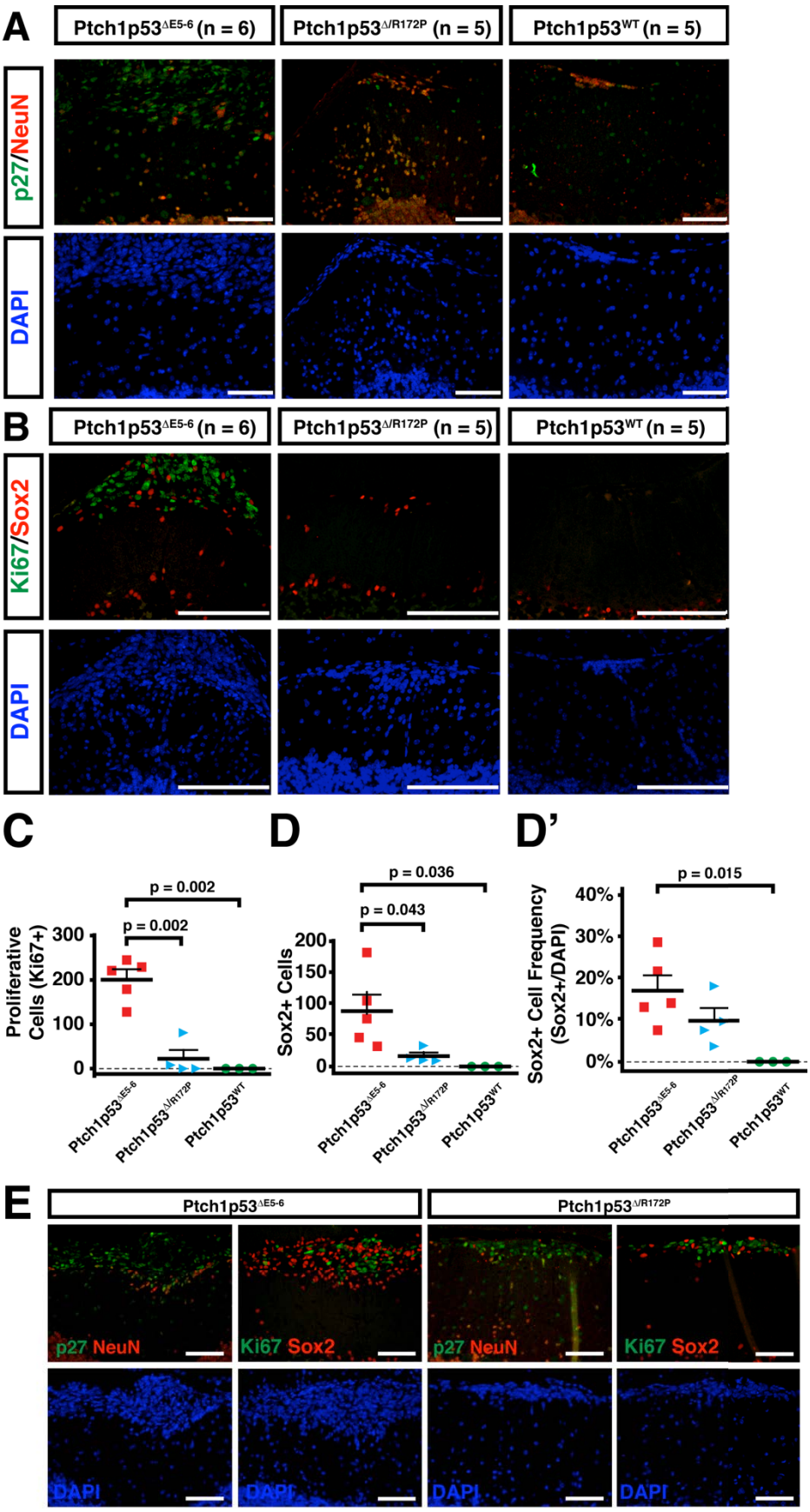
A
Ptch1p53ΔE5-6 (n = 6)
Ptch1p53Δ/R172P (n = 5)
Ptch1p53WT (n = 5)
p27/NeuN
DAPI
B
Ptch1p53ΔE5-6 (n = 6)
Ptch1p53Δ/R172P (n = 5)
Ptch1p53WT (n = 5)
Ki67/Sox2
DAPI
C
p = 0.002
p = 0.002
Proliferative Cells (Ki67+)
300
200
100
0
Ptch1p53ΔE5-6
Ptch1p53Δ/R172P
Ptch1p53WT
D
p = 0.036
p = 0.043
Sox2+ Cells
200
150
100
50
0
Ptch1p53ΔE5-6
Ptch1p53Δ/R172P
Ptch1p53WT
D'
p = 0.015
Sox2+ Cell Frequency (Sox2+/DAPI)
40%
30%
20%
10%
0%
Ptch1p53ΔE5-6
Ptch1p53Δ/R172P
Ptch1p53WT
E
Ptch1p53ΔE5-6
Ptch1p53Δ/R172P
p27 NeuN
Ki67 Sox2
p27 NeuN
Ki67 Sox2
DAPI
DAPI
DAPI
DAPI

Figure 21: Sox2-positive cells are only elminiated by radiation in the presence of p53 apoptotic response

(A) Co-localization of p27 and NeuN in PNL following P21-P35 radiation treatment in order to assess senescence and differentiation of treated PNL in the Ptch1p53$^{\Delta E5\text{-}6}$, Ptch1p53$^{\Delta/R172P}$ and Ptch1p53^{WT} models.
(B) Co-localization of Sox2 and Ki67 in PNL following P21-P35 treatment demonstrating the response of the Sox2-positive population to prolonged radiation.
(C) Quantification of total number of proliferative cells (Ki67+) in treated P35 PNLs.
(D-D') Quantification of total number of Sox2-positive cells (D) and Sox2-positive cell frequency (D') in treated P35 PNLs demonstrates retention in models without wild type p53.
(E) Co-localization of Sox2 and Ki67 in sections from outlier samples in the Ptch1p53$^{\Delta E5\text{-}6}$ and Ptch1p53$^{\Delta/R172P}$ models, showing the highest Sox2 cluster in Ptch1p53$^{\Delta E5\text{-}6}$ and the most proliferative cluster in Ptch1p53$^{\Delta/R172P}$ model. Note that frequent Sox2 corresponds with low Ki67, and likewise frequent Ki67 corresponds with lower Sox2. Additionally, co-localization of p27 and NeuN in adjacent sections demonstrates that NeuN and p27 often occur along the edges of clusters, whereas proliferative cells occupy the center of the cluster.

Scale, 200 um. Error bars represent Mean + SEM. Unpaired, two-tailed students t-tests were used to determine p-values.

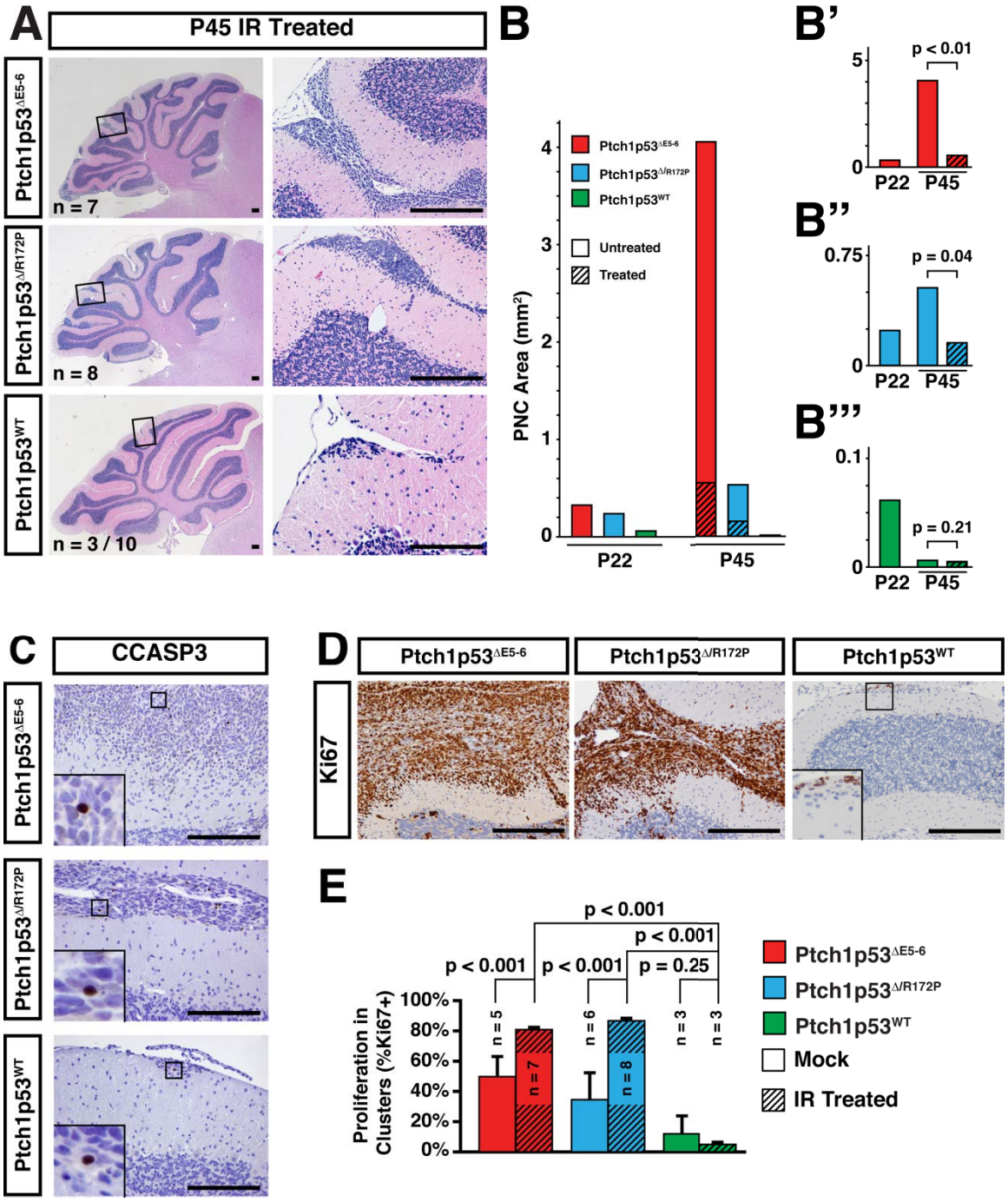
A
P45 IR Treated
Ptch1p53ΔE5-6
Ptch1p53Δ/R172P
Ptch1p53WT
n = 7
n = 8
n = 3 / 10
B
Ptch1p53ΔE5-6
Ptch1p53Δ/R172P
Ptch1p53WT
Untreated
Treated
PNC Area (mm²)
P22
P45
B'
p < 0.01
B''
p = 0.04
B'''
p = 0.21
C
CCASP3
D
Ki67
E
p < 0.001
p < 0.001
p < 0.001
p < 0.001
p = 0.25
Proliferation in Clusters (%Ki67+)
n = 5
n = 7
n = 6
n = 8
n = 3
n = 3
Mock
IR Treated

Figure 22: Impaired p53 Response Permits Enrichment of Proliferative Cells following Radiation of Pre-neoplastic Lesions

(A) H&E images taken from P21-P35 treated P46 mutants from the Ptch1p53$^{\Delta E5\text{-}6}$, Ptch1p53$^{\Delta/R172P}$, and Ptch1p53^{WT} models following a long-term IR treatment scheme, in which mice were subjected to a 2gray per day dose for a total of 10 days beginning at P21 and ending at P35. High magnification images Highlight PNLs in the treated brains.
(B) Quantification of PNL area, in mm2, comparing untreated P22 and P45 (solid bars) and P45 following long term IR treatment (striped).
(B'-B''') Enlarged charts of each mutant model show PNL area of Ptch1P53$^{\Delta E5\text{-}6}$ (B'), Ptch1P53$^{\Delta/R172P}$ (B'') and Ptch1P53^{WT} (B''').
(C) Immunohistochemistry of P46 PNL treated from P21-P35 for cleaved Caspase-3. Inset shows boxed region in high magnification.
(D) Immunohistochemistry of P46 PNL treated from P21-P35 for Ki67. Inset shows boxed region in high magnification.
(E) Quantification of proliferation in PNLs from the Ptch1p53$^{\Delta E5\text{-}6}$, Ptch1p53$^{\Delta/R172P}$, and Ptch1p53^{WT} models in untreated (Solid bars) and treated (Striped bars) mutants at P45.
Scale, 200 um. Error bars represent Mean + SEM. Unpaired, two-tailed students T-Tests were used to determine p-values.

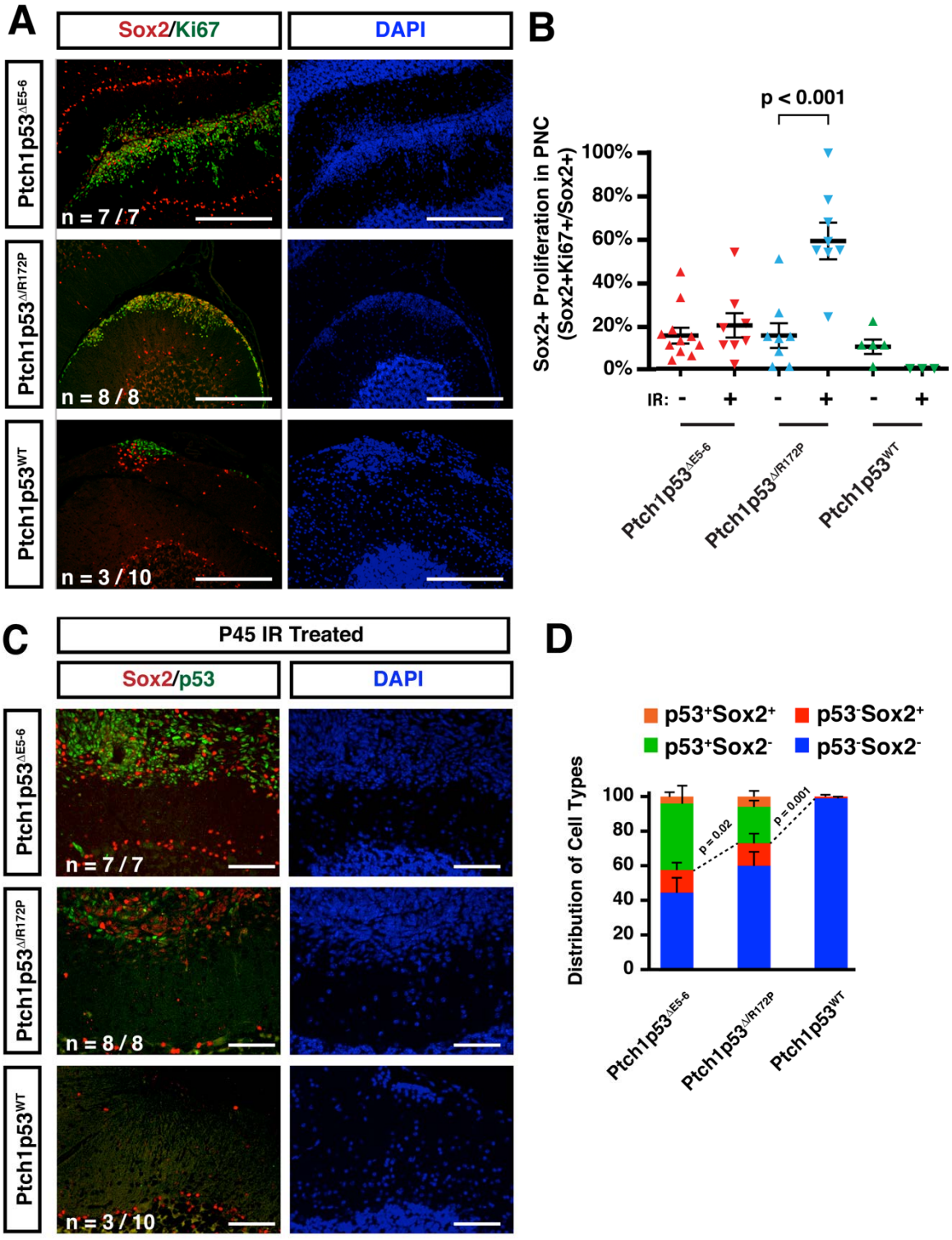
A
Sox2/Ki67
DAPI
Ptch1p53ΔE5-6
Ptch1p53Δ/R172P
Ptch1p53WT
n = 7 / 7
n = 8 / 8
n = 3 / 10
B
p < 0.001
Sox2+ Proliferation in PNC
(Sox2+Ki67+/Sox2+)
100%
80%
60%
40%
20%
0%
IR: - + - + - +
Ptch1p53ΔE5-6
Ptch1p53Δ/R172P
Ptch1p53WT
C
P45 IR Treated
Sox2/p53
DAPI
Ptch1p53ΔE5-6
Ptch1p53Δ/R172P
Ptch1p53WT
n = 7 / 7
n = 8 / 8
n = 3 / 10
D
p53+Sox2+
p53-Sox2+
p53+Sox2-
p53-Sox2-
Distribution of Cell Types
100
80
60
40
20
0
p = 0.02
p = 0.001
Ptch1p53ΔE5-6
Ptch1p53Δ/R172P
Ptch1p53WT

Figure 23: Sox2-positive cells in the Ptch1p53$^{\Delta E5\text{-}6/R172P}$ model represent a treatment-resistant population

(A) Co-localization of Sox2 and Ki67 in P46 PNL following P21-P35 treatment demonstrating the restored proliferative activity of PNL following prolonged radiation treatment. Only 3 of 10 (30%) Ptch1p53^{WT} mice retained proliferative PNL.

(B) Quantification of the rate of proliferation of the Sox2-positive cell population relative to the total Sox2-positive population (Sox2+;Ki67+ / Sox2+) in treated P46 PNLs.

(C) Co-localization of Sox2 and p53 in P46 PNL following P21-P35 treatment, with DAPI as a counterstain.

(D) Quantification of co-localization frequency of Sox2 and p53. Significantly fewer p53 positive cells were seen between each model, but no significant difference was found between Sox2-positive cell frequency.

Scale, 200 um. Error bars represent Mean + SEM. Unpaired, two-tailed students t-tests were used to determine p-values.

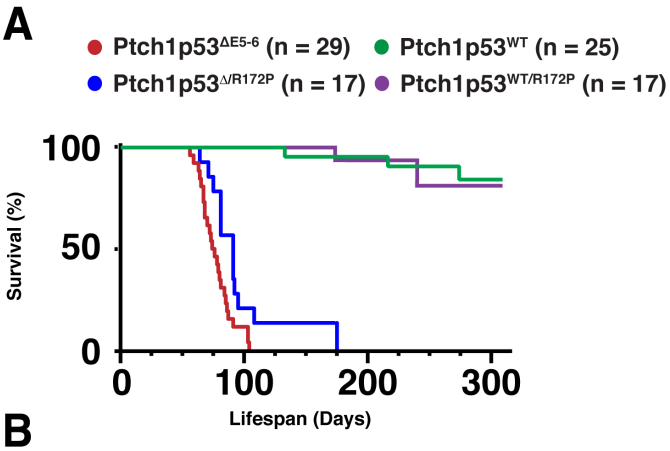

A'

	IR TRT	Median Survival	Tumor Pen.	p =
Ptch1p53$^{\Delta E5-6}$	-	64	100%	0.048
	+	75	100%	
Ptch1p53$^{\Delta/R172P}$	-	84	100%	0.39
	+	86	100%	
Ptch1p53^{WT}	-	159	38%	0.035
	+	187	12%	
Ptch1p53$^{WT/R172P}$	-	160	44%	0.025
	+	202	10.5%	

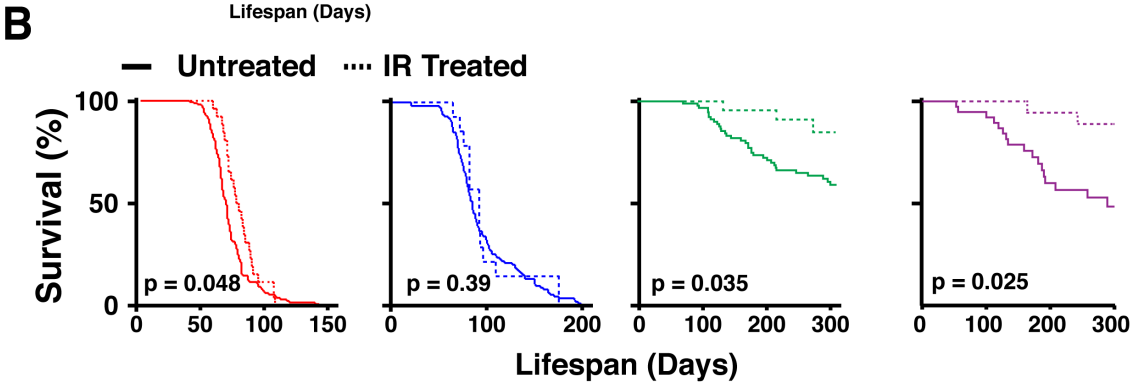

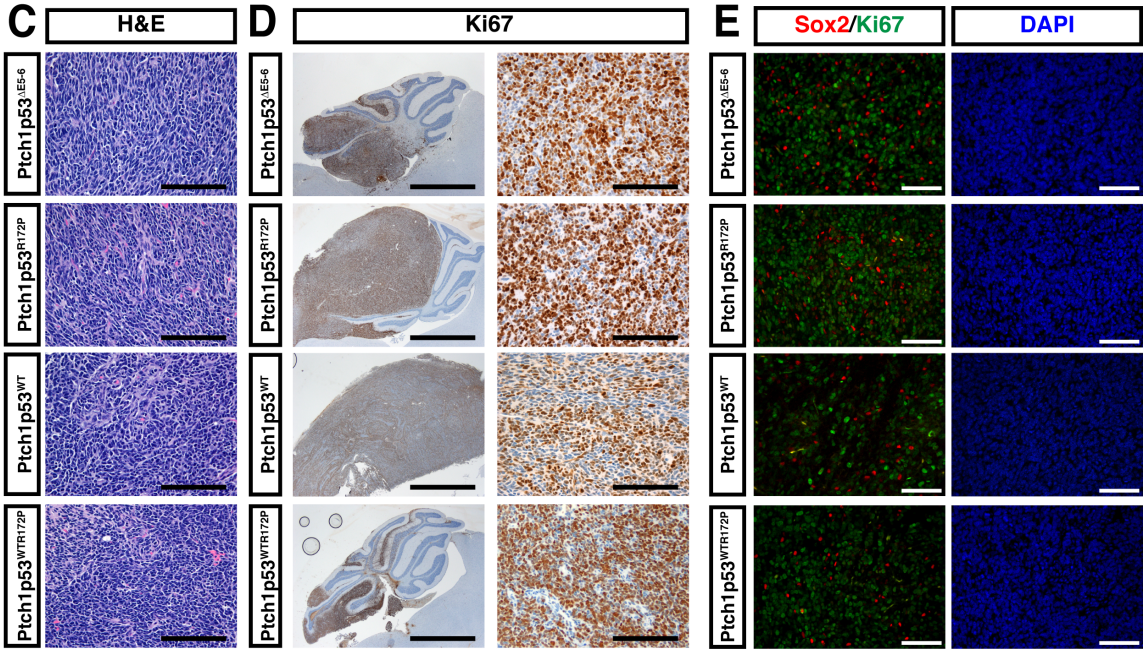

Figure 24: Treatment of Pre-neoplastic Lesions Requires Functional p53-mediated Apoptotic Response

(A) Kaplan-Meier survival curve of Ptch1p53$^{\Delta E5\text{-}6}$, Ptch1p53$^{\Delta/R172P}$, Ptch1p53^{WT} and Ptch1p53$^{WT/R172P}$ models following the long-term IR treatment scheme.

(A') Table demonstrating Median Survival and Tumor Penetrance of each model.

(B) Comparison of untreated and treated survival within each mutant model. (p, Log-rank (Mantel-Cox) test)

(C) High magnification H&E images show cellular morphology in MBs arising in the Ptch1p53$^{\Delta E5\text{-}6}$, Ptch1p53$^{\Delta/R172P}$, Ptch1p53^{WT} and Ptch1p53$^{WT/R172P}$ models from mice treated from P21-P35.

(D) Low and high magnification immunohisological images demonstrate Ki67 in treated Ptch1p53$^{\Delta E5\text{-}6}$, Ptch1p53$^{\Delta/R172P}$, Ptch1p53^{WT} and Ptch1p53$^{WT/R172P}$ models.

(E) Immunofluorescent co-labeling using anti-Sox2 and anti-Ki67 antibodies on treated Ptch1p53$^{\Delta E5\text{-}6}$, Ptch1p53$^{\Delta/R172P}$, Ptch1p53^{WT} and Ptch1p53$^{WT/R172P}$ MB.

Scale Represents 100 um in high mag images and 1mm in low mag image (D). Hematoxylin counterstain was used in DAB staining. DAPI counterstain was used in fluorescent images.

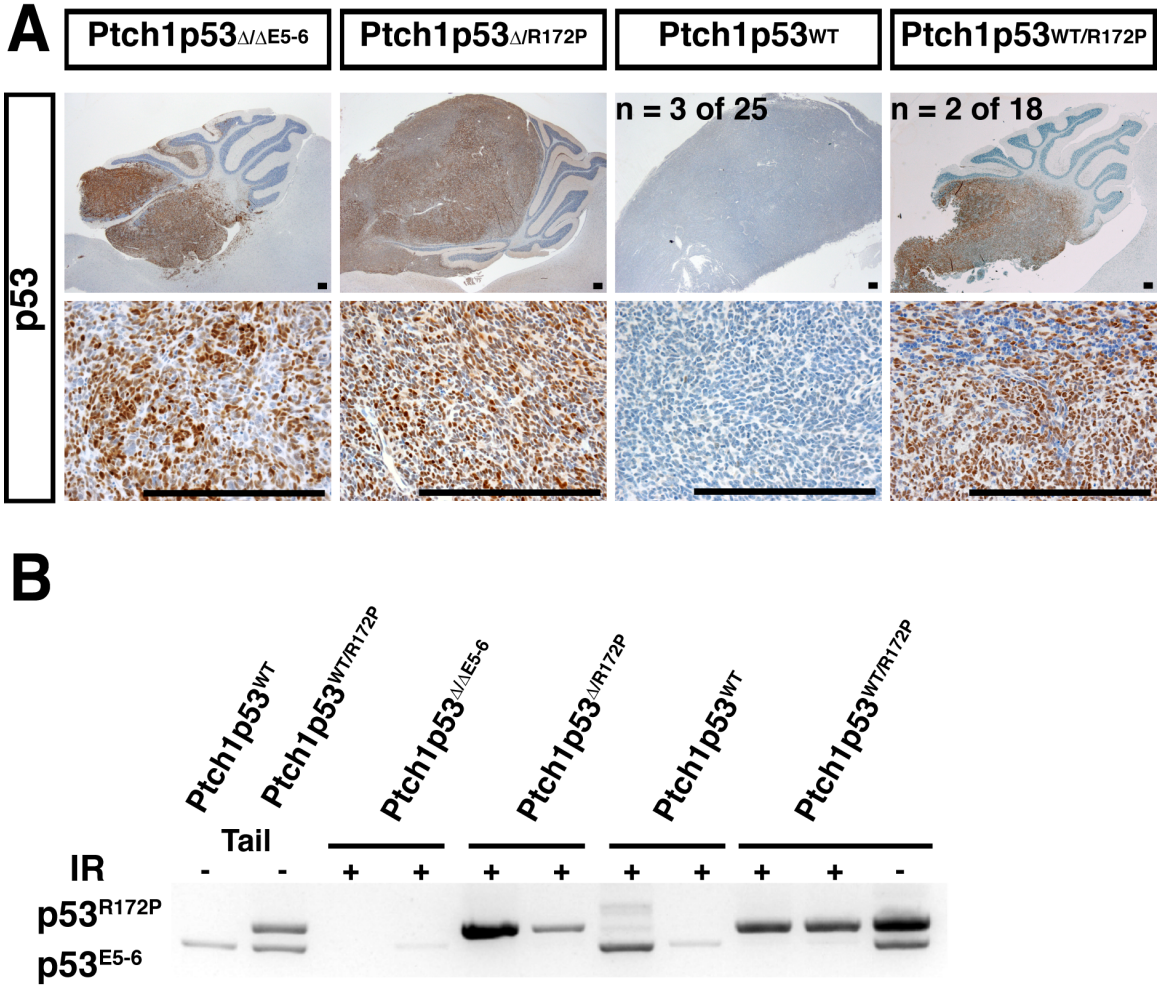

Figure 25: Radiation Induced Stress Drives Loss of Wild Type p53

(A) Low and high magnification images of immunohistochemistry images using the anti-p53 antibody with end-stage MBs treated with the long-term IR treatment of 2gray per day dose for a total of 10 days beginning at P21 and ending at P35. Note the inclusion of the Ptch1p53WT$^{/R172P}$ model, which differs from the Ptch1p53^{WT} model only after IR treatment.

(B) Genotyping of p53^{R172P} from treated MBs reveal acquired LOH in the Ptch1p53$^{WT/R172P}$ model.

Scale, 200 um. Error bars represent Mean + SEM. Unpaired, two-tailed students T-Tests were used to determine p-values.

Chapter IV: Materials and Methods

4.1 Mouse Models

Male and female mice carrying a floxed p53 ($p53^{E5\text{-}6}$) allele were maintained on a mixed C57Bl6/129Svj genetic background (Wang et. al., 2009). The $p53^{R172P}$ mouse strain was backcrossed into C57Bl6 background prior to introduction into the p53 colony, where it was crossed into the mixed p53 background. As described previously, the *hGFAP-Cre* mouse (Zhuo et. al., 2001) was initially produced on the FVB background, but was backcrossed into the mixed background for greater than five generations prior to integration into the p53 colony. The $Ptch1^{+/-}$ model (Goodrich et. al., 1997) was bred into and maintained on a mixed C57Bl6/129Svj genetic background prior to crossing into the $p53^{E5\text{-}6}$ colony. Control mice from the $p53^{\Delta E5\text{-}6/R172P}$;*hGFAP-Cre*$^{-}$;$Ptch1^{+/-}$ were collected and were phenotypically indistinguishable from $p53^{E5\text{-}6/E5\text{-}6}$;*hGFAP-Cre*$^{-}$$Ptch1^{+/-}$. Littermates were used within experimental procedures as often as possible to minimize variance.

Control and mutant animals were sacrificed either at experimental endpoints, specifically postnatal day 8, 22, or 46, or as determined by veterinary assessment. Veterinary assessment was focused around brain tumor incidence, as indicated by neurological symptoms, including loss of balance, head tilt, ataxia, hydrocephalus/macrocephaly, and seizure, with a small portion of mice instead sacrificed due to body tumors, typically lymphoma or sarcoma, particularly in germline p53 models. Control mice were also sacrificed after 350 days if no tumor was in evidence, and brains were collected and processed to verify the lack of tumor. Samples were collected either by perfusion using phosphate buffered saline followed by 4% paraformaldehyde (for paraffin embedding), or collected with a brief perfusion using only phosphate buffered saline prior to dissection, with one half the brain frozen using a liquid nitrogen bath and the other half brain placed into a 4% paraformaldehyde solution. A

subset of control and mutant animals was injected with BrdU, at the concentration of 50 μg per gram body weight, with 3 injections at 2 hour intervals for mice at postnatal day 22 and 46 and 5 injections at 2 hour intervals for mice sacrificed due to neurological symptoms. BrdU treated animals were sacrificed in the same fashion as untreated animals two hours after the final injection.

Following sacrifice, perfused tissue was processed through a sequence of dehydration steps prior to paraffin embedding. Embedded tissue was sectioned sagittally at 5 μm thickness, and affixed to Superfrost Plus microscope slides (Fisher Scientific). Sections were stained at regular intervals with hematoxylin and eosin stain to allow assessment of the MBs arising within the mouse model. Stained slides were assessed for the presence of mitotic figures, nuclear molding, and anaplastic cell morphology. Additionally, sections were stained by immunohistochemistry to further confirm typical MB markers (See below).

4.2 Irradiation

Matched littermates with MBs were treated with ionizing radiation using a RadSource 2000 with a Mouse Irradiation Fixture and Head Shield (Braintree Scientific Inc.), limiting radiation to the head and neck, and received a single dose of 20 Gray radiation and collected after 4 hours or a single dose of 4 Gray and collected after 24 hours. Matched littermates were treated with 2 Gray per Day beginning in their 4th week, typically between postnatal day 21 and 23, and received radiation 5 times a week for 2 weeks. All mice in this study were cared for according to guidelines approved by the Animal Care and Use Committee of the University of Michigan as well as the Institutional Animal Care and Use Committee of Childrens National Medical Center.

4.3 Histology, Immunohistochemistry and Immunofluorescence

Pre-neoplastic lesions were assessed using guidelines established by (Pazzaglia et. al., 2006, Mille et. al., 2014). Tumors were classified using the WHO guidebook for MB assessment criteria (Louis et. al., 2007). Diagnosis was reached based on hematoxylin

and eosin staining, as well as DAB with established MB markers.

Perfused tissue was dehydrated prior to embedding in paraffin. Parrafin embedded tissue was sectioned at 5 um, and adjacent sections were used in immunohistochemistry and immunofluorescent analysis. Tissue sections were rehydrated by sequential treatment with xylene, ethanol and water, prior to an eight minute antigen retrival using Retrieve-All antigen unmasking system (Covance) heated in coplin jars. Following retrieval, tissue was permeabalized using triton X-100 and then blocked with 3.5% goat or donkey serum, depending on antibody selection. For immunohistochemistry, blocked tissue was was incubated with primary antibody overnight at 4°C, prior to application of alkaline-phosphatase secondary antibody (Vector) at 1:400 dilution for 1 hour at room temperature. Following secondary antibody, the Avidin/Biotin Complex peroxidase system was used for 30 minutes. Following this, DAB was applied and slides were counterstained with nuclear marker hematoxylin. For immuno-fluorescent procedures, blocked tissue was incubated with primary antibody overnight at 4°C, prior to application of fluorescence conjugated secondary antibody, either Alexa488, Alexa555 or Alexa647 (Invtirogen), at 1:400 concentration for 1 hour at room temperature. Slides were counterstained with DAPI, and imaged using a fluorescent microscope. Immunofluorescent quantification was assayed by imaging multiple tumor regions, whereas DAB quantification was assessed in high magnification images and supplemented with automatic quantification using ImageJ. Whole mount images of perfused brains were taken using a dissection microscope (Olympus) with a variable objective on a solid background, using an integrated ruler to maintain scale. Brains were imaged in multiple orientations, with the medial brain used to assess cerebellar area. Pre-neoplastic lesion volume was assessed based on multiple H&E stained sections at 200-micrometer intervals.

The following primary antibodies were used:
p53-CM5 (1:500, rabbit, Leica, p53-CM5P-L)
Sox2 (1:200, goat, Santa Cruz, SC-17320)
BLBP (1:500, rabbit, AbCam, AB-32423)
NeuN (1:500, mouse, Millipore, MAB-377)
Nestin (1:100, mouse, Millipore, MAB-353)

Cleaved Caspase-3 (1:500, rabbit, Cell Signaling, 9661S)
Ki-67 (1:500, rabbit, Abcam, AB15580)
Ki-67 (1:500, mouse, BD, 550609)
BrdU (1:500, rat, Abcam, AB-6326)
p27 (1:500, mouse, BD, 610242)
Olig2 (1:2,000, rabbit, Millipore, AB-9610)
GFAP (1:1,000, rabbit, Dako, Z0334)
Synaptophysin (1:200, rabbit, Covance, SIG-3261)
p21 (1:200, mouse, BD, 556430)

4.4 TP53-DNA Structure, Plasmid Construction, Cell Culture, Transfection and Co-immunoprecipitation for Mutant P53 Analysis

Structure of TP53DBD-DNA complex was based upon the published crystal structure of the TP53DBD-DNA complex (Cho et. al., 1994; Kitayner et. al., 2006). Each of the TP53/p53 deletions and mutations used in this study was labeled in the structure of TP53DBD-DNA complex. Plasmids containing full-length human wild type p53 (pC53-SN3) and MDM2 were gifts from Dr. Yi Sun's lab at University of Michigan, Ann Arbor. The full length of wild type TP53, TP53R175H, TP53 inframe deletion of Exon 5 and 6 (human TP53 version of p53Δ5-6) and TP53 in-frame deletion of Exon 5 to 8 (p53ΔDBD with no the DNA-Binding Domain [DBD]) were amplified by PCR and reconstructed into pCDNA3.1/Flag-His vector (Invitrogen, Carlsbad, CA, USA). The full-length of mouse Mdm2 was amplified from mouse MEF cells with primers:

Forward 5' ATGTGCAATACCAAC 3'
Reverse 5' AGTTGAAGTAAGTTAGCAC 3'

Mdm2 was recombined into pLentilox RSV GFP vector (Core facility of University of Michigan). p53-specific siRNA(s) or mismatched siRNA oligos were constructed into lentiviral vector with H1 promoter (gifts from Dr. Yi Sun's lab). The targeting sequences chosen for mouse p53 (NM_011640.3) mRNA are:

GTACATGTGTAATAGCTCC (Sequence 1),
CAGTCTACTTCCCGCCATA (Sequence 2) and
GTAGATGTCTAATAGCTGC (mismatch siRNA).
Mouse p53 siRNA sequence 1 is from a previously published paper (Dirac and

Bernards, 2003); sequence 2 is from RANi Codex (http://cancan.cshl.edu/cgi-bin/Codex/Codex.cgi). All plasmids were verified by targeted Sanger sequencing. HEK293T and HCT116 TP53-/- human cell lines were grown in DMEM containing 10% FBS, 100U/ml penicillin, and 100ug/ml streptomycin at 37ºC in 5% CO_2. Transfection was performed with SuperFect transfection reagent (Qiagen) and lentivirus was produced by co-transfecting individual plasmids together with pCMVΔR8.9 and pVSV-G plasmids into HEK293T cells. For coimmunoprecipitation assay, HEK293T cells were co-transfected with indicated plasmids. Single transfection with one of the plasmids alone was used as control. 24 hours later, cells were harvested and lysed on ice using 500ul lysis buffer (50 mM Tris-HCl, pH 7.5, 150 mM NaCl, 1 mM EDTA PH 8.0, 0.5% NP40) in the presence of protease inhibitors. The detergent-soluble fraction was recovered by centrifugation at 4oC for 20 min at 12000 rpm and the supernatants were subjected to immunoprecipitation. 400ul of the supernatant was incubated with mouse anti-Flag antibody (M2, Sigma-Aldrich) and protein G PLUS-Agarose beads (Santa Cruz) with gentle rotation at 4oC for 4 hours. The beads were washed four times with lysis buffer and precipitates were eluted with 2XSDS-PAGE sample buffer and analyzed by Western blotting.

4.5 Western Blot

Snap-frozen tissue samples from wild type control brains and tumors were homogenized in Pierce RIPA Buffer (Thermo Scientific) (10 µl buffer/1 mg tissue), mixed 1:1 with Laemmli Sample Buffer (BioRad) and boiled at 100°C for 8 minutes. Samples were then subjected to SDS-PAGE using the Criterion TGX Precast gels (BioRad) and transferred onto PVDF membranes (Millipore). The membranes were blocked in 5% non-fat milk prepared in TBST and prior to an overnight incubation with primary antibodies at 4°C. Next the membranes were washed with TBST and incubated in horseradish peroxidase (HRP)-conjugated secondary antibodies at room temperature for 1 hour. Signal was detected using Pierce ECL Western Blotting Substrate (Thermo Scientific). The primary antibodies used in this study were as follows:

p53 (1:1000, rabbit, Leica, p53-CM5P-L)

M2/Anti-Flag (1:1000, mouse, Sigma, F3165)
GFP (1:3000, rabbit, Santa Cruz, SC-8334)
MDM2 (1:500, mouse, (Xiufang et. al., 2014))
p21 (1:500, mouse, BD, 556430)
β-Actin (1:5,000-10,000, mouse, Sigma-Aldrich, A-5441)

HRP-conjugated secondary antibodies were: anti-mouse (1:5,000-1:10,000, goat, BioRad, 170-6516) and anti-rabbit (1:5,000-1:10,000, goat, BioRad, 170-6515).

4.6 Genotyping

Genetic analysis of mice in the colony used genomic DNA extracted from P18-P21 tail snips incubated overnight at 50°C in SDS-EDTA TAE Buffer plus Proteinase K, prior to mixing the resultant solution with 70% isopropanol (1:1), allowing DNA to precipitate. Precipitate was then transferred and diluted into ultrapure water prior to PCR analysis for the Cre insert, p53 loxP recombination, $p53^{R172P}$, and the Ptch1 knockout allele using the Taq 2X MeanGreen Master Mix (Empyrical BioScience) in conjuncture with the following primers:

$p53^{R172P}$
$p53^{R172P}$A 5- ACCTGTAGCTCCAGCACTGG -3
$p53^{R172P}$B 5- ACAAGCCGAGTAACGATCAGG -3
p53 flox
p53.i6 5 - GCTGCAGGTCACCTGTAG - 3
p53.e7 5- CATGCAGGAGCTATTACACA -3
p53.e4 5- TGGGACAGCCAAGTCTGTTA -3
hGFAP-Cre
ICres 5- CCGTTTGCCGGTCGTGGG -3
ICreas 5- CGTATATCCTGGCAGCGATC -3
Ptch1
PtcNeoF3 5- TGGGGTGGGATTAGATAAATGCC -3
PtcR3 5- TGTCTGTGTGTGCTCCTGAATCAC -3

4.7 Sequencing

Total RNA was isolated from MBs arising within the Ptch1, Ptch1p53, and Ptch1p53 mutants, as well as control cerebellum from both WT and Ptch1p53WT mice,

by means of the RNEasy kit (Qiagen), as well as the AllPrep DNA/RNA Mini Kit (Qiagen). cDNA synthesis was performed using QuantiTect Reverse Transcription Kit (Qiagen). The cDNA product, following quality assessment and measurement of concentration, were used to sequence exons of the p53 allele. The p53 normal and mutant transcripts, encoding the entire open reading frame, was amplified with primers 1 and 2, purified, and sequenced. To improve sequence quality, shorter product was prepared combining primers 1 and 4, 3 and 8, and 7 and 2, which were amplified, purified and sequenced as well. Additionally, exons comprising the p53 DNA-binding domain (E4-8) were analyzed using genomic DNA specific to individual exons. cDNA sequencing primers are listed below:

P1, 5'- AGGTAGCGACTACAGTTAGGGG -3'
P2, 5'- TGAAGTCATAAGACAGCAAGGAG -3'
P3, 5'- CCTGCCATCACCTCAC -3'
P4, 5'- GGAAGCCATAGTTGCC -3'
P5, 5'-TCTGTTATGTGCACGTACTC -3'
P6, 5'- CGGGTGGCTCATAAGG -3'
P7, 5'- GCCGGCTCTGAGTATA -3'
P8, 5'- TGTGATGATGGTAAGGA -3'

Sequencing primers used with genomic DNA are listed below:

p53.E4F 5'- GCTGGTAGGCTGAGAACACA -3'
p53.E4R 5'- ACAGGCTGAAGAGGAACCCC -3'
p53.E5F 5'- CCTTGACACCTGATCGTTAC -3'
p53.E5R 5'- GAGCAAGAATAAGTCAGAAGC -3'
p53.E6F 5'- ACTGGCAGCCTCCCATCTT(C)C -3'
p53.E6R 5'- CTAGAAAGTCAACATCAGTC -3'
p53.E7F 5'- CTAGACTGATGTTGACTTTC -3'
p53.E7R 5'- CTGGGGAAGAAACAGGCTAA -3'
p53.E8F 5'- CTTGTGCTGGTCCTTTTCTTG -3'
p53.E8R 5'- GAGGTGACTTTGGGGTGAAG -3'

4.8 Quantitative RT-PCR

Both RNAs and genomic DNAs were extracted from cell lines, control tissues and MBs using the AllPrep DNA/RNA Mini Kit (Qiagen). cDNA for RT-PCR was generated through the QuantiTect Reverse Transcription Kit (Qiagen).. QuantiTect SYBR green

Master Mix (Qiagen), and all PCR experiments were conducted using Applied Biosystems 7500 Real-Time PCR System. Results were analyzed using ΔCT between targets and were quantified through a standard curve based method; each sample was run in triplicate and normalized to the expression of the housekeeping gene GADPH. The following primers were used for quantitative reverse transcriptase PCR (qRT-PCR):

p21
5' CACAGCTCAGTGGACTGGAA 3'
5' ACCCTAGACCCACAATGCAG 3'
Puma
5' GCGGCGGAGACAAGAAGA 3'
5' AGTCCCATGAAGAGATTGTACATGAC 3'
Gli1
5' GCTCCGCAAACACGTGAAGA 3'
5' GCCGGATCCTCCTTCCCTTT 3'
Gli2
5' TCTAGTCCACGTGTGACCCC 3'
5' AGGTCCGAATCATGCGTTGT 3'
N-Myc
5' AGGAAGCACTCCCCCATATT 3'
5' CCGCCGAAGTAGAAGTCATC 3'
Gapdh
5' ACCCAGAAGACTGTGGATGG 3'
5' CACATTGGGGGTAGGAACAC 3'

4.9 Cell Culture and Chromosome Assay

Primary cell cultures were isolated from malignant tumor taken from untreated mice when mice showed neurological symptoms. MBs were rinsed in 4ºC PBS prior to dissection, and tissue was then transferred into chilled DMEM medium. Tissue was gently minced prior to enzymatic cell dissociation using 37ºC Accutase (Innovative Cell Technologies). Following digestion, cells were transferred to serum-free self-renewal medium (Molofsky et al., 2003). Cells were fed with fresh media ever 3-5 days and passaged every 1-2 weeks, based on observed growth rate, with cells plated onto 6-well ultra-low attachment surface polystyrene plates (Corning). Excess cells were frozen using liquid nitrogen storage.

Chromosome analyses were conducted using primary cell lines based on a karyotyping protocol provided by Dr. David Ferguson's laboratory (Ferguson et al., 2000). Following splitting, cells at or below two passages were allowed to recover for 24 hours prior to incubation with Colcemid (KaryoMax, Gibco, Life Technologies) for 1 hour to arrest proliferation at metaphase. Cells were then incubated in 37°C 0.4% KCl prior to fixation in 4°C Methanol:Glacial acetic acid (3:1) fixative overnight. Fixed cells were dropped onto Superfrost Plus microscope slides (Fisher Scientific), and then stained with DAPI. Chromosomes of metaphase cells were analyzed.

4.10 Statistics

Kaplan-Meier survival curves were prepared using Prism, and included mice sacrificed due to brain tumor, body tumor and veterinary concerns, as well as aged control mice, and compared using the Mantel-Cox test. Histology and whole mount area quantification was determined using ImageJ (NIH). Cell number was counted manually and verified with ImageJ cell counter. Whenever possible, quantification was conducted using multiple replicates taken from discrete regions of the brain as well as multiple sections when possible. Student's 2-tailed t-test was used for the comparison of areas, cell numbers and staining frequency. Data were presented as Mean +/- Standard Error of the Mean (SEM), and $p < 0.05$ was considered to be statistically significant.

Chapter V: Discussion and Future Directions

The objective of my thesis project is to understand how most MBs are capable of forming without requiring inactivation of the p53 pathway, despite the fact that individuals with Li-Fraumeni syndrome carrying TP53 mutations have an increased risk of developing SHH-MBs. In this thesis, I used two mutant *p53* alleles to identify two populations of GCPs with differential sensitivity to p53-pathway activation, corresponding with p53-activation sensitive and resistant GCPs (Figure 26). In identifying the GCP population(s) sensitive to p53-pathway activation, I show that this type of GCP is effectively protected by a robust and sustained p53-mediated apoptotic response, and appear to form SHH-MBs only when TP53 mutations occur as an early event in the context of Li-Fraumeni patients with germline TP53 mutations. Despite a robust p53-mediated apoptotic response, a subset of GCPs forms SHH-MBs without disrupting the p53 pathway. This type of GCP appears to be resistant to p53-pathway activation upon oncogenic stress by Ptch1 loss, and thus do not present selective pressure to disrupt p53 during tumorigenesis. The concept of differential p53-pathway activation within GCPs offers a compelling model explaining how SHH-MBs may show increased incidence in germline mutant *TP53* individuals but rarely acquire somatic mutations to *TP53* (Pazzaglia et. al., 2006, Kool et. al., 2014).

5.1 p53-activation sensitive GCPs during cerebellar development

All SHH-MBs with germline *TP53* mutations arose during childhood (ages 4 - 17), suggesting that p53 may play a role in regulating cerebellar stem and progenitor cells, including GCPs, the cell(s) of origin for SHH-MBs (Rausch et. al., 2012, Northcott et. al., 2012, Kool et. al., 2014). Despite the increased SHH-MB incidence associated with germline *TP53* mutation, studies using germline *p53* mutation produced no overt defects in the cerebellum (Donehower et. al., 1992, Jacks et. al., 1994). Likewise, p53 conditional inactivation mutants, although capable of promoting SHH-MB with low

penetrance, typically did not feature cerebellar defects, suggesting that p53 is not required for proper cerebellar development (Wang et. al, 2009). However, when p53 is hyper-activated, such as in the *Mdm2*$^{puro/\Delta E7-9}$ mutant - producing 70% less Mdm2 protein – it was observed that the size of the developing EGL was reduced, and that the *Ptch1*$^{+/-}$;*Mdm2*$^{puro/\Delta E7-9}$ model produced no PNLs (Malek et. al., 2011). These p53 gain-of-function studies suggest that p53 activation is normally a tightly constrained process in GCPs, limited by the inherent p53-Mdm2 negative feedback loop but capable of potent response when de-repressed. Using p53$^{\Delta E5-6}$ as a marker for p53 activation, I identified a population of rare p53-actvating GCPs comprising less than 1% of the highly proliferative outer EGL. Surprisingly, in spite of the lack of p53-pathway activation, only 50% of p53$^{\Delta E5-6}$-positive GCPs were proliferative compared to the 90% frequency observed in surrounding outer EGL, suggesting that cells undergoing stress-activated p53 as well as a p53 independent cell-cycle arrest function. Introduction of even a single allele of *p53*^{R172P} was capable of reducing p53-positive cells by more than 75%, showing that a p53-activation sensitive GCP population exists during development and will be rapidly targeted by p53 activation. As MBs occur at low frequency in the p53$^{\Delta/\Delta E5-6}$ model (Wang et. al., 2009), it is likely that the p53-activation sensitive population has the potential to give rise to SHH-MBs, suggesting that p53-pathway activation eliminates tumorigenic cells. Thus, p53-sensitive GCPs that would typically be eliminated through p53-pathway activation are capable of undergoing oncogenic transformation and becoming MBs, mirroring the increased frequency for SHH-MBs in Li-Fraumeni patients (Zhukova et al. 2013; Kool et al. 2014). Overall, these results show that a rare GCP population activates p53 during cerebellar development, but this population is tightly regulated by the Mdm2-p53 negative feedback loop. Even with the introduction of mutant *p53*$^{\Delta E5-6}$, a p53-independent cell-cycle arrest mechanism(s) targets these p53-positive GCPs, explaining why previous studies have not detected these p53 positive cells during cerebellar development.

5.2 p53-activation sensitive GCPs and SHH-MB formation

In the developing cerebellum, I observed a proliferative GCP population that would accumulate $p53^{\Delta E5\text{-}6}$. One of the novel findings of this study was identification of $p53^{\Delta E5\text{-}6}$-positive cluster in the P8 EGL following loss of *Ptch1*, potentially representing the earliest detectable MB-precursor cells. Although located amongst a highly proliferative population, the $p53^{\Delta E5\text{-}6}$-clusters possessed several traits demonstrating abnormal behavior, including disruption of the boundary between outer and inner EGL and failure to undergo neuronal differentiation. Unlike many p53 positive cells in the outer EGL, the $p53^{\Delta E5,6}$-positive cells within clusters remained highly proliferative, comparable to the normal proliferative rate observed in GCPs of the adjacent outer EGL. Curiously, the majority of these $p53^{\Delta E5\text{-}6}$-positive clusters were Sox2-positive, a marker typically associated with cerebellar stem cells, suggesting that GCPs de-differentiate and acquire stem-like characteristics during an oncogenic transformation event (Oliver et. al., 2005, Ahlfeld et. al., 2013). Hyperactive SHH pathway activation has been shown to lead to increased Sox2 expression (Ahlfeld et. al. 2013), potentially indicating that *Ptch1* loss, previously suggested as an early event in SHH-MB initiation (Tamayo-Orrego et. al., 2016), may be a trigger leading to GCP de-differentiation into Sox2-positive stem-like cells. Just as frequent $p53^{\Delta E5\text{-}6}$ accumulation was noted in GCPs, both PNLs and SHH-MBs produced in the Ptch1p53$^{\Delta/\Delta E5\text{-}6}$ model maintained a high frequency of p53 positive cells throughout MB progression, demonstrating that stress would likely eliminate these cells if p53 activity had not already been lost. In turn, the Ptch1p53$^{\Delta/\Delta E5\text{-}6}$ model is capable of rapid MB induction, which is only possible when p53 activity is completely lost – demonstrated by the 38% increase in median survival following introduction of a single $p53^{R172P}$ hypomorph allele. These results demonstrate the presence of a p53-activation sensitive population of GCPs that are effectively protected from tumorigenesis by a robust p53-mediated apoptotic response during cerebellar development. Only when p53 is inactivated as an early event, analogous to the context of Li-Fraumeni syndrome, it is possible for these p53-activation sensitive GCPs to progress to form SHH-MBs (Zhukova et al. 2013; Kool et al. 2014).

5.3 p53-activation resistant GCPs during cerebellar development

Although functional p53 was able to reduce SHH-MB penetrance, I still observed a 36% tumor penetrance in the Ptch1p53^{WT} model. These tumors formed without requiring mutation of p53 and retained the ability for the p53 pathway to activate following genotoxic stress. The presence of a functional p53 response demonstrates that SHH-MBs are capable of forming without requiring p53 pathway inactivation, although it is possible that they have acquired p53-pathway alterations sufficient to limit pathway activation (Wasylishen and Lozano 2016). The formation of SHH-MBs without p53 pathway inactivation suggests the existence of a p53-activation resistant population of GCPs during cerebellar development. These GCPs, in spite of oncogenic stress induced by Ptch1 loss, are not put under selective pressure sufficient to necessitate complete inactivation of the p53 pathway. Based on these observations, I predicted that p53-activation resistant cell populations would be present in all Ptch1$^{+/-}$ mice. In support of this idea, PNLs of the *Ptch1*$^{+/-}$*p53*$^{\Delta E5\text{-}6/\Delta E5\text{-}6}$ and *Ptch1*$^{+/-}$*p53*$^{\Delta E5\text{-}6/R172P}$ models consisted of a high p53 and low p53 variant, which I attribute its cell of origin to p53-activation sensitive and resistant GCPs, respectively. The concept of distinct GCP populations with differential sensitivity to p53-pathway activation has previously been proposed, when it was demonstrated that GCPs at P0.5 had minimal response to radiation, whereas GCPs at P10 were radiation sensitive, eliciting a strong p53-mediated apoptotic response (Pazzaglia et. al., 2006). Further, irradiation was capable of inducing increased SHH-MB incidence if P0.5 cerebellum was stressed while causing a decrease in incidence when P10 cerebellum was treated (Pazzaglia et. al., 2002). The existence of distinct temporal windows for GCP to respond to p53 was demonstrated in a CRISPR/CAS9 model, where embryonic inactivation of Ptch1 lead to SHH-MB initiation regardless of p53 function, but postnatal Ptch1 inactivation could only produce widespread SHH-MBs when p53 was also inactivated (Zuckermann et. al. 2015). Likewise, differential times of Ptch1 *Math1-CreER*/*Ptch1*$^{flox/flox}$ These studies and my observations suggest the existence of a p53-activation resistant GCP population capable of producing SHH-MBs, and suggests that this GCP population may possess inherent differences from p53-activation sensitive GCPs that correspond with differences in p53 activity between early and late GCPs.

These observations seem to support my initial model, showing that there are two paths capable of giving rise to SHH-MB. Along one path, p53-activation sensitive GCPs would be eliminated unless *TP53* mutation occurs in the germline or early development. However, SHH-MBs forming on this path represents a highly aggressive SHH-MB variant, with reduced treatment response and a higher degree of genomic instability (Northcott et. al., 2012, Zhukova et. al., 2013, Kool et. al., 2014). The other path contains SHH-MBs that form from a p53-activation resistant population, which never undergo sufficient selective pressure to necessitate the loss of wild type p53, and therefore are capable of a p53-mediated response to treatment.

5.4 A connection between p53-activation resistant GCPs and Sox2-positive cells

Previous studies have identified that Sox2-positive cells are a stem-like population in SHH-MBs capable of resisting chemotherapy and inducing recurrence (Ahlfeld et. al., 2013, Vanner et. al., 2014). My results demonstrate that Sox2-positive cells were present in PNLs and SHH-MBs, and that these cells are resistant to p53-pathway activation, with less than 10% of Sox2-positive stem-like cells expressing $p53^{\Delta E5\text{-}6}$, thereby providing a mechanism explaining the observed resistance to radiation and chemotherapy (Vanner et. al., 2014). Even following high dose radiation, only 30-40% of Sox2-positive cells were found to stabilize p53, demonstrating that, even upon induced genotoxic stress, Sox2-positve cells are still relatively resistant to p53-pathway activation. Infrequent activation of p53 in Sox2-positive cells suggests that these cells may represent a potential source for p53-activation resistant SHH-MBs. One of the common theories surrounding stem-like cells in human cancer is that these cells are able to survive therapy and initiate recurrent disease (Vanner et. al., 2014). Activation of p53 by radiation during SHH-MB progression produced a differential response between Sox2-positive and Sox2-negative cells. Within both the $Ptch1^{p53R172P}$ and $Ptch1p53^{WT}$ models, activation of p53-mediated cell cycle arrest robustly drove Sox2-negative cells out of the cell cycle and induced neuronal differentiation. However, only in models retaining wild type p53 activity was it possible to eliminate Sox2-positive cells and reduce the incidence of SHH-MBs. These data explain that the treatment resistance

observed in Sox2-positive cells is likely a result of constrained p53-response, although how the p53 response is constrained in these cells requires additional study. Further, this treatment was sufficient to put a selective pressure on developing SHH-MBs, leading to the loss of the $p53^{WT}$ allele in SHH-MBs from the $Ptch1^{+/-}p53^{WT/R172P}$ model. These observations match with recurrent human MBs, which frequently gain mutations to *TP53* (Hill et. al., 2015, Morrissy et. al. 2016).

5.5 Differential roles of p53 signaling in SHH-MB progression and treatment

Following cerebellar development, the EGL is depopulated with GCPs migrating to the IGL, but hyper-activation of the SHH pathway interferes with this process, leading to the formation of PNLs (Oliver et. al., 2005). A recent study from the Charron lab suggested that SHH-MB initiation and progression are primarily hindered by the p53-mediated senescence response (Tamayo-Orrego et. al., 2016). In this study, the $Ptch1^{+/-}$ model was used to demonstrate enrichment of cell-cycle arrest/senescence proteins P21 and $P16^{Ink4A}$ in PNLs but not in SHH-MBs, which was taken as evidence that these SHH-MBs overcame the senescence response that had limited their progression into tumor (Tamayo-Orrego et. al., 2016). Using my mutant p53 models, I show that, in comparison $Ptch1^{+/-}p53^{WT/WT}$, the $Ptch1^{+/-}p53^{R172P}$ model, which losses p53-mediated apoptotic response, contains a four-fold increase in the number of PNLs observed after cerebellar maturation, suggesting that activation of p53 mediated apoptosis is a crucial barrier for p53-activation sensitive GCPs. Radiation treatment of PNLs led to p53-mediated cell-cycle arrest and differentiation, although it was insufficient to remove Sox2-positive cells. This suggests that activation of the p53-mediated senescence response is capable of limiting SHH-MB progression but was incapable of targeting Sox2-positive cells. As such, although senescence response may play a role in removing cells during GCP progression, my data demonstrates that successfully targeting PNLs requires the retention of the p53-mediated apoptotic response, thereby suggesting that p53-mediated senescence, while capable of limiting tumor progression, is not the mechanism by which p53 prevents SHH-MB occurrence.

Just as p53-mediated apoptosis was crucial to remove GCPs, so too was the p53 apoptotic response crucial for SHH-MB treatment. Using a *SmoM2;Math1-Cre* mouse in conjunction with either conditional deletion of *p53* or *Bax*, the gene encoding p53 apoptotic effector Bax, it was shown that the radiation response of SHH-MBs is highly dependent on p53-mediated apoptotic response (Crowther et. al., 2016). Similarly, I found that when p53 activation was enhanced with radiation, only a complete wild type p53 response was capable of successfully eliminating SHH-MB. Although many PNL cells were removed through p53-mediated cell-cycle arrest by activation of $p53^{R172P}$, this was insufficient to target a highly aggressive compartment of cells, which remained capable of producing SHH-MBs in spite of treatment. These findings provide evidence that, unlike most tumors where chemotherapy and radiation response is p53 pathway independent, SHH-MB treatment response is reliant on retained p53 function. This concurs with in vitro and in vivo data showing that activation of the p53 response by MDM2 inhibitor Nutlin-3 provided a potent suppressive effect on SHH-MBs (Kunkele et. al., 2012). This could also hold true for other cancers without mutant *TP53*, such as pediatric low-grade glioma. My study provides a clear association between *p53* mutation and treatment response, showing that the apoptotic effects of radiation treatment in SHH-MBs are almost entirely p53-pathway dependent.

5.6 Future Directions

My model shows that two paths lead to the formation of SHH-MB, a p53-activation sensitive GCP population that form SHH-MBs in the context of Li-Fraumeni syndrome with germline *TP53* mutations (otherwise it would be eliminated by p53-mediated apoptosis during cerebellar development), and a p53-activation resistant GCP population that form SHH-MBs without selective pressure to disrupt the p53 pathway. This model opens up several potential future directions for the project: 1) I demonstrate that two distinct populations of GCPs, differential sensitivity to p53 activation, can give rise to SHH-MB, but do not understand the mechanism by which p53-resistant GCPs evade p53 upon oncogenic stress. 2) I have found Sox2-positive cells during different stages of SHH-MBs, and observed distinct characteristics between the behavior of these

cells, shifting from highly proliferative cells at early stages to quiescent cells in PNLs and SHH-MBs. It is unknown if these cells represent the same cell types, nor how they relate to neural stem and progenitor cells during cerebellar development.

My current data provide evidence for differential sensitivity in the p53-pathway activation in GCPs, but the mechanism(s) underlying differential p53-pathway activation remain unknown. Using $p53^{\Delta E5\text{-}6}$ as a marker, I will investigate the sensitivity of p53-pathway activation in distinct GCP populations during different stages of cerebellar development upon radiation-induced DNA damage or inducible *Ptch1* loss. I will compare treated and untreated GCPs at P0.5 and P8, and demonstrate if $p53^{\Delta E5\text{-}6}$ is accumulated in these GCPs. I expect that $p53^{\Delta E5\text{-}6}$ will not accumulate in P0.5 GCPs, but in P8 or later GCPs, and will characterize cells that activate p53. If p53 accumulation is observed in these mutants, I will then attempt to characterize the behavior and markers associated with $p53^{\Delta E5\text{-}6}$ positive GCPs. Characterizing these GCP populations may give insight into distinct cells of origin for p53-activation sensitive and resistant SHH-MBs.

I have identified three distinct populations of Sox2-positive cells during SHH-MB initiation and progression, a proliferative GCP-like cell, a quiescent SHH-MB stem-like cell, and a proliferative population of Sox2-positive cells observed in the radiation treated $Ptch1p53^{R172P}$ model. Previous studies have emphasized that Sox2-positve cells are a quiescent, stem-like population that are highly resistant to chemotherapy and radiation (Oliver et. al., 2005, Hambardzumyan et. al., 2008, Ahlfeld et. al., 2013, Vanner et. al., 2014). However, the relationship between these different Sox2-positive cell populations, as well as their similarity to Sox2-positive stem cells, remains uncertain. To address this question, I will introduce the *Sox2-GFP* allele into my current Ptch1p53 models to isolate each of these Sox2-positive populations, either using flow sorting or laser capture micro-dissection (Arnold et. al., 2011, Vanner et. al., 2014). By comparing the expression pattern of the Sox2-positive cell populations, I will be able to determine whether these are truly distinct cells, or if they are instead the same cell type responding to distinct environmental stimuli. Further, comparison of these cells to Sox2-positive stem cells will demonstrate whether they maintain a stem-like expression pattern and may provide hints

as to how these cells remain quiescent. Better understanding of the Sox2-positive cell populations during different stages of SHH-MB development may have implications for therapeutic approach, as these cells have been implicated as a key mechanism of SHH-MB recurrence.

5.7 Summary

In summary, I showed that SHH-MBs arise from at least two distinct GCP populations during cerebellar development, a p53-activation sensitive and resistant GCP. I demonstrate that a sustained p53-mediated apoptotic response is capable of eliminating p53-activation sensitive GCPs, which are only able to form SHH-MB when *TP53* mutation occurs as an early event such as germline mutations associated with Li-Fraumeni syndrome. These GCPs with p53 activation formed the earliest detectable PNLs, and gave rise to highly aggressive p53-mutant SHH-MBs. However, a population of p53-activation resistant GCPs was capable of forming p53-wild type SHH-MBs, which were effectively targeted by p53-mediated apoptosis following radiation treatment. By using radiation to enhance p53-mediated responses on developing PNLs, I showed that wild type p53 activation is capable of eliminating SHH-MBs, but this selective pressure led to the loss of wild type p53 in $Ptch1^{+/-}p53^{WT/R172P}$ mutants, recapitulating human recurrent MB. Of translational significance, I demonstrated the mutational status of p53 is of critical importance to predict treatment response of SHH-MBs. Further study of the characteristics of p53-activation sensitive and resistant GCPs may provide novel therapeutic approaches to the treatment of different types of SHH-MBs.

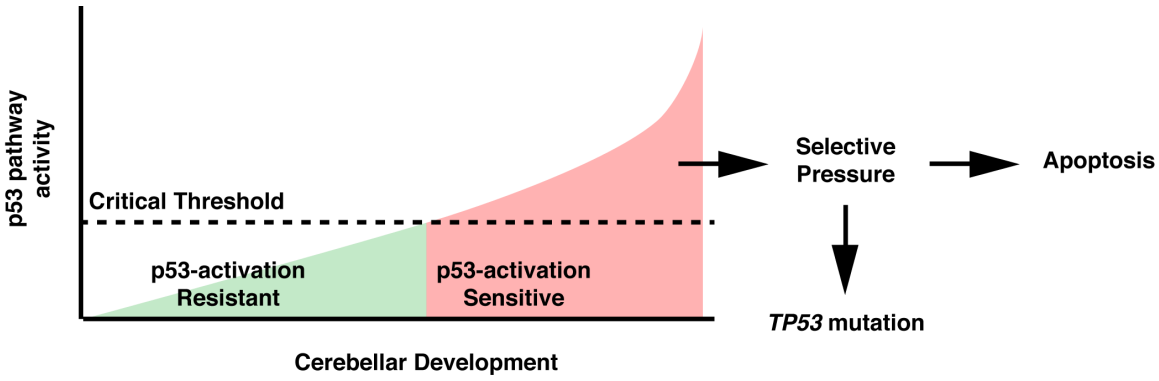

Figure 26: Proposed Model of p53 activation in cerebellar development and SHH-MB

Graphic illustration of p53-activation sensitivity in developing cerebellum. Early postnatal day 0.5 (P0.5) granule cell precursors (GCPs) are p53-activation resistant, whereas late postnatal day 10 (P10) GCPs are p53-activation sensitive. If p53 raises above a critical threshold, cells will be eliminated by selective pressure unless they mutate p53.

Works Cited

Abe, Y., Oda-Sato, E., Tobiume, K., Kawauchi, K., Taya, Y., Okamoto, K., Oren, M., and Tanaka, N. (2008). Hedgehog signaling overrides p53-mediated tumor suppression by activating Mdm2. Proc Natl Acad Sci U S A 105, 4838-4843.

Adesina, A. M., Nalbantoglu, J., and Cavenee, W. K. (1994). p53 gene mutation and mdm2 gene amplification are uncommon in MB. Cancer Res 54, 5649-5651.

Adolphe, C., Hetherington, R., Ellis, T., and Wainwright, B. (2006). Patched1 functions as a gatekeeper by promoting cell cycle progression. Cancer Res 66, 2081-2088.

Ahlfeld, J., Favaro, R., Pagella, P., Kretzschmar, H. A., Nicolis, S., and Schuller, U. (2013). Sox2 requirement in sonic hedgehog-associated MB. Cancer Res 73, 3796-3807.

Arnold, K., Sarkar, A., Yram, M. A., Polo, J. M., Bronson, R., Sengupta, S., Seandel, M., Geijsen, N., and Hochedlinger, K. (2011). Sox2(+) adult stem and progenitor cells are important for tissue regeneration and survival of mice. Cell Stem Cell 9, 317-329

Aruga, J., Inoue, T., Hoshino, J., and Mikoshiba, K. (2002). Zic2 controls cerebellar development in cooperation with Zic1. J Neurosci 22, 218-225.

Aruga, J., Minowa, O., Yaginuma, H., Kuno, J., Nagai, T., Noda, T., and Mikoshiba, K. (1998). Mouse Zic1 is involved in cerebellar development. J Neurosci 18, 284-293.

Baeza, N., Masuoka, J., Kleihues, P., and Ohgaki, H. (2003). AXIN1 mutations but not deletions in cerebellar MBs. Oncogene 22, 632-636.

Baker, S. J., Fearon, E. R., Nigro, J. M., Hamilton, S. R., Preisinger, A. C., Jessup, J. M., vanTuinen, P., Ledbetter, D. H., Barker, D. F., Nakamura, Y., et al. (1989). Chromosome 17 deletions and p53 gene mutations in colorectal carcinomas. Science 244, 217-221.

Barboza, J. A., Iwakuma, T., Terzian, T., El-Naggar, A. K., and Lozano, G. (2008). Mdm2 and Mdm4 loss regulates distinct p53 activities. Mol Cancer Res 6, 947-954.

Behesti, H., and Marino, S. (2009). Cerebellar granule cells: insights into proliferation, differentiation, and role in MB pathogenesis. Int J Biochem Cell Biol 41, 435-445.

Berman, D. M., Karhadkar, S. S., Hallahan, A. R., Pritchard, J. I., Eberhart, C. G., Watkins, D. N., Chen, J. K., Cooper, M. K., Taipale, J., Olson, J. M., and Beachy, P. A. (2002). MB growth inhibition by hedgehog pathway blockade. Science 297, 1559-1561.

Blaess, S., Corrales, J. D. and Joyner, A. L. (2006). Sonic hedgehog regulates Gli activator and repressor functions with spatial and temporal precision in the mid/hindbrain region. Development 133, 1799-1809.

Bouvard, V., Zaitchouk, T., Vacher, M., Duthu, A., Canivet, M., Choisy-Rossi, C., Nieruchalski, M., and May, E. (2000). Tissue and cell-specific expression of the p53-target genes: bax, fas, mdm2 and waf1/p21, before and following ionising irradiation in mice. Oncogene 19, 649-660.

Brachmann, D.G., Beckett, M., Graves, D., Haraf, D., Vokes, E., Weichselbaum, R.R.. (1993). *p53* mutation does not correlate with Radiosensitivity in 24 Head and Neck Cancer Cell Lines. Cancer Research 53, 3667-3669.

Brady, C. A., Jiang, D., Mello, S. S., Johnson, T. M., Jarvis, L. A., Kozak, M. M., Kenzelmann Broz, D., Basak, S., Park, E. J., McLaughlin, M. E., et al. (2011). Distinct p53 transcriptional programs dictate acute DNA-damage responses and tumor suppression. Cell 145, 571-583.

Chiang C, Litingtung Y, Lee E, Young KE, Corden JL, et al. (1996). Cyclopia and defective axial patterning in mice lacking sonic hedgehog gene function. Nature 383:407–13

Cho, Y., Gorina, S., Jeffrey, P. D., and Pavletich, N. P. (1994). Crystal structure of a p53 tumor suppressor-DNA complex: understanding tumorigenic mutations. Science 265, 346-355.

Cho, Y. J., Tsherniak, A., Tamayo, P., Santagata, S., Ligon, A., Greulich, H., Berhoukim, R., Amani, V., Goumnerova, L., Eberhart, C. G., et al. (2011). Integrative genomic analysis of MB identifies a molecular subgroup that drives poor clinical outcome. J Clin Oncol 29, 1424-1430.

Clevers, H. (2006). Wnt/beta-catenin signaling in development and disease. Cell 127, 469-480.

Crawford, J. R., MacDonald, T. J., and Packer, R. J. (2007). MB in childhood: new biological advances. Lancet Neurol 6, 1073-1085.

Crowther, A. J., Ocasio, J. K., Fang, F., Meidinger, J., Wu, J., Deal, A. M., Chang, S. X., Yuan, H., Schmid, R., Davis, I., and Gershon, T. R. (2016). Radiation Sensitivity in a Preclinical Mouse Model of Medulloblastoma Relies on the Function of the Intrinsic Apoptotic Pathway. Cancer Res 76:3211-3223

Dahmane, N., and Ruiz i Altaba, A. (1999). Sonic hedgehog regulates the growth and patterning of the cerebellum. Development 126, 3089-3100.

Deng, C., Zhang, P., Harper, J. W., Elledge, S. J., and Leder, P. (1995). Mice lacking p21CIP1/WAF1 undergo normal development, but are defective in G1 checkpoint control. Cell 82, 675-684.

Dirac, A. M., and Bernards, R. (2003). Reversal of senescence in mouse fibroblasts through lentiviral suppression of p53. J Biol Chem 278, 11731-11734.

Donehower, L. A., Harvey, M., Slagle, B. L., McArthur, M. J., Montgomery, C. A. Jr., Butel J. S., and Bradley, A. (1992). Mice deficient for p53 are developmentally normal but susceptible to spontaneous tumours. *Nature* **356**: 215-221.

Eberhart, C. G., and Burger, P. C. (2003). Anaplasia and grading in MBs. Brain Pathol 13, 376-385.

Eberhart, C. G., Chaudhry, A., Daniel, R. W., Khaki, L., Shah, K. V., and Gravitt, P. E. (2005). Increased p53 immunopositivity in anaplastic MB and supratentorial PNET is not caused by JC virus. BMC Cancer 5, 19.

Edlund, K., Larsson, O., Ameur, A., Bunikis, I., Gyllensten, U., Leroy, B., Sundstrom, M., Micke, P., Botling, J. and Soussi, T. (2012). Data-driven unbiased curation of

the TP53 tumor suppressor gene mutation database and validation by ultradeep sequencing of human tumors. Proc Natl Acad Sci U S A 109: 9551-9556.
el-Deiry, W. S., Harper, J. W., O'Connor, P. M., Velculescu, V. E., Canman, C. E., Jackman, J., Pietenpol, J. A., Burrell, M., Hill, D. E., Wang, Y., and et al. (1994). WAF1/CIP1 is induced in p53-mediated G1 arrest and apoptosis. Cancer Res 54, 1169-1174.
Eliyahu, D., Raz, A., Gruss, P., Givol, D., and Oren, M. (1984). Participation of p53 cellular tumour antigen in transformation of normal embryonic cells. Nature 312, 646-649.
Ellis, T., Smyth, I., Riley, E., Graham, S., Elliot, K., Narang, M., Kay, G. F., Wicking, C., and Wainwright, B. (2003). Patched 1 conditional null allele in mice. Genesis 36, 158-161.
Ellison, D. W. (2010). Childhood MB: novel approaches for the classification of a heterogeneous disease. Acta Neuropathol 120, 305-316.
Fan, X., and Eberhart, C. G. (2008). MB stem cells. J Clin Oncol 26, 2821-2827.
Fatemi, S. H. (2008). Reelin glycoprotein : structure, biology, and roles in health and disease, (New York: Springer).
Ferguson, D. O., Sekiguchi, J. M., Chang, S., Frank, K. M., Gao, Y., DePinho, R. A., and Alt, F. W. (2000). The nonhomologous end-joining pathway of DNA repair is required for genomic stability and the suppression of translocations. Proc Natl Acad Sci U S A 97, 6630-6633.
Finlay, C. A., Hinds, P. W., and Levine, A. J. (1989). The p53 proto-oncogene can act as a suppressor of transformation. Cell 57, 1083-1093.
Flora, A., Klisch, T. J., Schuster, G., and Zoghbi, H. Y. (2009). Deletion of Atoh1 disrupts Sonic Hedgehog signaling in the developing cerebellum and prevents MB. Science 326, 1424-1427.
Fogarty, M. P., Emmenegger, B. A., Grasfeder, L. L., Oliver, T. G., and Wechsler-Reya, R. J. (2007). Fibroblast growth factor blocks Sonic hedgehog signaling in neuronal precursors and tumor cells. Proc Natl Acad Sci U S A 104, 2973-2978.
Fucillo, M., Joyner, A. L., Fishell, G. (2006). Morphogen to mitogen: the multiple roles of hedgehog signaling in vertebrate neural development. Nature Rev Neuro 7, 772-783
Gajjar, A. J., and Robinson, G. W. (2014). MB-translating discoveries from the bench to the bedside. Nature reviews Clinical oncology 11, 714-722.
Garre, M. L., Cama, A., Bagnasco, F., Morana, G., Giangaspero, F., Brisigotti, M., Gambini, C., Forni, M., Rossi, A., Haupt, R., et al. (2009). MB variants: age-dependent occurrence and relation to Gorlin syndrome--a new clinical perspective. Clin Cancer Res 15, 2463-2471.
Gazit, R., Krizhanovsky, V., and Ben-Arie, N. (2004). Math1 controls cerebellar granule cell differentiation by regulating multiple components of the Notch signaling pathway. Development 131, 903-913.
Gibson, P., Tong, Y., Robinson, G., Thompson, M. C., Currle, D. S., Eden, C., Kranenburg, T. A., Hogg, T., Poppleton, H., Martin, J., et al. (2010). Subtypes of MB have distinct developmental origins. Nature 468, 1095-1099.
Gilbertson, R. J., and Ellison, D. W. (2008). The origins of MB subtypes. Annual review of pathology 3, 341-365.

Giordana, M. T., Schiffer, P., Lanotte, M., Girardi, P. and Chio, A. (1999). Epidemiology of adult MB. Int. J. Cancer, 80: 689–692.
Goodrich, L. V., Milenkovic, L., Higgins, K. M., and Scott, M. P. (1997). Altered neural cell fates and MB in mouse patched mutants. Science 277, 1109-1113.
Gorlin R. J. and Goltz R. W. (1960). Multiple basal-cell epithelioma, jaw cysts and bifid ribs: a syndrome. New Eng J Med 262:908–912.
Hallahan, A. R., Pritchard, J. I., Hansen, S., Benson, M., Stoeck, J., Hatton, B. A., Russell, T. L., Ellenbogen, R. G., Bernstein, I. D., Beachy, P. A., and Olson, J. M. (2004). The SmoA1 mouse model reveals that notch signaling is critical for the growth and survival of sonic hedgehog-induced MBs. Cancer Res 64, 7794-7800.
Hamard, P. J., Barthelery, N., Hogstad, B., Mungamuri, S. K., Tonnessen, C. A., Carvajal, L. A., Senturk, E., Gillespie, V., Aaronson, S. A., Merad, M., and Manfredi, J. J. (2013). The C terminus of p53 regulates gene expression by multiple mechanisms in a target- and tissue-specific manner in vivo. Genes Dev 27, 1868-1885.
Hambardzumyan, D., Becher, O. J., Rosenblum, M. K., Pandolfi, P. P., Manova-Todorova, K., and Holland, E. C. (2008). PI3K pathway regulates survival of cancer stem cells residing in the perivascular niche following radiation in MB in vivo. Genes Dev 22, 436-448.
Hatton, B. A., Knoepfler, P. S., Kenney, A. M., Rowitch, D. H., de Alboran, I. M., Olson, J. M., and Eisenman, R. N. (2006). N-myc is an essential downstream effector of Shh signaling during both normal and neoplastic cerebellar growth. Cancer Res 66, 8655-8661.
He, X., Zhang, L., Chen, Y., Remke, M., Shih, D., Lu, F., Wang, H., Deng, Y., Yu, Y., Xia, Y., et al. (2014). The G protein alpha subunit Galphas is a tumor suppressor in Sonic hedgehog-driven MB. Nat Med 20, 1035-1042.
Hill, R. M., Kuijper, S., Lindsey, J. C., Petrie, K., Schwalbe, E. C., Barker, K., Boult, J. K., Williamson, D., Ahmad, Z., Hallsworth, A., et al. (2015). Combined MYC and P53 defects emerge at MB relapse and define rapidly progressive, therapeutically targetable disease. Cancer Cell 27, 72-84.
Hisada, M., Garber, J. E., Fung, C. Y., Fraumeni, J. F., Jr., and Li, F. P. (1998). Multiple primary cancers in families with Li-Fraumeni syndrome. J Natl Cancer Inst 90, 606-611.
Hooper, J. E., and Scott, M. P. (1989). The Drosopila patched Gene encodes a Putative Membrane Protein Required for Segmental Patterning. Cell 59, 751-765.
Huang, H., Mahler-Araujo, B. M., Sankila, A., Chimelli, L., Yonekawa, Y., Kleihues, P., and Ohgaki, H. (2000). APC mutations in sporadic MBs. Am J Pathol 156, 433-437.
Inga, A., Storici, F., Darden, T. A., and Resnick, M. A. (2002). Differential transactivation by the p53 transcription factor is highly dependent on p53 level and promoter target sequence. Mol Cell Biol 22, 8612-8625.
Jacks, T., Remington, L., Williams, B. O., Schmitt, E. M. , Halachmi, S., Bronson, R. T., and Weinberg, R. A. (1994). Tumor spectrum analysis in p53-mutant mice. Curr. Biol. **4**, 1–7.

Jenkins, J. R., Rudge, K., Redmond, S., and Wade-Evans, A. (1984). Cloning and expression analysis of full length mouse cDNA sequences encoding the transformation associated protein p53. Nucleic Acids Res 12, 5609-5626.
Jiang, J., and Hui, C. C. (2008). Hedgehog signaling in development and cancer. Developmental cell 15, 801-812.
Jiang, L., Kon, N., Li, T., Wang, S. J., Su, T., Hibshoosh, H., Baer, R., and Gu, W. (2015). Ferroptosis as a p53-mediated activity during tumour suppression. Nature 520, 57-62.
Jimenez, G. S., Nister, M., Stommel, J. M., Beeche, M., Barcarse, E. A., Zhang, X. Q., O'Gorman, S., and Wahl, G. M. (2000). A transactivation-deficient mouse model provides insights into Trp53 regulation and function. Nat Genet 26, 37-43.
Joerger, A. C., and Fersht, A. R. (2016). The p53 Pathway: Origins, Inactivation in Cancer, and Emerging Therapeutic Approaches. Annu Rev Biochem 85, 375-404.
Jones, D. T., Jager, N., Kool, M., Zichner, T., Hutter, B., Sultan, M., Cho, Y. J., Pugh, T. J., Hovestadt, V., Stutz, A. M., et al. (2012). Dissecting the genomic complexity underlying MB. Nature 488, 100-105.
Jones, S. N., Roe, A. E., Donehower, L. A., and Bradley, A. (1995). Rescue of embryonic lethality in Mdm2-deficient mice by absence of p53. Nature 378, 206-208.
Kandel ER, Schwartz JH, Jessell TM. 2000. Principles of Neural Science, 4th Edtition. McGraw-Hill, New York. ISBN 0-8385-7701-6
Kawauchi, D., Robinson, G., Uziel, T., Gibson, P., Rehg, J., Gao, C., Finkelstein, D., Qu, C., Pounds, S., Ellison, D. W., et al. (2012). A mouse model of the most aggressive subgroup of human MB. Cancer Cell 21, 168-180.
Kessler, J. D., Hasegawa, H., Brun, S. N., Emmenegger, B. A., Yang, Z. J., Dutton, J. W., Wang, F., and Wechsler-Reya, R. J. (2009). N-myc alters the fate of preneoplastic cells in a mouse model of MB. Genes Dev 23, 157-170.
Kim, J., Aftab, B. T., Tang, J. Y., Kim, D., Lee, A. H., Rezaee, M., Kim, J., Chen, B., King, E. M., Borodovsky, A., Riggins, G. J., Epstein, E. H. Jr, Beachy, P. A., and Rudin, C. M. (2013). Itraconazole and arsenic trioxide inhibit hedgehog pathway activation and tumor growth associated with acquired resistance to smoothened antagonists. *Cancer Cell*, *23*, 23–34.
Kim, J. Y., Nelson, A. L., Algon, S. A., Graves, O., Sturla, L. M., Goumnerova, L. C., Rowitch, D. H., Segal, R. A., and Pomeroy, S. L. (2003). MB tumorigenesis diverges from cerebellar granule cell differentiation in patched heterozygous mice. Dev Biol 263, 50-66.
Kimonis, V. E., Goldstein, A. M., Pastakia, B., Yang, M. L., Kase, R., DiGiovanna, J. J., Bale, A. E., and Bale, S. J. (1997). Clinical manifestations in 105 persons with nevoid basal cell carcinoma syndrome. Am J Med Genet 69, 299-308.
Kimura, H., Stephen, D., Joyner, A., and Curran, T. (2005). Gli1 is important for MB formation in Ptc1+/- mice. Oncogene 24, 4026-4036.
Kitayner, M., Rozenberg, H., Kessler, N., Rabinovich, D., Shaulov, L., Haran, T. E., and Shakked, Z. (2006). Structural basis of DNA recognition by p53 tetramers. Molecular cell 22, 741-753.
Klein, C., Butt, S. J., Machold, R. P., Johnson, J. E., and Fishell, G. (2005). Cerebellum- and forebrain-derived stem cells possess intrinsic regional character. Development 132, 4497-4508.

Knoepfler, P. S., Cheng, P. F., and Eisenman, R. N. (2002). N-myc is essential during neurogenesis for the rapid expansion of progenitor cell populations and the inhibition of neuronal differentiation. Genes Dev 16, 2699-2712.

Kool, M., Jones, D. T., Jager, N., Northcott, P. A., Pugh, T. J., Hovestadt, V., Piro, R. M., Esparza, L. A., Markant, S. L., Remke, M., et al. (2014). Genome sequencing of SHH-MB predicts genotype-related response to smoothened inhibition. Cancer Cell 25, 393-405.

Korshunov, A., Remke, M., Kool, M., Hielscher, T., Northcott, P. A., Williamson, D., Pfaff, E., Witt, H., Jones, D. T., Ryzhova, M., et al. (2012). Biological and clinical heterogeneity of MYCN-amplified MB. Acta Neuropathol 123, 515-527.

Kress, M., May, E., Cassingena, R., and May, P. (1979). Simian virus 40-transformed cells express new species of proteins precipitable by anti-simian virus 40 tumor serum. Journal of virology 31, 472-483.

Kunkele, A., De Preter, K., Heukamp, L., Thor, T., Pajtler, K. W., Hartmann, W., Mittelbronn, M., Grotzer, M. A., Deubzer, H. E., Speleman, F., et al. (2012). Pharmacological activation of the p53 pathway by nutlin-3 exerts anti-tumoral effects in MBs. Neuro-oncology 14, 859-869.

Lahav, G., Rosenfeld, N., Sigal, A., Geva-Zatorsky, N., Levine, A. J., Elowitz, M. B., and Alon, U. (2004). Dynamics of the p53-Mdm2 feedback loop in individual cells. Nat Genet 36, 147-150.

Lane, D. P., and Crawford, L. V. (1979). T antigen is bound to a host protein in SV40-transformed cells. Nature 278, 261-263.

Lee, Y., Miller, H. L., Russell, H. R., Boyd, K., Curran, T., and McKinnon, P. J. (2006). Patched2 modulates tumorigenesis in patched1 heterozygous mice. Cancer Res 66, 6964-6971.

Lewandowicz, G. M., Harding, B., Harkness, W., Hayward, R., Thomas, D. G., and Darling, J. L. (2000). Chemosensitivity in childhood brain tumours in vitro: evidence of differential sensitivity to lomustine (CCNU) and vincristine. Eur J Cancer 36, 1955-1964.

Li, P., Du, F., Yuelling, L. W., Lin, T., Muradimova, R. E., Tricarico, R., Wang, J., Enikolopov, G., Bellacosa, A., Wechsler-Reya, R. J., and Yang, Z. J. (2013). A population of Nestin-expressing progenitors in the cerebellum exhibits increased tumorigenicity. Nat Neurosci 16, 1737-1744.

Li, T., Kon, N., Jiang, L., Tan, M., Ludwig, T., Zhao, Y., Baer, R., and Gu, W. (2012). Tumor suppression in the absence of p53-mediated cell-cycle arrest, apoptosis, and senescence. Cell 149, 1269-1283.

Lin, S. C., Lee, K. F., Nikitin, A. Y., Hilsenbeck, S. G., Cardiff, R. D., Li, A., Kang, K. W., Frank, S. A., Lee, W. H., and Lee, E. Y. (2004). Somatic mutation of p53 leads to estrogen receptor alpha-positive and -negative mouse mammary tumors with high frequency of metastasis. Cancer Res 64, 3525-3532.

Linzer, D. I., and Levine, A. J. (1979). Characterization of a 54K dalton cellular SV40 tumor antigen present in SV40-transformed cells and uninfected embryonal carcinoma cells. Cell 17, 43-52.

Liu G, Parant JM, Lang G, Chau P, Chavez-Reyes A, El-Naggar AK, Multani A, Chang S, Lozano G. (2004). Chromosome stability, in the absence of apoptosis, is

critical for suppression of tumorigenesis in Trp53 mutant mice. Nat Genet. 36(1):63-8.
Liu, G., Terzian, T., Xiong, S., Van Pelt, C. S., Audiffred, A., Box, N. F., and Lozano, G. (2007). The p53-Mdm2 network in progenitor cell expansion during mouse postnatal development. J Pathol 213, 360-368.
Lorenz, A., Deutschmann, M., Ahlfeld, J., Prix, C., Koch, A., Smits, R., Fodde, R., Kretzschmar, H. A., and Schuller, U. (2011). Severe alterations of cerebellar cortical development after constitutive activation of Wnt signaling in granule neuron precursors. Mol Cell Biol 31, 3326-3338.
Louis, D. N., Ohgaki, H., Wiestler, O. D., Cavenee, W. K., Burger, P. C., Jouvet, A., Scheithauer, B. W., and Kleihues, P. (2007). The 2007 WHO classification of tumours of the central nervous system. Acta neuropathologica 114, 97-109.
Ludwig, R. L., Bates, S., and Vousden, K. H. (1996). Differential activation of target cellular promoters by p53 mutants with impaired apoptotic function. Mol Cell Biol 16, 4952-4960.
Malek, R., Matta, J., Taylor, N., Perry, M. E., and Mendrysa, S. M. (2011). The p53 inhibitor MDM2 facilitates Sonic Hedgehog-mediated tumorigenesis and influences cerebellar foliation. PLoS One 6, e17884.
Malkin, D., Li, F. P., Strong, L. C., Fraumeni, J. F., Jr., Nelson, C. E., Kim, D. H., Kassel, J., Gryka, M. A., Bischoff, F. Z., Tainsky, M. A., and et al. (1990). Germ line p53 mutations in a familial syndrome of breast cancer, sarcomas, and other neoplasms. Science 250, 1233-1238.
Mao, J., Ligon, K. L., Rakhlin, E. Y., Thayer, S. P., Bronson, R. T., Rowitch, D., and McMahon A. P. (2006). A novel somatic mouse model to survey tumorigenic potential applied to the Hedgehog pathway. Cancer Res 66, 10171-10178.
Marigo, V, Johnson, R. L., Vortkamp, A., and Tabin, C. J. (1996). Sonic hedgehog differentially regulates expression of GLI and GLI3 during limb development. Dev Bio 180, 273-283.
Marino, S., Vooijs, M., van Der Gulden, H., Jonkers, J., and Berns, A. (2000). Induction of MBs in p53-null mutant mice by somatic inactivation of Rb in the external granular layer cells of the cerebellum. Genes Dev 14, 994-1004.
Marzban, H., Del Bigio, M. R., Alizadeh, J., Ghavami, S., Zachariah, R. M., and Rastegar, M. (2015). Cellular commitment in the developing cerebellum. Frontiers in cellular neuroscience 8, 450.
Matsuo, S., Takahashi, M., Inoue, K., Tamura, K., Irie, K., Kodama, Y., Nishikawa, A., and Yoshida, M. (2013). Thickened area of external granular layer and Ki-67 positive focus are early events of MB in Ptch1(+)/(-) mice. Experimental and toxicologic pathology : official journal of the Gesellschaft fur Toxikologische Pathologie 65, 863-873.
Merchant, T. E., Schreiber, J. E., Wu, S., Lukose, R., Xiong, X., and Gajjar, A. (2014). Critical combinations of radiation dose and volume predict intelligence quotient and academic achievement scores after craniospinal irradiation in children with MB. Int J Radiat Oncol Biol Phys 90, 554-561.
Mille, F., Tamayo-Orrego, L., Levesque, M., Remke, M., Korshunov, A., Cardin, J., Bouchard, N., Izzi, L., Kool, M., Northcott, P. A., et al. (2014). The Shh receptor

Boc promotes progression of early MB to advanced tumors. Developmental cell 31, 34-47.
Miyazawa, K., Himi, T., Garcia, V., Yamagishi, H., Sato, S., and Ishizaki, Y. (2000). A role for p27/Kip1 in the control of cerebellar granule cell precursor proliferation. J Neurosci 20, 5756-5763.
Molofsky, A. V., Pardal, R., Iwashita, T., Park, I. K., Clarke, M. F., and Morrison, S. J. (2003). Bmi-1 dependence distinguishes neural stem cell self-renewal from progenitor proliferation. Nature 425, 962-967.
Morrissy, A. S., Garzia, L., Shih, D. J., Zuyderduyn, S., Huang, X., Skowron, P., Remke, M., Cavalli, F. M., Ramaswamy, V., Lindsay, P. E., et al. (2016). Divergent clonal selection dominates MB at recurrence. Nature 529, 351-357.
Moxon-Emre, I., Bouffet, E., Taylor, M. D., Laperriere, N., Scantlebury, N., Law, N., Spiegler, B. J., Malkin, D., Janzen, L., and Mabbott, D. (2014). Impact of craniospinal dose, boost volume, and neurologic complications on intellectual outcome in patients with MB. J Clin Oncol 32, 1760-1768.
Nakano, K., and Vousden, K. H. (2001). PUMA, a novel proapoptotic gene, is induced by p53. Molecular cell 7, 683-694.
Northcott, P. A., Korshunov, A., Witt, H., Hielscher, T., Eberhart, C. G., Mack, S., Bouffet, E., Clifford, S. C., Hawkins, C. E., French, P., et al. (2011). MB comprises four distinct molecular variants. J Clin Oncol 29, 1408-1414.
Northcott, P. A., Lee, C., Zichner, T., Stutz, A. M., Erkek, S., Kawauchi, D., Shih, D. J., Hovestadt, V., Zapatka, M., Sturm, D., et al. (2014). Enhancer hijacking activates GFI1 family oncogenes in MB. Nature 511, 428-434.
Nüsslein-Volhard, C., and Wieschaus, E. (1980). Mutations affecting segment polarity in Drosophilia. Nature 287, 795-801.
O'Keefe, K., Li, H., and Zhang, Y. (2003). Nucleocytoplasmic shuttling of p53 is essential for MDM2-mediated cytoplasmic degradation but not ubiquitination. Mol Cell Biol 23, 6396-6405.
Oda, K., Arakawa, H., Tanaka, T., Matsuda, K., Tanikawa, C., Mori, T., Nishimori, H., Tamai, K., Tokino, T., Nakamura, Y., and Taya, Y. (2000). p53AIP1, a potential mediator of p53-dependent apoptosis, and its regulation by Ser-46-phosphorylated p53. Cell 102, 849-862.
Oliver, T. G., Grasfeder, L. L., Carroll, A. L., Kaiser, C., Gillingham, C. L., Lin, S. M., Wickramasinghe, R., Scott, M. P. and Wechsler-Reya, R. J. (2003). Transcriptional profiling of the Sonic hedgehog response: A critical role for N-Myc in proliferation of neuronal precursors. Proc Natl Acad Sci USA 100, 7331-7336.
Oliver, T. G., Read, T. A., Kessler, J. D., Mehmeti, A., Wells, J. F., Huynh, T. T., Lin, S. M., and Wechsler-Reya, R. J. (2005). Loss of patched and disruption of granule cell development in a pre-neoplastic stage of MB. Development 132, 2425-2439.
Palmer, S. L., Armstrong, C., Onar-Thomas, A., Wu, S., Wallace, D., Bonner, M. J., Schreiber, J., Swain, M., Chapieski, L., Mabbott, D., et al. (2013). Processing speed, attention, and working memory after treatment for MB: an international, prospective, and longitudinal study. J Clin Oncol 31, 3494-3500.

Pan, Y., Wang, C., and Wang, B. (2009). Phosphorylation of Gli2 by Protein kinase A is required for Gli2 processing and degradation and the Sonic Hedgehog-regulated mouse development. J Biol Chem 282, 10846-10852.
Pant, V., Xiong, S., Chau, G., Tsai, K., Shetty, G., and Lozano, G. (2016). Distinct downstream targets manifest p53-dependent pathologies in mice. Oncogene.
Parada, L. F., Land, H., Weinberg, R. A., Wolf, D., and Rotter, V. (1984). Cooperation between gene encoding p53 tumour antigen and ras in cellular transformation. Nature 312, 649-651.
Parsons, D. W., Li, M., Zhang, X., Jones, S., Leary, R. J., Lin, J. C., Boca, S. M., Carter, H., Samayoa, J., Bettegowda, C., et al. (2011). The genetic landscape of the childhood cancer MB. Science 331, 435-439.
Pazzaglia, S., Mancuso, M., Atkinson, M. J., Tanori, M., Rebessi, S., Majo, V. D., Covelli, V., Hahn, H., and Saran, A. (2002). High incidence of MB following X-ray-irradiation of newborn Ptc1 heterozygous mice. Oncogene 21, 7580-7584.
Pazzaglia, S., Tanori, M., Mancuso, M., Gessi, M., Pasquali, E., Leonardi, S., Oliva, M. A., Rebessi, S., Di Majo, V., Covelli, V., et al. (2006). Two-hit model for progression of MB preneoplasia in Patched heterozygous mice. Oncogene 25, 5575-5580.
Pei, Y., Moore, C. E., Wang, J., Tewari, A. K., Eroshkin, A., Cho, Y. J., Witt, H., Korshunov, A., Read, T. A., Sun, J. L., et al. (2012). An animal model of MYC-driven MB. Cancer Cell 21, 155-167.
Pfaff, E., Remke, M., Sturm, D., Benner, A., Witt, H., Milde, T., von Bueren, A. O., Wittmann, A., Schottler, A., Jorch, N., et al. (2010). TP53 mutation is frequently associated with CTNNB1 mutation or MYCN amplification and is compatible with long-term survival in MB. J Clin Oncol 28, 5188-5196.
Po, A., Ferretti, E., Miele, E., De Smaele, E., Paganelli, A., Canettieri, G., Coni, S., Di Marcotullio, L., Biffoni, M., Massimi, L., et al. (2010). Hedgehog controls neural stem cells through p53-independent regulation of Nanog. Embo J 29, 2646-2658.
Polyak, K., Xia, Y., Zweier, J. L., Kinzler, K. W., and Vogelstein, B. (1997). A model for p53-induced apoptosis. Nature 389, 300-305.
Pöschl, J., Stark, S., Neumann, P., Gröbner, S., Kawauchi, D., Jones, D. T., Northcott, P. A., Lichter, P., Pfister, S. M., Kool, M., Schüller, U. (2014). Genomic and transcriptomic analyses match MB mouse models to their human counterparts. Acta Neuropathol. 128, 123-36.
Rausch, T., Jones, D. T., Zapatka, M., Stutz, A. M., Zichner, T., Weischenfeldt, J., Jager, N., Remke, M., Shih, D., Northcott, P. A., et al. (2012). Genome sequencing of pediatric MB links catastrophic DNA rearrangements with TP53 mutations. Cell 148, 59-71.
Reeber, S. L., White, J. J., George-Jones, N. A., and Sillitoe, R. V. (2012). Architecture and development of olivocerebellar circuit topography. Frontiers in neural circuits 6, 115.
Riley, T., Sontag, E., Chen, P., and Levine, A. (2008). Transcriptional control of human p53-regulated genes. Nat Rev Mol Cell Biol 9, 402-412.
Robinson, G., Parker, M., Kranenburg, T. A., Lu, C., Chen, X., Ding, L., Phoenix, T. N., Hedlund, E., Wei, L., Zhu, X., et al. (2012). Novel mutations target distinct subgroups of MB. Nature 488, 43-48.

Rodriguez, F. J., Eberhart, C., O'Neill, B. P., Slezak, J., Burger, P. C., Goldthwaite, P., Wu, W., and Giannini, C. (2007). Histopathologic grading of adult MBs. Cancer 109, 2557-2565.

Rohatgi, R., Milenkovic, L., and Scott, M. P. (2007). Patched1 regulates hedgehog signaling at the primary cilium. Science 317, 372-376.

Romer, J. T., Kimura, H., Magdaleno, S., Sasai, K., Fuller, C., Baines, H., Connelly, M., Stewart, C. F., Gould, S., Rubin, L. L., and Curran, T. (2004). Suppression of the Shh pathway using a small molecule inhibitor eliminates MB in Ptc1(+/-)p53(-/-) mice. Cancer Cell 6, 229-240.

Rossi, A., Caracciolo, V., Russo, G., Reiss, K., and Giordano, A. (2008). MB: from molecular pathology to therapy. Clin Cancer Res 14, 971-976.

Roussel, M. F., and Hatten, M. E. (2011). Cerebellum development and MB. Curr Top Dev Biol 94, 235-282.

Salero, E., and Hatten, M. E. (2007). Differentiation of ES cells into cerebellar neurons. Proc Natl Acad Sci U S A 104, 2997-3002.

Schilling, K., Oberdick, J., Rossi, F., and Baader, S. L. (2008). Besides Purkinje cells and granule neurons: an appraisal of the cell biology of the interneurons of the cerebellar cortex. Histochem Cell Biol 130, 601-615.

Schuller, U., Heine, V. M., Mao, J., Kho, A. T., Dillon, A. K., Han, Y. G., Huillard, E., Sun, T., Ligon, A. H., Qian, Y., et al. (2008). Acquisition of granule neuron precursor identity is a critical determinant of progenitor cell competence to form Shh-induced MB. Cancer Cell 14, 123-134.

Schwechheimer, K., Wiedenmann, B., and Franke, W. W. (1987). Synaptophysin: a reliable marker for MBs. Virchows Archiv A, Pathological anatomy and histopathology 411, 53-59.

Segal, R. A., Goumnerova, L. C., Kwon, Y. K., Stiles, C. D., and Pomeroy, S. L. (1994). Expression of the neurotrophin receptor TrkC is linked to a favorable outcome in MB. Proc Natl Acad Sci U S A 91, 12867-12871.

Shakhova, O., Leung, C., van Montfort, E., Berns, A., and Marino, S. (2006). Lack of Rb and p53 delays cerebellar development and predisposes to large cell anaplastic MB through amplification of N-Myc and Ptch2. Cancer Res 66, 5190-5200.

Shih, D. J., Northcott, P. A., Remke, M., Korshunov, A., Ramaswamy, V., Kool, M., Luu, B., Yao, Y., Wang, X., Dubuc, A. M., et al. (2014). Cytogenetic prognostication within MB subgroups. J Clin Oncol 32, 886-896.

Smith, M. J., Beetz, C., Williams, S. G., Bhaskar, S. S., O'Sullivan, J., Anderson, B., Daly, S. B., Urquhart, J. E., Bholah, Z., Oudit, D., et al. (2014). Germline mutations in SUFU cause Gorlin syndrome-associated childhood MB and redefine the risk associated with PTCH1 mutations. J Clin Oncol 32, 4155-4161.

Soussi, T. (2010). The history of p53. A perfect example of the drawbacks of scientific paradigms. EMBO Rep 11, 822-826.

Stone, D. M., Hynes, M., Armanini, M., Swanson, T. A., Gu, Q., Johnson, R. L., Scott, M. P., Pennica, D., Goddard, A., Phillips, H., Noll, M., Hooper, J. E., de Sauvage, F., and Rosenthal, A. (1996). The tumour-suppressor gene patched encodes a candidate receptor for Sonic hedgehog. Nature 384, 129–134.

Suh, Y. A., Post, S. M., Elizondo-Fraire, A. C., Maccio, D. R., Jackson, J. G., El-Naggar, A. K., Van Pelt, C., Terzian, T., and Lozano, G. (2011). Multiple stress signals activate mutant p53 in vivo. Cancer Res 71, 7168-7175.

Sutter, R., Shakhova, O., Bhagat, H., Behesti, H., Sutter, C., Penkar, S., Santuccione, A., Bernays, R., Heppner, F. L., Schuller, U., et al. (2010). Cerebellar stem cells act as MB-initiating cells in a mouse model and a neural stem cell signature characterizes a subset of human MBs. Oncogene 29, 1845-1856.

Szak, S. T., Mays, D., and Pietenpol, J. A. (2001). Kinetics of p53 binding to promoter sites in vivo. Mol Cell Biol 21, 3375-3386.

Tabori, U., Baskin, B., Shago, M., Alon, N., Taylor, M. D., Ray, P. N., Bouffet, E., Malkin, D., and Hawkins, C. (2010). Universal poor survival in children with MB harboring somatic TP53 mutations. J Clin Oncol 28, 1345-1350.

Tamayo-Orrego, L., Wu, C. L., Bouchard, N., Khedher, A., Swikert, S. M., Remke, M., Skowron, P., Taylor, M. D., and Charron, F. (2016). Evasion of Cell Senescence Leads to MB Progression. Cell reports 14, 2925-2937.

Tanori, M., Pasquali, E., Leonardi, S., Casciati, A., Giardullo, P., De Stefano, I., Mancuso, M., Saran, A., and Pazzaglia, S. (2013). Developmental and oncogenic radiation effects on neural stem cells and their differentiating progeny in mouse cerebellum. Stem Cells 31, 2506-2516.

Thomas, W. D., Chen, J., Gao, Y. R., Cheung, B., Koach, J., Sekyere, E., Norris, M. D., Haber, M., Ellis, T., Wainwright, B., and Marshall, G. M. (2009). Patched1 deletion increases N-Myc protein stability as a mechanism of MB initiation and progression. Oncogene 28, 1605-1615.

Thompson, J., George, E. O., Poquette, C. A., Cheshire, P. J., Richmond, L. B., de Graaf, S. S., Ma, M., Stewart, C. F., and Houghton, P. J. (1999). Synergy of topotecan in combination with vincristine for treatment of pediatric solid tumor xenografts. Clin Cancer Res 5, 3617-3631.

Thompson, M. C., Fuller, C., Hogg, T. L., Dalton, J., Finkelstein, D., Lau, C. C., Chintagumpala, M., Adesina, A., Ashley, D. M., Kellie, S. J., et al. (2006). Genomics identifies MB subgroups that are enriched for specific genetic alterations. J Clin Oncol 24, 1924-1931.

Tokino, T., and Nakamura, Y. (2000). The role of p53-target genes in human cancer. Critical reviews in oncology/hematology 33, 1-6.

Vanner, R. J., Remke, M., Gallo, M., Selvadurai, H. J., Coutinho, F., Lee, L., Kushida, M., Head, R., Morrissy, S., Zhu, X., et al. (2014). Quiescent sox2(+) cells drive hierarchical growth and relapse in sonic hedgehog subgroup MB. Cancer Cell 26, 33-47.

Wang, V. Y., and Zoghbi, H. Y. (2001). Genetic regulation of cerebellar development. Nat Rev Neurosci 2, 484-491.

Wang, Y., Yang, J., Zheng, H., Tomasek, G. J., Zhang, P., McKeever, P. E., Lee, E. Y., and Zhu, Y. (2009). Expression of mutant p53 proteins implicates a lineage relationship between neural stem cells and malignant astrocytic glioma in a murine model. Cancer Cell 15, 514-526.

Ward, R. J., Lee, L., Graham, K., Satkunendran, T., Yoshikawa, K., Ling, E., Harper, L., Austin, R., Nieuwenhuis, E., Clarke, I. D., et al. (2009). Multipotent CD15+ cancer stem cells in patched-1-deficient mouse MB. Cancer Res 69, 4682-4690.

Wasylishen, A.R., Lozano, G. (2016). Attenuating the p53 Pathway in Human Cancers: Many Means to the Same End. *Cold Spring Harb Perspect Med* **6**.
Wechsler-Reya, R. J., and Scott, M. P. (1999). Control of neuronal precursor proliferation in the cerebellum by Sonic Hedgehog. Neuron 22, 103-114.
Weiner, H. L., Bakst, R., Hurlbert, M. S., Ruggiero, J., Ahn, E., Lee, W. S., Stephen, D., Zagzag, D., Joyner, A. L., and Turnbull, D. H. (2002). Induction of MBs in mice by sonic hedgehog, independent of Gli1. Cancer Res 62, 6385-6389.
Wetmore, C., Eberhart, D. E., and Curran, T. (2000). The normal patched allele is expressed in MBs from mice with heterozygous germ-line mutation of patched. Cancer Res 60, 2239-2246.
Wetmore, C., Eberhart, D. E., and Curran, T. (2001). Loss of p53 but not ARF accelerates MB in mice heterozygous for patched. Cancer Res 61, 513-516.
White, J. J., and Sillitoe, R. V. (2013). Development of the cerebellum: from gene expression patterns to circuit maps. Wiley interdisciplinary reviews Developmental biology 2, 149-164.
Wu, C. C., Shete, S., Amos, C. I., and Strong, L. C. (2006). Joint effects of p53 germline mutation and sex on cancer risk in Li-Fraumeni Syndrome. Cancer Research 66, 8287-8292
Wu, X., Northcott, P. A., Dubuc, A., Dupuy, A. J., Shih, D. J., Witt, H., Croul, S., Bouffet, E., Fults, D. W., Eberhart, C. G., et al. (2012). Clonal selection drives genetic divergence of metastatic MB. Nature 482, 529-533.
Xia, M., Knezevic, D., Tovar, C., Huang, B., Heimbrook, D. C., and Vassilev, L. T. (2008). Elevated MDM2 boosts the apoptotic activity of p53-MDM2 binding inhibitors by facilitating MDMX degradation. Cell Cycle 7, 1604-1612.
Xiong, X., Zhao, Y., Tang, F., Wei, D., Thomas, D., Wang, X., Liu, Y., Zheng, P., and Sun, Y. (2014). Ribosomal protein S27-like is a physiological regulator of p53 that suppresses genomic instability and tumorigenesis. eLife 3, e02236.
Yaguchi Y., Yu T., Ahmed M. U., Berry M., Mason I., and Basson M. A. (2009). Fibroblast growth factor (FGF) gene expression in the developing cerebellum suggests multiple roles for FGF signaling during cerebellar morphogenesis and development. Developmental Dynamics 238, 2058-2072
Yang, Z. J., Ellis, T., Markant, S. L., Read, T. A., Kessler, J. D., Bourboulas, M., Schuller, U., Machold, R., Fishell, G., Rowitch, D. H., et al. (2008). MB can be initiated by deletion of Patched in lineage-restricted progenitors or stem cells. Cancer Cell 14, 135-145.
Yauch, R. L., Dijkgraaf, G. J., Alicke, B., Januario, T., Ahn, C. P., Holcomb, T., Pujara, K., Stinson, J., Callahan, C. A., Tang, T., et al. (2009). Smoothened mutation confers resistance to a Hedgehog pathway inhibitor in MB. Science 326, 572-574.
Yokota, N., Aruga, J., Takai, S., Yamada, K., Hamazaki, M., Iwase, T., Sugimura, H., and Mikoshiba, K. (1996). Predominant expression of human zic in cerebellar granule cell lineage and MB. Cancer Res 56, 377-383.
Zauberman, A., Barak, Y., Ragimov, N., Levy, N., and Oren, M. (1993). Sequence-specific DNA binding by p53: identification of target sites and lack of binding to p53 - MDM2 complexes. Embo J 12, 2799-2808.

Zhukova, N., Ramaswamy, V., Remke, M., Pfaff, E., Shih, D. J., Martin, D. C., Castelo-Branco, P., Baskin, B., Ray, P. N., Bouffet, E., et al. (2013). Subgroup-specific prognostic implications of TP53 mutation in MB. J Clin Oncol 31, 2927-2935.

Zhuo, L., Theis, M., Alvarez-Maya, I., Brenner, M., Willecke, K., and Messing, A. (2001). hGFAP-cre transgenic mice for manipulation of glial and neuronal function in vivo. Genesis 31, 85-94.

Zindy, F., Knoepfler, P. S., Xie, S., Sherr, C. J., Eisenman, R. N., and Roussel, M. F. (2006). N-Myc and the cyclin-dependent kinase inhibitors p18Ink4c and p27Kip1 coordinately regulate cerebellar development. Proc Natl Acad Sci U S A 103, 11579-11583.